Novel Functions of C-terminus of HSC70-Interacting Protein (CHIP) in Mitophagy and Neuroprotection

By

Britney Nola Lizama

Dissertation
Submitted to the Faculty of the
Graduate School of Vanderbilt University
in partial fulfillment of the requirements
for the degree of

DOCTOR OF PHILOSOPHY
in
Neuroscience
August 10, 2018
Nashville, Tennessee

Approved:

Kevin D. Niswender, M.D., Ph.D.

BethAnn McLaughlin, Ph.D.

Fiona E. Harrison, Ph.D.

Joshua P. Fessel, M.D., Ph.D.

To my grandparents,
Francisco G. Lizama and Ester T. Lizama

ACKNOWLEDGMENTS

I express sincere thanks to my funding sources that supported this work: a predoctoral fellowship funded by the American Heart Association (14PRE2003500007), NIH grants NS050396 and R01ES022936, training grants funded by the NIH for the Initiative for Maximizing Student Diversity Program and the Neuroscience Graduate Program, travel and professional development scholarships funded by the Society for Neuroscience, and travel scholarships funded by the Howard Hughes Medical Institute and VUMC Clinical Program in Molecular Medicine.

I first want to acknowledge and express my gratitude for my thesis advisor, Dr. BethAnn McLaughlin. I have never experienced fear quite like the times that she found out that I was working in lab through holidays and severe weather, skipping lunches, and putting off doctor appointments. Beyond teaching me ways in which to be a better scientist, Dr. McLaughlin taught me what years of education and academia could not – that being a better person and strong role model is more impactful than any lab experiment.

I also want to thank my thesis committee members, Drs. Fiona Harrison, Joshua Fessel, and Kevin Niswender. I am ever grateful for your support and advice. I am also extremely thankful for your patience and support while I went through a mid-thesis crisis, where I struggled to see the many career paths possible. I am also grateful for Dr. Derek Riebau's mentorship, and I truly appreciate the experiences in the Neuro ICU with patients and families. Dr. Riebau helped me better understand the needs of patients and the realities of stroke recovery and treatment. I thank all the leaders, organizers, and mentors of diversity programs, especially those from the UA MARC program, the Vanderbilt IMSD program, and the Society for Neuroscience Scholars program. They showed me the path for success when I didn't know how to begin. I could not have done this on my own.

My family deserves all the appreciation I can possibly give. My parents, James and Brigid Borja, have been the cornerstone of the kind of person I am today – from developing my creativity in the arts as

well as science, to establishing a “get it done, no excuses” work ethic. My grandparents, Francisco and Ester Lizama, have been the kindling to my education, and without their support I would have had a very different life trajectory. My brother, sister, and nephew are my unconditional fans, and I can only hope to be the role model they deserve. I thank my best friend Steven for bearing witness to the metamorphoses of the person I am and sticking with me anyway.

I want to thank my lab sister, Amy, for her unfiltered advice and all-in support. I also thank all the members of the McLaughlin lab, especially my undergraduate mentees. They have been a joy to teach and watch grow into their chosen professional fields I also thank fellow grad students Liz and Emily for helping me cope through this academic journey and I hope our paths cross again. Last, but not least, I want to thank Brian for truly uncensored commentary and kitchen table talk-therapy, and for being the inspiration to keep moving forward.

TABLE OF CONTENTS

LIST OF TABLES

Table

LIST OF FIGURES

Figure

LIST OF ABBREVIATIONS

4-HNE	4-hydroxy-2-nonenal
ADH	Alcohol dehydrogenase
ADP	Adenosine diphosphate
ANOVA	Analysis of variance
Atg5	Autophagy-related protein 5
Atg12	Autophagy-related protein 12
Atg16	Autophagy-related protein 16
ATP	Adenosine triphosphate
Baf	Bafilomycin A1
BAG-1	Bcl-2-associated athanogene 2
BSA	Bovine serum albumin
CHIP	C-terminus of HSC70 interacting protein
CNS	Central nervous system
C-terminus	Carboxy terminus
DAPI	4,6-diamidino-2-phenylindole
DIV	Days in vitro
DJ-1	*PARK7* protein deglycase
DMEM	Dulbecco's modified eagle medium
DMSO	Dimethyl sulfoxide
Drp1	Dynamin-related protein 1
DTT	Dithiothreitol
EDTA	Ethylenediaminetetraacetic acid
EGTA	Ethyl glycol tetraacetic acid

ER	Endoplasmic reticulum
ETC	Electron transport chain FBS Fetal bovine serum
Fk2	Antibody against mono – and polyubiquitinated proteins
GAPDH	Glyceraldehyde 3-phosphate dehydrogenase
GDAP-1	Ganglioside-induced differentiation-associated protein 1
GFP	Green fluorescent protein
GSTα4	Glutathione S-transferase α4
HBSS	Hank's balanced salt solution
HEPES	4-(2-hydroxyethyl)-1-piperazineethaanesulfonic acid
Het	Heterozygous
HIP	HSC70 interacting protein
HOP	HSC70 organizing protein
HRP	Horseradish peroxidase
HSC70	Heat shock cognate 70
HSF1	Heat shock factor 1
HSP	Heat shock protein
HSP40	Heat shock protein 40
HSP70	Heat shock protein 70
HSP72	Heat shock protein 72
HSP90	Heat shock protein 90
IBR	In-between RING
IMM	Inner mitochondrial membrane

K_{ATP}	ATP-dependent potassium channel
KO	Knockout
LC3	Microtubule-associated protein light chain III
LDH	Lactate dehydrogenase
MAP2	Microtubule-associated protein 2
MDH	Malate dehydrogenase
MEF	Mouse embryonic fibroblast
MEM	Minimum essential medium
Mfn1	Mitofusin 1
Mfn2	Mitofusin 2
Miro	Mitochondrial Rho GTPase
NaCl	Sodium chloride
NINDS	National Institute of Neurological Disorders and Stroke
NMDA	*N*-methyl-D-aspartate nNOS Nitric oxide synthase
N-terminus	Amino terminus
O_2	Oxygen
OGD	Oxygen glucose deprivation
OMM	Outer mitochondrial membrane
OPA1	Optic Atrophy 1
PBS	Phosphate buffer saline
PCR	Polymerase chain reaction
PC	Preconditioning

PCC	Pearson Correlation Coefficient
PD	Parkinson's disease
PI	Propidium iodide
PINK1	PTEN-induced putative kinase 1
PND	Postnatal day
PVDF	Polyvinylidene difluoride
RING	Really interesting new gene
ROS	Reactive oxygen species
RT	Room temperature
SDS	Sodium dodecyl sulfate
SEM	Standard error of the mean
siRNA	Small interfering RNA
SOD	Superoxide dismutase
STUB1	STIP1 homology and U-box containing protein 1
TBS	Tris-buffered saline
TBST	Tris-buffered saline/Tween 20
TIA	Transient ischemic attack
TOM20	Translocase of outer membrane 20
TPR	Tetratricopeptide repeat domain
UBL	Ubiquitin-like
UPR	Unfolded Protein Response
VDAC	Voltage-dependent anion channel

WT	Wildtype

CHAPTER 1

INTRODUCTION

1.1 Ischemic Stroke and Neuroprotection

Ischemic stroke encompasses 87% of all strokes in the United States and is the fourth most common cause of death in the country (Go et al., 2013). It is also the leading cause of long-term disability in adults (Go et al., 2013). By 2030, an additional 3.4 million people above 18 years will have had a stroke, and the prevalence of stroke survivors is projected to increase (Writing Group et al., 2016).

During an ischemic stroke, a plaque or clot in a blood vessel results in loss of oxygen and glucose to the areas of the brain the vessel normally supplies causing neuronal excitotoxicity characterized by excessive glutamate release and hyperstimulation of NMDA receptors (Murphy et al., 1989). Once the plaque or clot has been removed or dissolved, re-introduction of oxygen promotes a second wave of reactive oxygen species (ROS) generation (Young et al., 2004).

Several clinical trials have used antioxidants and free radical scavengers as a means to decrease the morbidity and mortality associated with ischemic stroke (Margaill et al., 2005) with only modest improvement. One of the reasons for the limited success of these studies is that treatments in animal models are often administered at a predetermined time before or immediately after controlled ischemic onset. Stroke, however, is spontaneous and unforeseen, often meaning that patients do not reach a hospital quickly enough or within tested time windows for treatment. For example, less than 3% of adult patients qualify for receiving tissue plasminogen activator (tPA), a clot-buster and only FDA-approved drug for the treatment of ischemic stroke (often given in conjunction with antioxidant treatment in animals), because it must be administered intravenously within 4.5 hours of stroke onset (Powers et al., 2018).

Modeling Neuroprotection: Ischemic Preconditioning

While prolonged ischemia is damaging to neurons, strong experimental evidence suggests that transient ischemic attack (TIA) prior to a more severe ischemic event can be neuroprotective (Kitagawa et al., 1990; Gidday, 2006). This phenomenon, "ischemic preconditioning", can be elicited by a number of subtoxic stressors in addition to ischemia (Gidday, 2006) and has become a valuable paradigm for studying endogenous adaptive pathways in animal and cell culture models.

Over the past 25 years, many *in vivo* and *in vitro* models of PC have been developed, revealing specific windows in which protection is maximal. Early PC is elicited mainly by post-translational modifications that recede within hours after stress, providing a very narrow window of protection. Classical PC evokes new protein synthesis and lasts for days to weeks in *in vivo* models (Stetler et al., 2009; Stetler et al., 2014). We are most interested in the latter form of PC, as it provides a more pliable window in which to develop therapeutics that target the underlying adaptive pathways following an ischemic event.

Models of cerebral preconditioning share key features including: new protein synthesis, induction of heat shock proteins, activation of mitochondrial K_{ATP} channels, and spatially and temporally limited activation of caspases (McLaughlin et al., 2003; Gidday, 2006). We have increasingly come to appreciate that signaling pathways commonly associated with apoptosis and cell death can also be triggered during non-lethal, preconditioning events (McLaughlin et al., 2003; Brown et al., 2010).

Our working model of preconditioning suggests that ROS function as spatially- and temporally-controlled signals, and while we have identified a variety of redox-sensitive molecules that contribute to protection, there remain gaps in our understanding of the roles these molecules have on essential cellular processes including protein and organelle degradation.

HSP70 Is Necessary, But Not Sufficient for Preconditioning

Heat shock proteins (HSPs) constitute a highly conserved and functionally interactive network of chaperone proteins. While some HSPs are constitutively expressed, others are inducible in response to chemical, environmental and physiological stressors. Collectively, HSPs work to disaggregate, refold, and re-nature misfolded proteins in order to avoid otherwise fatal consequences. As such, many knockout models of heat shock proteins, the HSP transcription factor, HSF1, and HSP co-chaperones often exhibit severe abnormalities in their cardiovascular, reproductive and nervous systems, decreased growth rates and overall body size and increased aging phenotypes, all of which are associated with early mortality (Dickey et al., 2008; Hashimoto-Torii et al., 2014; Kim et al., 2013; Min et al., 2008; Wacker et al., 2009).

HSP70 is a cytosolic, stress-inducible chaperone that binds to multiple co-chaperones to form a protein triage complex. The function of this complex in either degrading or refolding client proteins depends on the assembly of co-chaperones. The "pro-folding" complex requires the recruitment of HIP and HOP with HSP70-HSP40 (Hohfeld et al., 2001). The "pro-degradation" complex requires the recruitment of BAG1 and CHIP with the HSP70-HSP40 complex, where CHIP ubiquitinates HSP70 client proteins for proteasomal degradation (Hohfeld et al., 2001). Given the essential functions of HSP70 in proteostasis and longevity, many groups have sought to overexpress HSP70 in models of acute and chronic stress, protein dysfunction, neurodegeneration, and aging, acquiring mixed results.

In models of heat stress, nitric oxide stress, and ataxia, HSP70 overexpression improves viability and is protective (Bellmann et al., 1996; Mosser et al., 2000; Cummings et al., 2001). However, chronic overexpression of HSP70 is deleterious, inhibiting normal development and reducing viability in Drosophila (Krebs and Feder, 1997). Additionally, in mouse models of chronic heart failure and atrial fibrillation, which is closely associated with ischemic stroke (Wolf et al., 1991; Adelborg et al., 2017),

HSP70 overexpression is not protective (Bernardo et al., 2015). In regards to preconditioning, where low-level stress evokes subsequent protection, HSP70 expression is necessary but not sufficient for neuroprotection. Only 50% of preconditioned neurons are spared in response to lethal stress despite the fact that all preconditioned neurons express HSP70 (McLaughlin et al., 2003). Taken together, these models reveal that HSP70 expression has acute protective functions, but is insufficient in long-term maintenance of the cellular milieu under chronic stress. This suggests that other proteins or pathways may be a limiting factor for maintaining protection. Given the central role of bioenergetic and redox signaling in stroke pathology, we hypothesized that mitochondria play a critical and underappreciated role in both preconditioning protection and chaperone biology.

1.2 Mitochondrial Function and Dysfunction

Redox and Energetic Homeostasis In the Central Nervous System

Eukaryotic cells rely on mitochondria for efficient generation of energy through the Krebs cycle and the electron transport chain (ETC). Indeed, eukaryotes contain an average of one billion ATP molecules, which turn over approximately three times per minute (Kornberg, 1989). The central nervous system (CNS) relies heavily on aerobic respiration for ATP production. The brain utilizes over 20% of total oxygen respired, as well as 0.3-0.8 μmol of glucose per gram of weight per minute (μmol/g/min) (Erecinska and Silver, 1989), producing approximately 25-32 μmol/g/min of ATP. Notably, nearly 50% of this pool is required to maintain cellular ion homeostasis alone (Erecinska and Silver, 1989), thus underscoring the necessity for efficient ATP production by active mitochondria.

While production of energy-rich ATP by aerobic respiration is adaptive, it also produces free oxygen-and nitrogen-radicals (Halliwell and Gutteridge, 1989). Not surprisingly, mitochondria produce the majority of ROS within neurons and approximately 3% of oxygen used for respiration captures

electrons inefficiently resulting in the generation of superoxide anions (Halliwell and Gutteridge, 1989). Given the elevated metabolic demand in neurons, maintaining redox homeostasis is crucial. ROS can modify protein structures and disrupt protein-protein interactions, oxidize lipids and alter membrane integrity, and damage DNA to disrupt normal protein synthesis (Halliwell and Gutteridge, 1989). Indeed, elevated ROS, decreased antioxidants, protein oxidation and lipid peroxidation are shared pathological features among neurological disorders (Faucheux et al., 2003; Chen et al., 2007; Hauser and Hastings, 2013; Rotblat et al., 2014; Dixit et al., 2017).

Mitochondrial morphology and intracellular localization are also dependent on metabolic demand (Mishra et al., 2015). Mitochondria are densely packed in dendrites and axon terminals, areas concentrated in ATP-dependent enzymes (Pysh and Khan, 1972; Chen and Chan, 2006). To meet such demands, neurons continuously undergo biogenesis, fusion, and fission of mitochondria. Indeed, alterations in mitochondrial quality control pathways are also associated with a host of neurological diseases (Chen and Chan, 2006; Detmer and Chan, 2007; Chan, 2012).

Discovery of Parkin and the Role of Mitochondria in Neurodegeneration

Much of what we now understand about mitochondrial quality control comes from seminal research on Parkinson's disease (PD), an age-related neurodegenerative disease characterized by loss of dopaminergic neurons in the substantia nigra pars compacta (SNpc). The resulting changes in dopaminergic tone within the basal ganglia cause hallmark symptoms of PD including cognitive decline, akinesia, bradykinesia and tremor. Approximately 10% of PD patients have inherited mutations in genes including: SNCA, LRRK2, PARK2, PARK7, and PINK1; however, the vast majority of PD is sporadic in nature, with no known family history (Klein and Westenberger, 2012).

Parkinson's is the second most prevalent neurodegenerative disease in the world affecting approximately 9,000,000 patients (Dorsey et al., 2007). Risk factors for sporadic PD include age, sex (males have a 1.5 time greater likelihood of developing PD), exposure to pesticides and fungicides, and contact with other environmental toxins (Gorell et al., 1997; Gorell et al., 1998; Van Den Eeden et al., 2003; Taylor et al., 2007). Individuals who have suffered concussive brain injury, most notably from participating in football, hockey, boxing and mixed-martial art combat, have a higher incidence of PD and PD-like symptoms (Gardner et al., 2015; Pearce et al., 2015; Mez et al., 2017).

The selective vulnerability of SNpc neurons to PD-induced degeneration has been linked to unique intrinsic properties of affected dopaminergic cells as well as circuit-specific factors such as requirements in firing activity, afferent neurochemical input and other regional specific features of the SNpc (Brichta and Greengard, 2014; Surmeier et al., 2017). One particularly appealing hypothesis first put forth by Jim Surmeier in 2010, incorporates aspects of these cell and circuit specific changes. This model features a critical role for the pacemaking properties of L-type calcium channels, whereby mitochondrial buffering of calcium entry through these channels increases mitochondrial oxidant production (Surmeier et al., 2010; Surmeier et al., 2011). The unique expression and activation of these channels may, therefore, place SNpc calcium buffering systems in peril. This hypothesis is also consistent with an important primary role for mitochondrial failure in mediating Parkinson's pathology (Ahlqvist et al., 1975).

Prior to widespread genetic analysis, the earliest and most reliable models of Parkinson's disease were developed by the labs of Flint Beal, Bill Langston and Tim Greenamyre using peripheral and central administration of pesticides, herbicides, drugs of abuse, and other agents (Betarbet et al., 2002; Schlossmacher et al., 2002; Beal and Lang, 2006). While compounds that induced PD-like degeneration and motor symptoms were structurally unique, they shared the underlying biochemical property of

blocking aerobic respiration (Tipton and Singer, 1993). Taken together with data from patient fibroblasts and imaging, these groundbreaking studies supported a central role of mitochondrial number, bioenergetic function, integrity and signaling in disease pathology (see reviews (Ding and Yin, 2012; Moon and Paek, 2015; Kang et al., 2016; Wang et al., 2016)). While our research focuses on acute injury, the molecules identified in PD research that regulate mitochondrial function also play critical roles during ischemic stress.

Each neuron must generate, repair, and replace hundreds to thousands of biologically active mitochondria in order to supply sufficient ATP and calcium buffering capacity to ensure cell viability (Erecinska and Silver, 1989; Chang and Reynolds, 2006; Chan, 2012; Golpich et al., 2017). Therefore, it is not difficult to envision why the demands of constant *de novo* mitochondrial biogenesis are overwhelming, compelling mitochondria to be able to combine resources via fission and fusion or to isolate functional mitochondria from those that need to be recycled via autophagic processes (mitophagy).

Mitofusin 1 (Mfn1) and Mitofusin 2 (Mfn2) assist in the fusion of the outer mitochondrial membrane (OMM), while Optic Atrophy 1 (Opa1) permits fusion of inner mitochondrial membranes (IMMs) (Chen and Chan, 2009). The fusion of mitochondrial membranes between organelles promotes ionic buffering and sharing of energetic resources. Indeed, stress-induced hyperfusion of mitochondria is a highly effective way for neurons to promote cell survival under acute stress, whereas under relaxed conditions cells are able to segregate damaged mitochondria (Chen and Chan, 2009). Hyperfusion occurs within minutes to hours after acute stress resulting in a highly interconnected mitochondrial network that enhances communication with the endoplasmic reticulum (van der Bliek, 2009). Fusion also allows diffusion of matrix content among mitochondria, diluting accumulated mitochondrial DNA mutations and oxidized proteins (Archer, 2013).

Mitochondrial fission reactions are regulated by Drp1, mitochondrial fission factor (Mff), and mitochondrial fission 1 protein (Fis1). These proteins are key in proper mitochondrial maintenance as they can affect the size, shape, and distribution of these organelles (Reddy et al., 2011). Cytosolic Drp1 translocates to the OMM and assembles with Fis1 and Mff, where it uses GTP hydrolysis to constrict the membranes of mitochondria until scission (Mears et al., 2011).

Cortical neuronal mitochondria have been the most widely studied primary neuronal culture system for mitochondrial dynamics. Mitochondria have equal fusion-fission and fission-fusion cycle rates of 0.023 cycles per mitochondrion per minute, or roughly one cycle completed for a single mitochondrion every 43 minutes (Cagalinec et al., 2013). In models of proteotoxicity in which mutant Huntington or Tau are overexpressed, mitochondrial fusion rates decrease, and mitochondria become shortened (Cagalinec et al., 2013). This is reversible by overexpression of the mitochondrial motility protein Miro (Cagalinec et al., 2013). While fusion rates depend on mitochondrial motility, fission rates depend on mitochondrial length. In cortical neurons, mitochondria will undergo fission more frequently when mitochondrial length exceeds 4 μm (Cagalinec et al., 2013). This constant cycling of mitochondrial fission and fusion is tightly regulated and subject to changes in the cellular proteome.

Within the last decade, the role of autophagy – the controlled process of intracellular "self-eating" – has been shown to play a critical and previously unappreciated role in neurodegeneration. During autophagy, signaling molecules called autophagy-related proteins (Atgs) initiate recruitment and formation of lipid bilayer vesicles (autophagosomes) that engulf targeted intracellular organelles and upon fusion with lysosomes, result in component degradation. Both neurons and glia undergo baseline autophagy essential for cell homeostasis (Cherra and Chu, 2008; Chen and Chan, 2009). Therefore, perturbations in autophagic proteins can promote aberrant death that is most profound in CNS (Hara et al., 2006; Komatsu et al., 2006). Defects in mitophagy, in particular, have been linked to PD as animals

with inherited mutations in PD genes have altered mitochondrial dynamics, cellular respiration, mitochondrial fission, fusion and mitophagy (Santos and Cardoso, 2012).

Parkin and PINK1 Interact to Regulate Mitophagy

The selective degradation of mitochondria is a multi-tiered system that can be triggered by single events or combination of stressors. Two distinct steps facilitate mitophagy: the priming of autophagic proteins and the selection of mitochondria for recycling (Ding et al., 2010; Egan et al., 2011; Greene et al., 2012; Itakura et al., 2012).

The E3-ubiquitin ligase Parkin works closely with PTEN-induced putative kinase 1 (PINK1) to control mitochondrial degradation via autophagy (mitophagy). PINK1 is a serine-threonine kinase that is constitutively synthesized and imported to all mitochondria, but cleaved from healthy mitochondria by inner-membrane proteases (Greene et al., 2012). In mitochondria that fail to maintain membrane potential, PINK1 accumulates on the OMM, where its catalytic kinase domain is exposed and able to phosphorylate OMM proteins as a signal for Parkin-mediated ubiquitination (Narendra et al., 2010; Lazarou et al., 2013). PINK1 can also phosphorylate the linker region of Parkin itself, facilitating the mitochondrial translocation of this E3 ligase (Kim et al., 2008). Mutations in PINK1 and Parkin have been found in patients with a subtype of early onset familial Parkinson's disease.

While disruption of PINK1 or Parkin results in mild cellular dysfunction, such models fail to capture the acute vulnerability to stress or pathological features of diseases like PD (Goldberg et al., 2003; Perez and Palmiter, 2005; Gispert et al., 2009). These data suggest that there are aspects of systems- or circuit- level functions that compensate for both PINK1 and Parkin, and that more studies are needed to identify other proteins that can be leveraged to more closely mimic the conserved pathological features of aging and disease.

The proteins that promote engulfment, dynamic changes in mitochondrial number and function, and compensation of the dopaminergic circuit that results in decades-long decline and motor manifestation of disease require a great deal more of study. For example, Nix proteins expressed on the OMM are a physical tether between mitochondrial lipid membranes and engulfing autophagosomes speckled with LC3 and GABARAP (Ding et al., 2010; Novak et al., 2010). This engulfment and the processes that precede it can occur in the absence of mitochondrial depolarization, which is often depicted as the common trigger of mitophagy. Moreover, in highly metabolic tissues, mitophagy can proceed in the absence of PINK1, suggesting that mitophagy is tissue- and context-dependent (McWilliams et al., 2018). Indeed, any number of cues such as signaling via the outer membrane kinase Ulk1 (Itakura et al., 2012; Lazarou et al., 2015), as well as the cytosolic chaperones HSP90 and Cdc37 (Weihofen et al., 2008; Joo et al., 2011) and the Nix-like protein Bnip3 (Lee et al., 2011), and triggers of the mitochondrial unfolded response (Jin and Youle, 2013) can all promote mitochondrial fission and Parkin recruitment.

We have shown that a structurally similar E3-ligase, C-terminal of HSC70-Interacting Protein (CHIP) is induced by acute neurologic stress and localizes to mitochondria. Yet, the molecular cues that promote CHIP translocation to mitochondria remain to be identified (Palubinsky et al., 2015). Post-mortem brain tissue from patients with a history of transient ischemic attack or ischemic stroke exhibit increased CHIP expression (Stankowski et al., 2011). Likewise, *in vitro* models of ischemia and heat shock promote CHIP expression and localization to mitochondria (Palubinsky et al., 2015). Acute stress induced by environmental toxins or bioenergetic dysfunction also increases the mitochondrial retention of full length PINK1 whereas total Parkin expression remains unchanged (Lee et al., 2015). Our data supports a model whereby CHIP, like Parkin, is recruited to mitochondria during acute stress, possibly through PINK1 stabilization and kinase activity.

Parkin Facilitates Mitophagy via Specific Structural Domains

The specific structural elements of Parkin that contribute to mitochondrial translocation suggest that the RING1 domain is a critical modulator of relocalization. Overexpression of RING1 mutants fail to rescue the mitochondrial morphological changes observed in KO animals, indicating that the RING1 domain is necessary (Rose et al., 2011). While the ubiquitin-like (UBL) domain is mutated in some patients with familial PD, Parkin does not require the UBL domain or the linker region to localize to mitochondria. Both the regulatory RING0 domain and the complete carboxy-terminal RING configuration of Parkin are also required for both mitochondrial translocation and subsequent mitochondrial degradation by mitophagy (Geisler et al., 2010).

In Drosophila, Parkin translocation is dependent on phosphorylation of residues S65, T175 and T217, but phosphorylation at these sites is not sufficient (Narendra et al., 2010; Kane et al., 2014). These data suggest that RING1 and UBL domain phosphorylation are critical regulators of Parkin translocation. PINK1 also phosphorylates Ser65 on ubiquitin molecules (pS65-Ub) ligated to proteins on the OMM. Phospho-ubiquitin then binds to Parkin's RING1 domain, inducing a conformational change that allows PINK1-mediated phosphorylation of Ser65 in the UBL domain of Parkin and increased E3 ligase activity (Kane et al., 2014; Kazlauskaite et al., 2014; Koyano et al., 2014; Nguyen et al., 2016; Aguirre et al., 2017).

Despite our increased understanding of PINK1-Parkin activity, many *in vitro* and Drosophila models of null or mutated PINK1 do not exhibit stress-induced Parkin translocation to failing mitochondria (Song et al., 2013). Much like Parkin KO animal models, mice deficient in PINK1 also fail to exhibit an overt behavioral phenotype or PD pathology (Kitada et al., 2009). PINK1 deficient animal models share more in common with Parkin-null animals than any other E3 ligase mutants or knockouts (Gispert et al., 2009). Given the lack of any overt phenotype, it is perhaps not surprising that Parkin

deletion does not alter baseline mitochondrial morphology in mice. Indeed, mitophagy can proceed unfettered in even Drp1 KO (Burman et al., 2017) and PINK1 KO animals (McWilliams et al., 2018). In studies by Kageyama and colleages, mitochondrial ubiquitination and localization of the autophagy adaptor protein, p62, occurred independently of Parkin (Kageyama et al., 2014).

Taken together, we have yet to develop a full understanding of the events that cause mitochondria to be engulfed and how endogenous signals like energetics and ROS combine with fusion and fission proteins to promote or halt mitophagy. We hypothesize that local, subcellular cues are essential to determining neuronal fate, and that under conditions of extreme ROS formation or energetic stress there are redundant opportunities for mitochondria to be recycled via mitophagy.

1.3 E3-ligases in Neurological Disease

Conservation of ubiquitination as a critical regulator of protein function from yeast to humans underscores the importance of this post-translational modification for eukaryotic life. Over the past two decades, ubiquitin has been linked to apoptosis, facilitating protein-protein interactions, promoting DNA transcription and cell repair (Grabbe et al., 2011; Hammond-Martel et al., 2012; Husnjak and Dikic, 2012; Zhao et al., 2014).

During the ubiquitination process, E1 enzymes activate ubiquitin via an ATP-dependent reaction, forming a thioester with ubiquitin's C-terminus. The activated ubiquitin is then transferred to a cysteine residue of an E2 ubiquitin conjugating enzyme. E3 ligases then carry out the final step in the ubiquitination cascade, catalyzing the transfer of ubiquitin from the E2 enzyme to a lysine residue of the substrate in a covalent manner (Reviewed by (Metzger et al., 2012)).

Three classes of E3 ligases facilitate this ubiquitin transfer by different mechanisms and are distinguished by their unique structural features. They are: the RING, the HECT, and the ring-between-

ring (RBR) E3 ligase proteins. RING family proteins catalyze the transfer of ubiquitin directly from an E2 enzyme to the substrate, whereas the HECT and RBR families facilitate the transfer of ubiquitin via a two-step trans-thioesterfication reaction (Metzger et al., 2012).

Parkin Is a Redox-Sensitive RING Finger Domain E3 Ligase

Parkin is unique in that the structure of the protein suggests that it is a classical RBR (Figure 1), yet based on cell free assays as well as *in situ* studies, it contains features of both RING and HECT E3 ligase activity (Riley et al., 2013). Notably, ligases containing the structures necessary for the trans-thioesterification reactions during ubiquitin transfer are more susceptible to changes in cell redox status (Riley et al., 2013; Groitl and Jakob, 2014).

Parkin is rich in methionine and cysteine residues, which are the most vulnerable amino acids to oxidative modification (Halliwell and Gutteridge, 1989), and HECT domains often contain multiple cysteine residues needed for trans-thioesterification (Kee and Huibregtse, 2007). Disruption of these catalytic residues by reactive oxygen species (ROS) has been shown to slow or halt substrate ubiquitination (Doris et al., 2012). Taken together, these data suggest that there are structural features of Parkin that make it uniquely vulnerable to aberrant redox modification or uniquely sensitive to detecting changes in redox environment as a mechanism to control bioactivity of the ligase. Indeed, it has been hypothesized that one factor that could contribute to the early death of SNpc neurons in PD is the high level of ROS produced in these cells (Choi et al., 2003).

In addition to the conserved RING1, IBR and RING2 domains, Parkin also contains an N-terminal UBL domain followed by a zinc-binding domain called RING0 (Hristova et al., 2009). Both the IBR and RING2 domains bind zinc in a similar topological manner, but differ from the canonical cross-brace fold conformation of RING1. Parkin's RING finger domains are additional sites of potential

structural vulnerability given that within a globular conformation, it binds two zinc ions in a histidine- and cysteine-rich motif. This structure promotes protein-protein interactions, but is also biochemically unstable and prone to oxidation as well as metal displacement by other divalent cations like cadmium and cobalt. The resulting changes in protein structure and function can be rapid, extremely unstable and lead to potentially toxic loss or gain of function alterations in activity (Hartwig, 2001). Indeed, metal ion disequilibrium has been implicated in environmental toxin induced Parkinson's disease (Gorell et al., 1997; Kwakye et al., 2016).

Through its C-terminal RING domain, Parkin is able to conjugate to a variety of E2 proteins (Shimura et al., 2000; Imai et al., 2002; Olzmann and Chin, 2008). The proteins and cofactors that regulate binding of Parkin with each of its E2 proteins *in vivo* remain poorly understood, yet are of great importance given that the ability of Parkin to bind unique combinations of E2 proteins regulates the fate of ubiquitinated clients (Fiesel et al., 2014). Several disease-associated mutations in PARK2 impair E3 ligase activity for a selective population of substrates, including growth factors, repair enzymes, and structural proteins (Shimura et al., 2000; Zhang et al., 2000; Imai et al., 2002).

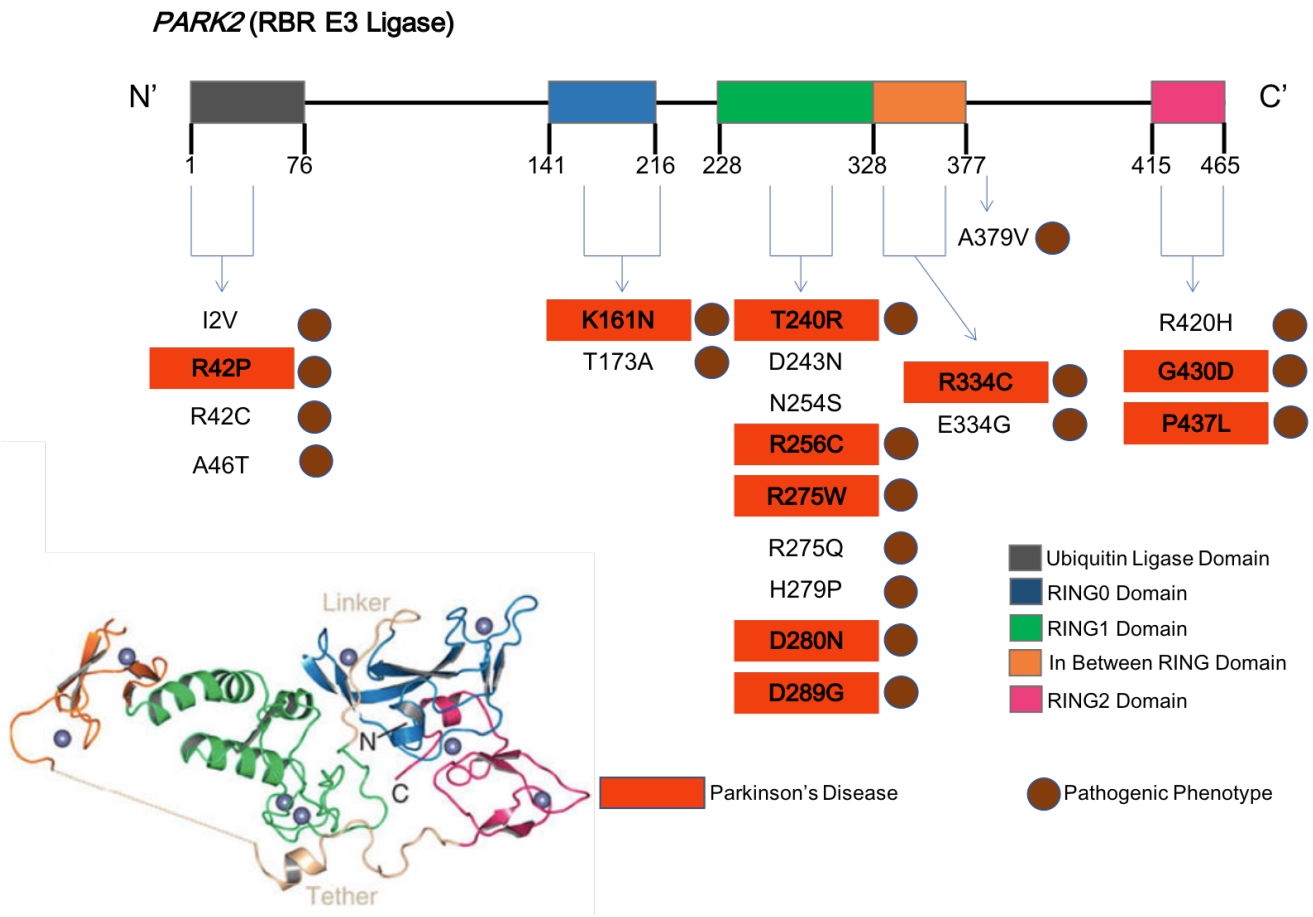

Figure 1: Parkin (PARK2) Structure and Mutations. The PARK2 gene contains few mutations in its ubiquitin ligase domain; most of the mutations appear in its RING domains, which bind two zinc ions in a histidine and cysteine-rich motif to facilitate the transthioesterfication reaction. (Figure adapted from (Riley et al., 2013; Lizama et al., 2017)).

Pathogenic Mutations in Parkin

Most of the pathogenic Parkin mutations in patients with PD occur in the linker region between the UBL and RING1 domains (Figure 1). Indeed, mutations in this region account for 43% of identified Parkin pathological changes (Parkinson's Disease mutations database); however, pathogenic mutations have been identified throughout the Parkin protein (Trempe et al., 2013) (Figure 1). For example, the RING1 mutant C289G, the RING2 mutant C441R, and the UBL mutant R42P all fail to translocate to

depolarized mitochondria (Hampe et al., 2006; Lee et al., 2010; Lazarou et al., 2013). On the other hand, the RING1 domain mutant R275W is recruited to mitochondria via a PINK1 dependent pathway yet fails to induce mitophagy (Geisler et al., 2010; Narendra et al., 2010) while mutants deficient in E3 ligase activity such as A240R and T415N not only associate with depolarized mitochondria but also induce formation of mitochondrial aggregates (Zhang et al., 2000; Sriram et al., 2005; Lee et al., 2010).

Mutations have also been found to increase E3 ligase activity of Parkin (Riley et al., 2013; Trempe et al., 2013), suggesting that the substrates with which Parkin interacts, the efficacy in which substrates are tagged with ubiquitin and delivered to the proteasome for degradation, and other aspects of function and localization of this protein are critical determinants of dopaminergic cell survival (Seirafi et al., 2015). A testament to this complexity is that not all Parkin substrates accumulate in Parkin knockout (KO) mice or PD patients, suggesting that either Parkin-mediated ubiquitination can be independent of proteasomal degradation or that redundant E3 ligases, such as CHIP can promote proteostasis when Parkin is mutated or absent (Imai et al., 2002; Schlossmacher et al., 2002; Moore et al., 2008; Chen et al., 2010).

CHIP Is an Essential U-box Domain E3 Ligase

In 2002, Imai and colleagues demonstrated that Parkin associates with Heat Shock Protein 70 (HSP70), where it facilitates ubiquitination and degradation of HSP70 client proteins. Interestingly, this interaction is interrupted by expression of the HSP70 co-chaperone and E3 ligase, CHIP. Upon dissociation from HSP70, Parkin can instead focus on turnover of the Pael-R receptors and presumably other substrates during ER-stress (Imai et al., 2002). Since it was discovered, interest in CHIP has rapidly expanded to PD and other neurodegenerative diseases (Kumar et al., 2012; Joshi et al., 2016), as acute CHIP overexpression *in vitro* improves cellular survival by removing damaged proteins and

decreasing proteotoxic stress in models of chronic neurological diseases (Dickey et al., 2007a; Rosser et al., 2007).

Despite heightened interest in CHIP, CHIP-specific substrates have been ill-defined and limited to known HSC/HSP70 client proteins, which include ataxin-3, p53, mutant tau, mutant huntingtin, and cystic fibrosis transmembrane conductance regulator (Arndt et al., 2007; Rosser et al., 2007). Given that most CHIP protein-protein interactions were derived from immunoprecipitation experiments that fail to capture *in vitro* and *in vivo* interactions (Stankiewicz et al., 2010; Kumar et al., 2012), more studies on specific binding partners of CHIP during physiological conditions are sorely needed.

CHIP is a 303 amino acid protein that is highly conserved across species (Ballinger et al., 1999). CHIP was originally discovered in a screen of tetracopeptide repeat (TPR) domain-containing enzymes, of which many participate in interactions with the heat shock protein family (Ballinger et al., 1999). CHIP contains an N-terminal TPR domain, a charged central domain, and a highly conserved C-terminal U-box domain that is necessary for its E3 ligase activity (Ballinger et al., 1999; Jiang et al., 2001) (Figure 2).

U-box E3 ligases are far less abundant than RING-finger proteins, with only seven identified in the human and mouse proteomes (Hatakeyama et al., 2001). The U-box domain is functionally and structurally similar to RING domains, but contains a hydrophobic core that lacks metal-chelating residues present in RING domain E3 ligases (Aravind and Koonin, 2000). One possibility is that this unique structure renders U-box E3 ligase activity resistant to oxidative modification, and thus a resilient scavenger for damaged proteins, lipids, and organelles during stress conditions.

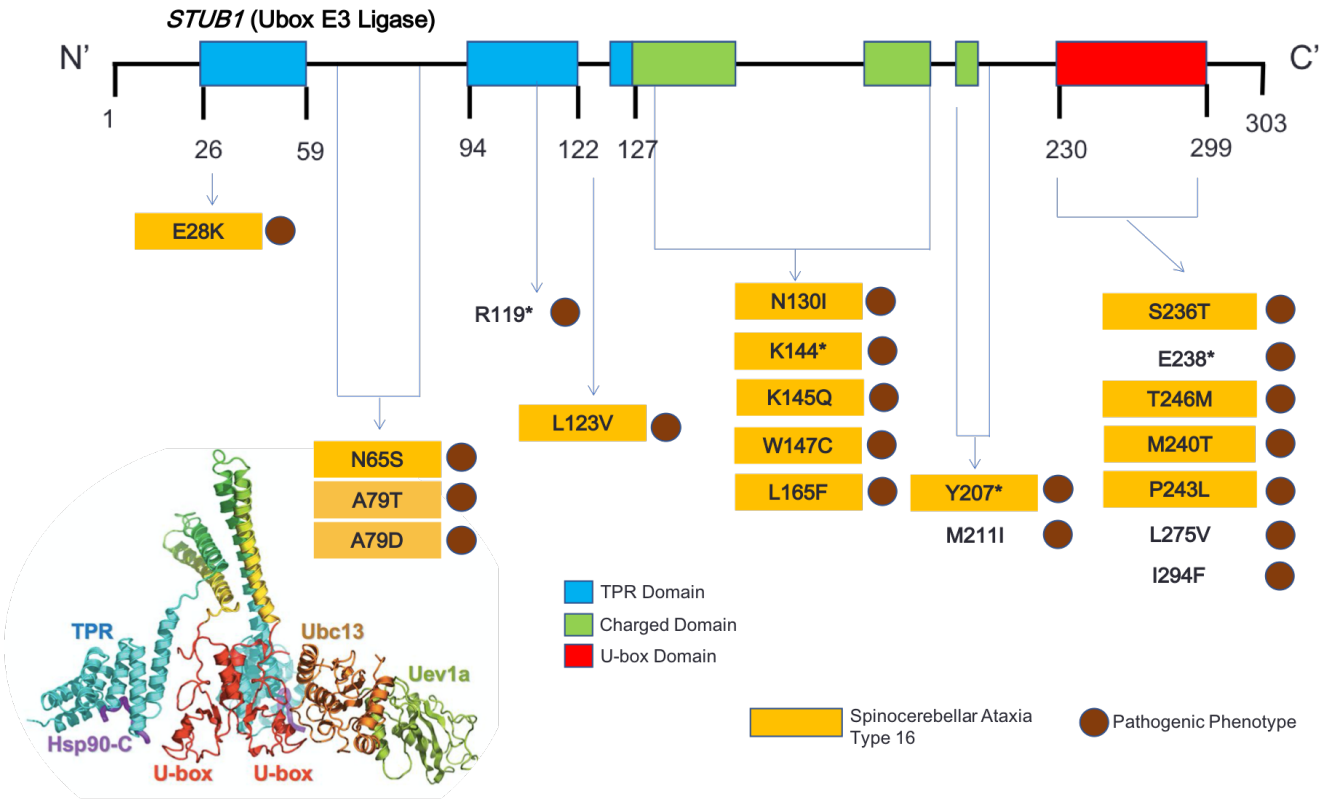

Figure 2: CHIP (STUB1) Structure and Mutations. STUB1 is the gene that encodes CHIP, an E3 ligase of the RING family with a C-terminal Ubox domain. Several pathogenic mutations were identified in CHIP in patients with particular forms of Spinocerebellar Ataxia (SCA). Mutations are located throughout the protein, suggesting loss of E3 ligase function is not the only important domain in this protein. (Figure adapted from (Pearl et al., 2008; Lizama et al., 2017)).

CHIP Mutations Result In Unique and Devastating Neurological Dysfunction

One might suspect that a Parkin surrogate like CHIP would have mild pathological features when deleted, similar to Parkin-null mice. In fact, quite the opposite is true. Severe motor impairments, mitochondrial failure, cardiovascular abnormalities, and early lethality observed in CHIP deficient animals suggest that this protein plays a critical role in aging, stress responsiveness and neurological function (Palubinsky et al., 2015). These features stand in stark contrast to Parkin-null mice, which are

long-lived and free of major hallmarks of PD or other degenerative diseases (Rial et al., 2014). Under conditions of energetic and oxidative stress, heat stress and hypoxia we, and others, have shown that CHIP expression is rapidly upregulated (Dai et al., 2003; Kim et al., 2005; Stankowski et al., 2011).

Within the past five years, whole-exome sequencing has led to the discovery of a number of mutations (13 missense; 2 nonsense) in CHIP in patients with recessive ataxia (Casarejos et al., 2014; Heimdal et al., 2014; Shi et al., 2014; Synofzik et al., 2014; Bettencourt et al., 2015) (Figure 2). Patients with recessive ataxia and spinocerebellar ataxia exhibit a progressive loss of motor control, gait abnormalities, and cerebellar atrophy (Heimdal et al., 2014; Shi et al., 2014). More recently, homozygous mutations in the STUB1 gene encoding CHIP resulting in a loss of function in CHIP activity have been linked to the rare genetic disorder Gordon Holms Syndrome in which patients present with hypogonadism and ataxia (Shi et al., 2014; Rubel et al., 2015). These phenotypes in humans are consistent with our observations in which male CHIP-deficient mice are infertile.

Pathogenic mutations in CHIP are found throughout the protein (Figure 2), and recent functional analyses of these mutations *in vitro* indicate that the consequence of these mutations is structurally destabilized CHIP (Pakdaman et al., 2017; Kanack et al., 2018). For example, the TPR mutation E28K and the U-box mutation T246M result in decreased CHIP dimerization and increased monomer and higher order oligomerization (Pakdaman et al., 2017). Interestingly, the predicted dysfunction of these mutations does not always correlate with location of the mutation. For instance, the U-box mutations M240T and T246M cause decreased HSP binding in addition to loss of E2 recruitment (Kanack et al., 2018). Similarly, the TPR mutations N65S and L123V cause decreased E2 recruitment in addition to decreaed HSP binding (Kanack et al., 2018). These data reveal that the domains of CHIP work cooperatively for HSP-mediated substrate identification and ubiquitination.

A

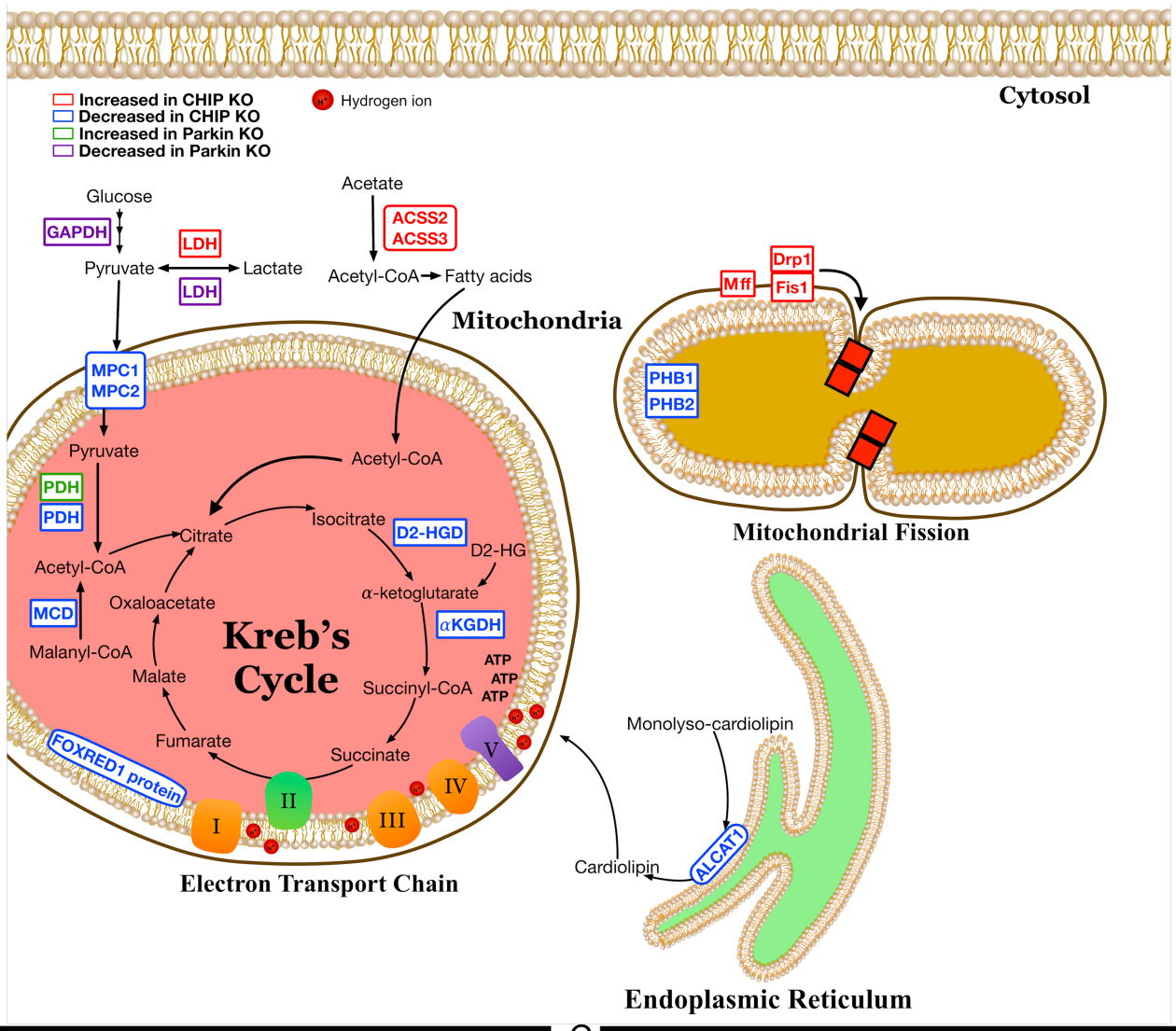

B

Energetics Proteins Altered in CHIP KO Animals	
Decreased in CHIP KO Mice	
Protein	*Fold Change*
Pyruvate Dehydrogenase	1.4
Mitochondrial Pyruvate Carrier Protein I	4.5
Mitochondrial Pyruvate Carrier Protein II	2.2
2-oxoglutarate dehydrogenase	4.0
Malonyl-CoA Decarboxylase	6.9
D-2-hydroxyglutarate dehydrogenase	2.9
FAD-dependent oxidoreductase proteIn I	2.5
Increased in CHIP KO Mice	
Protein	*Fold Change*
Lactate dehydrogenase	3.7
Acyl coA synthetase II	3.7
Acyl coA synthetase III	1.5

C

Mitochondrial Structural Proteins Altered in CHIP KO Animals	
Decreased in CHIP KO Mice	
Protein	*Fold Change*
Prohibitin	1.6
Prohibitin-2	2.3
Lysocardiolipin acyltransferase	8.8
Increased in CHIP KO Mice	
Protein	*Fold Change*
Dynamin-related protein I	7.8
Mitochondrial fission factor	5.5
Mitochondrial fission 1 protein	2.3

Figure 3: Loss of CHIP or Parkin Causes Mitochondrial Dysfunction and Energetic Imbalance via Redundant and Non-redundant Pathways. Proteomic analysis of whole brains from postnatal day 35 WT

and CHIP KO mice was performed to screen for alterations in protein expression. LC-MS/MS shotgun analyses of single gel fractions of all proteins were run and the proteins listed (B, C) are the subset of those significantly increased or decreased by CHIP KO compared to WT littermates based on spectral count data analyzed by QuasiTel (Palubinsky et al., In Preparation; Lizama, Under Review). Proteomic data from 2-month-old Parkin KO mouse cortices are described by Periquet and colleagues (Periquet et al., 2005). *A*. Diagram summarizing proteins altered by either CHIP KO or Parkin KO. Proteins increased in CHIP KO mice are labeled in red, while proteins decreased by CHIP loss are labeled in blue. Proteins increased in Parkin KO mice are labeled in green, while proteins decreased by Parkin loss are labeled in purple. *B*. Glycolytic enzymes pyruvate dehydrogenase (PDH) and lactate dehydrogenase (LDH) are increased and decreased, respectively, while mitochondrial pyruvate carrier proteins I and II (MPC1/MPC2), which affect pyruvate uptake into mitochondria, are increased by CHIP loss. Acyl CoA synthases II and III (ACSS2/ACSS3) are increased in CHIP KO. Loss of CHIP decreases expression of the Krebs cycle enzymes 2-oxoglutarate dehydrogenase (αKGDH), malonyl-CoA decarboxylase (MCD), and d-2-hydroxyglutarate dehydrogenase (D2-HGD). FAD-dependent oxidoreductase protein I (FOXRED1), which is crucial for respiratory complex 1 formation, is also decreased in CHIP KO. *C*. A key enzyme in cardiolipin localization and formation, lysocardiolipin acyltransferase (ALCAT1), is decreased in CHIP KO mice. Similarly, prohibitins (PHB1/PHB2), known to control cristae morphogenesis and respiratory chain assembly as well as to dictate levels of ROS within mitochondria via interactions with cardiolipin are also decreased when CHIP is absent. Three key fission proteins, dynamin-related protein 1 (Drp1), mitochondrial fission factor (Mff) and mitochondrial fission 1 protein (Fis1) are increased in CHIP KO mice. Figure adapted from (Lizama et al., 2017).

To better understand how CHIP deficiency elicits such a devastating phenotype, while Parkin deficient models do not, we compared Parkin and CHIP proteomic profiles (summarized in Figure 3). In doing so, we hoped to leverage the differences to identify mechanisms by which the CHIP protein may prove to be irreplaceable for long-term survival. We hypothesized that the CHIP KO proteomic profile will reveal changes critical to mitochondrial function, whereas the Parkin KO proteomic profile would reveal changes more in line with events that may only result in pathology after several decades. For instance, LDH is decreased in Parkin KO cortices, while PDH is increased, which is the opposite of findings in CHIP KO animals (Periquet et al., 2005). Moreover, a critical subunit of Krebs cycle enzyme succinate dehydrogenase is increased in Parkin KO (Periquet et al., 2005), while Krebs cycle enzymes in our CHIP KO screen are decreased. Taken together, these data underscore a compensatory role for Parkin mutated cells to increase metabolic pathways as a mechanism to deal with redox imbalance and protein oxidation. On the other hand, proteomic profiles from CHIP KO mice, wherein numerous energetics enzymes are decreased, suggest that these animals are unable to compensate. In combination with decreases in overall ATP levels in CHIP KO mice (Palubinsky et al., 2015), we suspect that these changes underlie the severe motor and behavioral phenotypes of CHIP-deficient mice.

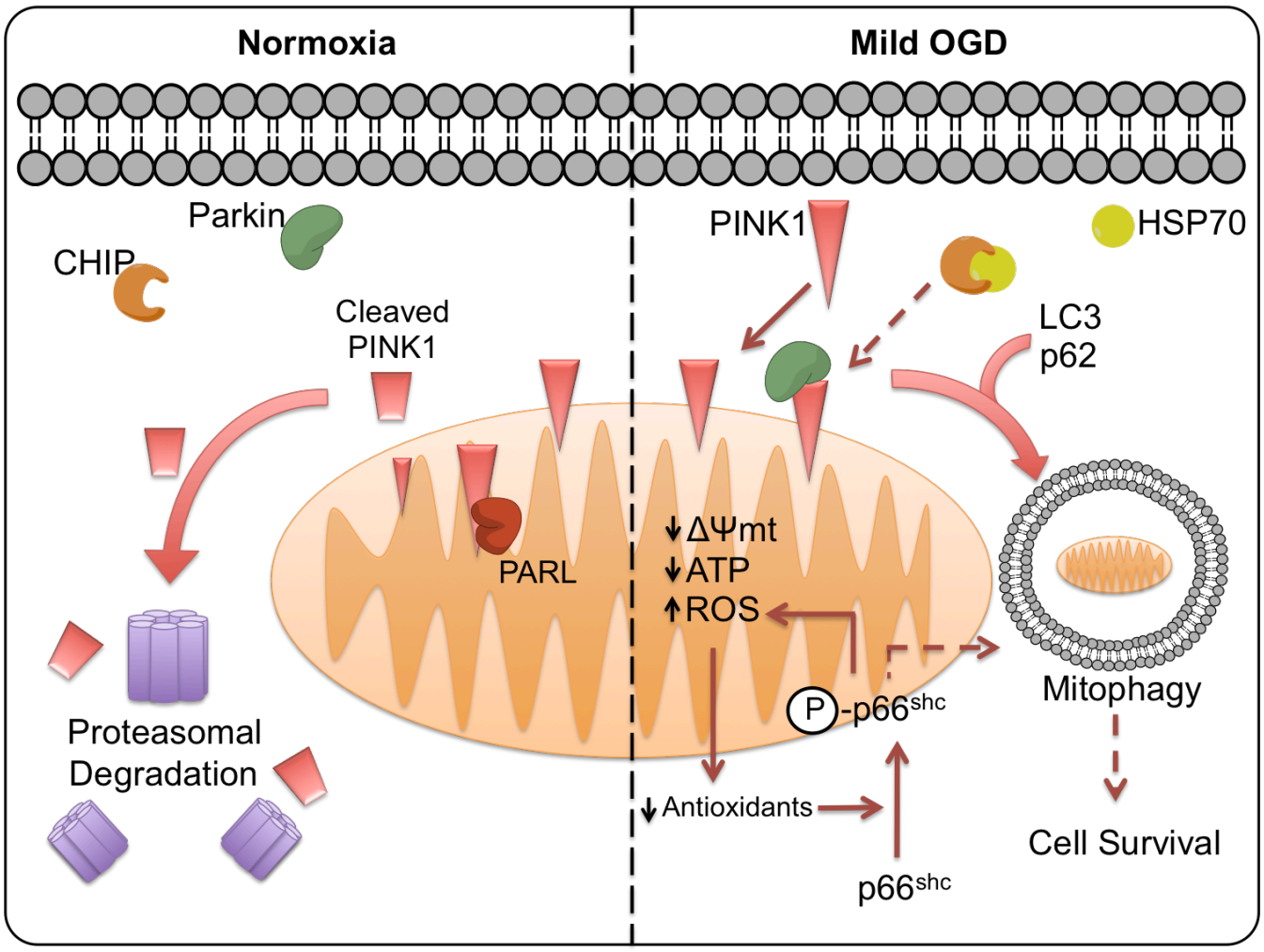

Figure 4: Model Depicting PINK1 and CHIP Interaction During Mild OGD That Contributes To Cell Survival Through Mitophagy and HSP70 Induction. During normoxia, PINK1 is targeted to mitochondria and swiftly cleaved by proteases and degraded via the proteasome. Inactive CHIP and Parkin are chiefly cytosolic. During mild OGD, PINK1 stabilizes on the outer mitochondrial membrane, recruiting Parkin through its kinase domain activity. Our hypothesis is that CHIP is also recruited to mitochondria through PINK1 activity to induce clearance of compromised mitochondria through mitophagy. Parallel processes also necessary for survival include activated p66shc and HSP70 induction, which negatively regulate the apoptotic pathway.

1.4 Rationale

CHIP, like HSP70, is inducible by ischemic stress, and loss of CHIP results in a uniquely devastating neurological phenotype. CHIP deficient animals exhibit pathology resembling early aging and degeneration, with increased aggregates of poly-ubiquinated proteins, increased oxidized proteins and lipids, and mitochondrial dysfunction. *In vitro* analyses of CHIP in primary neurons reveal that CHIP localizes to mitochondria under severe bioenergetic stress. This project aims to fill gaps in our understanding of the molecular cues and consequences of CHIP association with mitochondria during physiological and pathophysiological conditions.

1.5 Hypothesis

We hypothesize that the E3-ligase CHIP is essential for mitochondrial quality control and for determining whether neurons are preconditioned to withstand subsequent injury.

1.6 Thesis Specific Aims

To address the gaps in our understanding of CHIP function after bioenergetic stress and neuronal survival, I proposed the following specific aims:

Aim 1: Test the hypothesis that CHIP expression and localization to mitochondria are events associated with neuroprotection afforded by PC. Primary neuronal cultures, immunofluorescence imaging, subcellular fractionation, and biochemical analyses of protein expression will be used to determine the temporal and spatial localization of CHIP following non-lethal bioenergetic stress.

Aim 2: Test the hypothesis that mitophagy is associated with cell survival in preconditioned neurons. Immunofluorescence imaging and biochemical analyses of protein expression will be used to determine the temporal and spatial localization of PINK1 and autophagy-associated proteins, such as

LC3. Autophagic activity will also be manipulated during PC through pharmacological agents to assess whether mitophagy is protective to neurons following acute bioenergetic stress.

Aim 3: Test the hypothesis that alterations in CHIP expression and function promote mitochondrial dysfunction, disrupt mitophagy, and block neuroprotection. CHIP KO mouse embryonic fibroblasts (MEFs), acute siRNA-mediated knockdown of CHIP in WT primary neurons, and expression of mutant CHIP plasmids in CHIP KO primary neurons will be used to determine the critical functions of CHIP in mitophagy and neuronal survival during bioenergetic stress.

CHAPTER 2

C-TERMINUS OF HSC70-INTERACTING PROTEIN LOCALIZES TO MITOCHONDRIA AND IS NECESSARY FOR SURVIVAL FOLLOWING ACUTE BIOENERGETIC STRESS

2.1 Abstract

C-terminus of HSC70-interacting protein (CHIP, STUB1) is a ubiquitously expressed cytosolic E3-ubiquitin ligase. CHIP-deficient mice exhibit cardiovascular stress and motor dysfunction prior to premature death. This phenotype is more consistent with animal models in which master regulators of autophagy are affected rather than with the mild phenotype of classic E3-ubiquitin ligase mutants. The cellular and biochemical events that contribute to neurodegeneration and premature aging in CHIP KO models remain poorly understood. Electron and fluorescent microscopy demonstrates that CHIP deficiency is associated with greater numbers of mitochondria, but these organelles are swollen and misshapen. Acute bioenergetic stress triggers CHIP induction and re-localization to mitochondria where it plays a role in the removal of damaged organelles. This mitochondrial clearance is required for protection following low-level bioenergetic stress in neurons. CHIP expression overlaps with stabilization of the redox stress sensor PTEN-inducible kinase 1 (PINK1) and is associated with increased LC3-mediated mitophagy. Introducing human promoter-driven vectors with mutations in either the E3 ligase or TPR domains of CHIP in primary neurons derived from CHIP-null animals enhances CHIP accumulation at mitochondria. Exposure to autophagy inhibitors suggests the increase in mitochondrial CHIP is likely due to diminished clearance of these CHIP-tagged organelles. Proteomic analysis of WT and CHIP KO mouse brains from both sexes reveals proteins essential for maintaining energetic, redox and mitochondrial homeostasis undergo significant changes in expression dependent upon genotype. Together these data support the use of CHIP deficient animals as a predictive model of age-related degeneration with selective neuronal proteotoxicity and mitochondrial failure.

2.1 Introduction

The HSP70 complex is capable of blocking neurodegeneration triggered by a host of genetic mutations, physiological events and environmental stressors (Franklin et al., 2005; Gestwicki and Garza, 2012). HSP70 binding partners alter the localization, activity and expression of the chaperone complex itself and its client proteins. E3 ligases, such as Parkin and C-terminus of HSC70-Interacting Protein (CHIP), regulate HSP70-mediated protein degradation (Ballinger et al., 1999; Jiang et al., 2001). CHIP is a 303 amino acid cytosolic protein that contains an N-terminal TPR domain regulating HSP/HSC70-docking, a helix-loop-helix domain, and a C-terminal Ubox domain that is necessary for binding to E2-conjugating enzymes (Ballinger et al., 1999; Jiang et al., 2001; Xu et al., 2008). CHIP is unique among E3 ligases in that its expression is induced by acute bioenergetic stress and in post-mortem samples from patients with stroke (Stankowski et al., 2011; Lizama et al., 2017). CHIP is also unique in that it forms asymmetric homodimers, which have not been observed in other E3 ligase proteins and are only formed in higher vertebrates, suggesting it may perform distinctive roles in cell biology (Zhang et al., 2005; Ye et al., 2017).

Further evidence of the unique attributes of CHIP can be found in studies demonstrating that mice deficient in CHIP have pervasive dysfunction far more robust than would be predicted based on a primary role as a conventional E3 ligase. CHIP insufficiency results in decreased life expectancy, profound lipid oxidation, as well as poor performance on behavioral assessments of motor function and anxiety (McLaughlin et al., 2012; Palubinsky et al., 2015). Indeed, CHIP knockout (KO) animals are unable to complete even simple behavioral assessments given their moribund nature.

Mutations in CHIP have been identified in patients with an early-onset, recessive form of spinocerebellar ataxia, in which mutations in major structural domains confer loss of CHIP function (Heimdal et al., 2014; Shi et al., 2014; Synofzik et al., 2014; Bettencourt et al., 2015). Patients exhibit

unifying symptoms that include progressive deterioration in muscle coordination and tone, speech difficulty, and cerebellar atrophy. Yet, symptom heterogeneity exists among patients with CHIP mutations, which include dementia, hypogonadism, and epilepsy. Such variable observations support a role for CHIP beyond the cerebellum, where CHIP mutations can cause a multidimensional, multisystemic degenerative disease (Hayer et al., 2017).

In this work, we sought to understand the underpinnings of the devastating phenotype caused by CHIP loss by evaluating CHIP's role in cell signaling employing neuronal models of an acute pathophysiological stress. Using a combination of cellular imaging, proteomics, biochemistry, molecular targeting and ultrastructural assays, we determined that CHIP deficiency results in radical mitochondrial reorganization not seen in other E3 ligase deficient animals. These data reinforce a model in which CHIP functions are more in keeping with a role as an essential autophagy regulator than a standard E3 ligase. Taken together, our data supports the use of these animals as a powerful and robust model of neurological dysfunction induced by mitochondrial failure and secondary proteotoxicity.

2.3 Materials and Methods

Materials and Reagents

Tissue culture: Fetal bovine serum (SH30070.03) was obtained from Hyclone. Dulbecco's modified Eagle's medium (DMEM, 11995) with high glucose, minimum essential medium (MEM, 51200), Neurobasal medium, B27 supplement (17504044), N2 supplement (17502048), 0.25% Trypsin–EDTA, trypan blue stain 0.4%, and penicillin-streptomycin (15140-122) were purchased from Invitrogen. LipoJet *In Vitro* Transfection Kit (Ver. II) was purchased from SignaGen.

Western blotting: XT-MOPS running buffer, Tris-Glycine transfer buffer, Criterion Bis-Tris gels, Laemmli buffer, and precision plus protein all blue standards were purchased from Bio-Rad

Laboratories. Membrane-blocking solution was from Zymed. Hybond P polyvinylidene difluoride membranes were acquired from GE Healthcare. Gel Code Blue Stain Reagent and Western Lightning Chemiluminescence Reagent Plus were obtained from Thermo Scientific.

For Western blotting, CHIP (PC711) antibody was purchased from Calbiochem. Antibody for p62 was obtained from Cell Signaling Technology (5114). LC3 for Western blotting was obtained from MBL International (PD014), and for immunofluorescence LC3 was obtained from Abcam (ab62116). HSP70/HSP72 (SPA-811), and HSC70 antibodies (SPA-816) were purchased from Enzo Life Science, Inc. PINK1 (BC100-494) and TOM20 (H00009804-M01) antibodies were purchased from Novus Biologicals. CHIP (sc-133066) antibody for immunofluorescence was purchased from Santa Cruz Biotechnology.

Unless otherwise stated, all other chemicals were purchased from Sigma-Aldrich.

Experimental Design and Statistical Analysis

Statistical analyses were performed using GraphPad Prism version 5.03. Error bars indicate standard error of the mean (s.e.m) and statistical significance was assessed by one-way ANOVA followed by Bonferroni *post-hoc* analysis (Fig. 1C, Fig. 3A, Fig. 7A, Table 1, Table 2, Table 3), unpaired Student's t-test (Fig. 1E, Fig. 2D, Fig. 4E, Fig. 5A, Fig. 6B, Fig. 7B, Fig. 7C), Mann-Whitney analysis (Fig. 4F), or two-way ANOVA (Fig. 5B). Experimental replicates labeled as "n" were derived from at least 3 independent cell cultures or animals as indicated and are described further in each Methods section.

Maintenance of CHIP WT and KO Mouse Colony

The Institutional Animal Care and Use Committee at Vanderbilt University Medical Center

approved all animal husbandry and experiments. Parental mouse lines were previously described (Dai et al., 2003). All mice were maintained on a mixed background of C57BL/6 and 129SvEv for 8 or 9 generations. Further backcrossing exacerbates the early lethality observed in CHIP KO animals resulting in a less than 5% survival at birth. As CHIP KO male mice are sterile, heterozygous matings were used to maintain the colony. Generating CHIP KO animals from heterozygous crossings occurs at non-Mendelian rates because of preferential reabsorption and cannibalism of KO animals that are often runted. Genotyping was performed by PCR with DNA from tail clippings using primers for the CHIP allele. Primers were purchased from XXIDT and the sequences of the reverse and forward primers used are 5' TGA CAC TCC TCC AGT TCC CTG AG 3' and 5' AAT CCA CGA GGC TCC GCC TTT 3', respectively.

Rat Primary Neuronal Culture

Forebrain cultures were prepared from embryonic day 18.5 Sprague-Dawley rats as previously described (Stankowski et al., 2011). Briefly, forebrain was dissociated and the resultant cell suspension was adjusted to 750,000 cells/well in 6-well tissue culture plates containing five, 12-mm poly-L-ornithine-treated coverslips/well. Plating media was composed of 84% (v/v) Dulbecco's modified MEM, 8% (v/v) Ham's F12-nutrients, 8% (v/v) fetal bovine serum, 24 U/ml penicillin, 24 μg/ml streptomycin, and 80 μM L-glutamine.

Cultures were maintained at 37°C, 5% CO_2, and media was partially replaced every 2 – 3 days. Glial cell proliferation was inhibited after two days in culture with 2 μM cytosine arabinoside, and cells were maintained thereafter in Neurobasal media supplemented with 2% B27 and 2% NS21 until 17 days *in vitro* (Chen et al., 2008). B27 was then removed from the feeding media and cultures were maintained in Neurobasal supplemented with NS21 only. This preparation yields a 98% neuronal culture with a

mature complement of NMDA receptors (Zeiger et al., 2010). All experiments were conducted between DIV20-27.

Neuronal Bioenergetic Stress

Neurons were exposed to brief periods of bioenergetic stress by removing oxygen and glucose in order to trigger mitochondrial stress signaling. Oxygen-and-glucose deprivation (OGD) was performed as described with minor modifications (Palubinsky et al., 2015). Briefly, a complete media exchange was performed by transferring coverslips into wells containing deoxygenated, glucose-free Earle's balanced salt solution (150 mM NaCl, 2.8 mM KCl, 1 mM $CaCl_2$, and 10 mM HEPES; pH 7.3). Cultures were placed in an anaerobic chamber (Billups-Rothberg) for various durations (15–90 minutes) at 37°C. OGD was terminated by moving coverslips into 6- or 24-well plates containing MEM, 0.01% (w/v) BSA, 2.5% (v/v) HEPES, and 2x N2 (MEM/BSA/HEPES/N2). After 18–24 hours, neuronal viability was assessed visually as well as via LDH assays.

Viability Assay of Rat Primary Neurons

Cell viability was assessed using a lactate dehydrogenase (LDH)-based *in vitro* toxicity kit (Sigma), which colorimetrically determines the amount of LDH released into the culture media from dead and dying neurons.In order to account for variation in total LDH content, raw LDH values were normalized to the toxicity caused by 90-minute OGD, which, at 24 hours, results in 100% neuronal cell death in this system. Viability is also confirmed visually with corresponding brightfield images.

Preconditioning and CHIP siRNA Knockdown in Rat Primary Neurons

Primary neuronal cultures were grown for 20-25 days *in vitro* after which they were exposed to

low-level bioenergetic stress (15-minute OGD) and immediately returned to normoxia in MEM/HEPES/BSA/N2 medium. For studies of mitophagy, neurons were incubated in bafilomycin A1 (BafA; 1 nM) 30 minutes prior to, during, and after OGD. Twenty-four hours following preconditioning, neurons were exposed to 90-minute OGD and viability was determined 24 hours later using LDH assays and visual confirmation.

CHIP small interfering RNA (siRNA) was obtained from QIAGEN Science (50-CCAGCTGGAGATGGA GAGTTA-30) (Stankowski et al., 2011). Using the LipoJet Transfection Kit, CHIP siRNA (25 nM) and green-fluorescent protein (GFP; 2 μg) were added dropwise into each well of a 6-well dish containing neurons in 2 ml of growth medium. Six hours after addition of transfection reagents, cells underwent a complete medium change. CHIP siRNA transfected cells were harvested 24–72 hours post-transfection in TNEB lysis buffer (50 mM Tris-Cl, pH 7.8, 2 mM EDTA, 150 mM NaCl, 8 mM β-glycerophosphate, 100 μM sodium orthovanadate, 1% [v/v] Triton X-100, and protease inhibitor (P8340) diluted 1:1000) and extracts were prepared for Western blotting. Pilot experiments revealed optimal knockdown of CHIP expression at 24 hours (Fig. 5a), and this time point was used for all subsequent studies of acute CHIP knockdown.

Western Blotting of Primary Neuronal Lysate

For *in vitro* lysates, all cell lysis and harvesting steps took place on ice. Cells were washed twice with ice- cold 1x phosphate-buffered saline (PBS), and following the second wash, 150–400 μL of TNEB lysis buffer was added.

Approximately 100-200 μL of lysate was re-suspended in an equal volume of Laemmli buffer with β-mercaptoethanol (1:20). Protein samples were heated to 95°C for 10 minutes and stored at -20°C. Equal protein concentrations were determined by DC Protein Assay Kit II and samples were separated

on 4-12% Criterion Bis-Tris gels. Proteins were transferred to PVDF membranes and blocked in methanol for 5 minutes. Following 10 minutes of drying, the membranes were incubated overnight with antibodies detecting CHIP, HSP70, HSC70, TOM20, p62, PINK1, or LC3 in 5% non-fat dry milk in TBS-Tween (0.1%) or in Membrane Blocking Solution at 4°C. Membranes were washed three times with TBS-Tween, and incubated with horseradish peroxidase conjugated secondary antibodies for 1 hour at room temperature (RT). Following three washes in TBS-Tween, protein bands were visualized using Western Lightning© chemiluminescence plus enhanced luminol reagent. Western blots were analyzed using NIH Image (Scion ImageJ) to determine the mean relative densities of each protein band, and fold changes were calculated using untreated cultures as controls. Data represent results from at least 3 independent experiments as indicated in figure legends.

CHIP WT and KO Mouse Primary Neuronal Culture

Forebrain cultures were prepared from embryonic day 18 mice generated by heterozygous matings as described (Palubinsky et al., 2015). Briefly, mice were decapitated and the entire brain was stored individually in Hibernate E medium (HE-Pr; Brain Bits) at 4°C, while tails were processed for genotyping. Once PCR was concluded, WT and KO brains were pooled by genotype and dissection continued with cortical tissue digestion in 0.025% trypsin for 20 minutes, followed by mechanical dissociation. Resultant cell suspensions were plated at 600,000 cells/ml.

Cultures were maintained at 37°C, 5% CO_2 in growth media comprising a volume-to-volume mixture of 84% (v/v) DMEM, 8% (v/v) Ham's F12-nutrients, 8% (v/v) fetal bovine serum, 24 U/ml penicillin, 24 μg/ml streptomycin, and 80 μM L-glutamine. Before plating, 2x N2 and 2% NS21 (v/v) supplements were added to growth media. Glial proliferation was inhibited after two days in culture via the addition of 2 μM cytosine arabinoside, after which cultures were maintained in Neurobasal medium

containing 2% B27 (v/v), 2x N2, and 2% NS21 (v/v) supplements with antibiotics for two weeks. One week before experiments, neurons were maintained in Neurobasal medium containing 2% (v/v) NS21 and antibiotics only. All experiments were conducted 20–25 days following dissociation.

CHIP Plasmid Design and Transfection

Plasmids were generated by and purchased from ProNovus Bioscience, LLC. Mammalian expression vectors for hCHIP, hCHIP K30A and hCHIP H260Q are based on pcDNA3.1 (Qian et al., 2006). The human CHIP promoter sequence was used in order to induce CHIP expression by endogenous transcription factors. For detection by immunofluorescence, a mCherry expression sequence was added to the 3' end of the CHIP sequence using a 3xGGGGS linker. Sequences are summarized in Appendix A. Using the LipoJet Transfection Kit, plasmid (5 μg) was added dropwise into each well of a 6-well dish containing neurons in 2 ml of growth medium. Six hours after transfection cells underwent a complete medium change, and experiments were carried out the following day.

Immunofluorescence of Primary Neurons

Cells were fixed in 4% paraformaldehyde (PFA) and then permeabilized with 0.1% Triton X-100 as previously described (Palubinsky et al., 2015). Primary antibody was diluted in 1% BSA overnight at 4°C. Cells were washed with 1x PBS for a total of 30 minutes and incubated in Cy-2, Cy-3, or Alexa-Fluor 350 secondary antibodies (1:500) for 60 minutes at RT. Cells were counterstained with 4,6-diamidino-2-phenylindole (DAPi) to observe nuclei. Coverslips were mounted on glass slides using ProLong Gold (Fisher; P3693), and fluorescence was observed with a Zeiss Axioplan microscope at 63x or 40x, where indicated.

Cell Counting and Colocalization of Immunofluorescent Primary Neurons

Cell counts of primary neuronal cultures prepared for immunofluorescence staining of PINK1 and MAP2, and of CHIP and MAP2, were carried out using ImageJ FIJI version 2.0.0-rc-43/1.50e. Cell counts were performed by two blinded investigators. Statistical significance was determined by two-tailed unpaired *t*-test with $p<0.05$ using GraphPad Prism software.

Colocalization analysis of mouse primary neurons stained with CHIP and TOM20 were performed using Coloc2 in FIJI. Twenty to 30 fields per condition were chosen at random and measured by blinded investigators. Background was accounted for by using a Rolling-Ball Background Subtraction of 50. Neurons were outlined using the polygon drawing tool. Point Spread Function (PSF) was calculated and set to 1.0, and Costes Randomizations was set to 10.

Generation of WT and CHIP KO Mouse Embryonic Fibroblast (MEF) Cultures

Fibroblast cell lines were developed based on previous protocols (Xu, 2005). Briefly, embryonic day 13 mouse pups generated by heterozygous matings were decapitated and internal organs were removed. Tail samples were taken and all remaining epidermal tissue was minced and placed in individual conical tubes containing 2 mL of 0.25% trypsin-EDTA and digested at 4°C for 18 hours followed by 30 minutes at 37°C. Meanwhile tails were processed for genotyping (Palubinsky et al., 2015). Once PCR and digestion was concluded, WT and KO tissue was pooled, an equal volume of MEF media (84% (v/v) DMEM, 10% (v/v) fetal bovine serum, 24 U/ml penicillin, and 24 mg/ml streptomycin) was added and the tissue was mechanically dissociated using a 5 mL pipette, triturating ~20 times. Any remaining tissue was allowed to settle while the supernatant was transferred to a new tube. Five mL of MEF media was added to the tissue pellet, trituration was repeated and supernatant was collected and added to the initial cell suspension. Trituration and transfer were repeated a final time and

the entire resultant cell suspension was plated in a T75 flask and maintained at 37°C, and 5% CO_2 until cells reached 85% confluency at which point they were passaged. Immortalization was achieved via repeated passaging (roughly 25 passages). Following immortalization, all experiments were carried out using MEFs between passages 10-20.

Transmission Electron Microscopy of MEFs

WT and CHIP KO MEFs were grown to 60-80% confluency and fixed in 2.5% glutaraldehyde with 0.1 M cacodylate buffer, pH 7.4 at RT then transferred to 4°C overnight. Samples were further processed in the Vanderbilt University Medical Center Cell Imaging Shared Resource. Cells were washed, scraped, pelleted, and underwent several exchanges of fixative and dehydrating solvents. Samples were fixed in 2.5% gluteraldehyde in 0.1 M cacodylate buffer, pH 7.4 at RT for 1 hour then transferred to 4ºC overnight. The samples were washed in 0.1 M cacodylate buffer, then incubated 1 hour in 1% osmium tetraoxide at RT then washed with 0.1 M cacodylate buffer. Subsequently, the samples were dehydrated through a graded ethanol series and then three exchanges of 100% ethanol. Next, the samples were incubated for 5-minutes in 100% ethanol and propylene oxide (PO) followed by 2 exchanges of pure PO. Samples were then infiltrated with 25% Epon 812 resin and 75% PO for 30 minutes at RT. Next, they were infiltrated with Epon 812 resin and PO [1:1] for 1 hour at RT then overnight at RT. The next day, samples went through a [3:1] (resin: PO) exchange for 3-4 hours, then were incubated with pure epoxy resin overnight. Samples were then incubated in two more changes of pure epoxy resin and allowed to polymerize at 60°C for 48 hours. Thin sections (70-80 nm) were cut using an ultramicrotome and mounted onto copper grids. The sections were stained with 2% uranyl acetate and Reynold's lead citrate before imaging at 26,000x and 67,000x on an electron microscope (Philips T12 equipped with an AMT CCD camera system, FEI).

MitoTracker Labeling and Immunofluorescence of MEFs

WT and CHIP KO MEFs were grown to 60-80% confluency on glass coverslips. MitoTracker Orange staining was performed as previously described (Palubinsky et al., 2015). Briefly, MitoTracker (Fisher; M7511) was added to live cell cultures at a final concentration of 790 nM and incubated at 37°C for 45 minutes. Coverslips were washed with 1x PBS, fixed with 4% (v/v) PFA, permeabilized with 0.1% Triton X-100, washed again with 1x PBS, and then blocked with 8% (w/v) BSA diluted in 1x PBS. After 25 minutes in BSA, coverslips were incubated overnight at 4°C in primary antibody against β-tubulin diluted in 1% (w/v) BSA. Following primary antibody incubation, cells were washed with 1x PBS for a total of 30 minutes and incubated in Alexa 350 secondary antibody in 1% BSA for one hour. Cells were next washed for a total of 30 minutes in 1x PBS and coverslips were mounted using Prolong Gold.

Using ImageJ FIJI, a total of 120 WT MEF cells and 169 CHIP KO MEF cells from two individual cultures were analyzed. Images were thresholded using an adaptive algorithm and particles were analyzed for total count, area, and perimeter. Area and perimeter values were then used to calculate mitochondrial circularity ($circularity = 4\pi(area/perimeter^2)$), where values closer to 0 are less circular (i.e. ellipses, crescents, and complex tubular structures) and values close to 1 are perfectly circular.

Proteomic Analysis of WT and CHIP KO Brains

Tissue Preparation and Precipitation

Whole brains from postnatal day 35 WT mice (4 male, 4 female) and CHIP KO mice (4 male, 4 female) were removed and immediately placed into a glass dounce containing 1 ml of ice-cold TNEB lysis buffer. Brains were homogenized on ice (35 strokes), sonicated at 6 watts for 10 seconds and passed through a 40 micron cell strainer then through a 0.2 micron filter affixed to a 10 ml syringe.

Protein assays were completed and all samples were adjusted to 2 mg in 1mL of TNEB. Samples were precipitated by adding 3 mL of ice-cold ethanol, vortexing and incubating on ice for 3 minutes. Following incubation, samples were spun at 3000 *x rpm* (1819 *g*) for 10 minutes at 4°C. Upon removal of the supernatant, pellets were incubated in a 2:1 mixture of chloroform and ice-cold methanol for 3 minutes and centrifuged at 3000 *x rpm* (1819 *g*) for 10 minutes. Following the spin, pellets were washed 3 times in 1 ml of ice-cold methanol. After the third wash, pellets were re-suspended in 1 ml of 0.5% SDS and sonicated at 6 watts for 10 pulses. Following sonication, 10 µl of sample was added to 8 µl of 4X sample buffer and 2 µl of 1 M DTT. This portion of the sample was heat denatured at 95°C for 10 minutes while the rest of the sample was used for protein assay.

Peptide Preparation

Peptides were prepared as previously described (Ham, 2005). Briefly, equal protein amounts of each sample were loaded onto a 10% Bis-Tris gel with empty lanes in between samples and separated at 180V for 30 minutes. Simply Blue Safe Stain was used to visualize all protein bands and allow for each sample to be cut horizontally into ~13 fractions. Each horizontal fraction was then cut vertically into ~1 mm cubes and placed in a microcentrifuge tube. One hundred µl of 100 mM ammonium bicarbonate (AmBic) was added to each fraction tube.

Samples were reduced with 5 mM DTT in AmBic for 30 minutes at 60°C with shaking. Samples were then alkylated with 10 mM iodoacetamide in AmBic for 20 minutes in the dark at RT. Any remaining Safe Stain dye was removed with additional 100 µl washes in 50 mM AmBic /acetonitrile (1:1, v/v). Once clear of all dye, gel pieces were dehydrated in 100% acetonitrile. Next, samples were rehydrated in 200 µl of 25 mM AmBic containing 300 ng of trypsin gold (Promega) and incubated at 37^{o}C overnight. Following trypsinization, peptides were extracted from the gel via 3, 20 minute washed

in 200 µl of 60% aqueous acetonitrile containing 1% formic acid and evaporated to dryness *in vacuo*. Lastly, peptides were re-suspended in 30% aqueous acetonitrile containing 0.1% formic acid and stored at -80^{o}C (Ham, 2005).

Mass Spectrometry

Protein digests were lyophilized and re-suspended in water prior to solid phase extraction with a Waters Oasis HLB cartridge. Prior to use, cartridges were activated with 1 ml of acetonitrile and equilibrated with 2 ml of water. Peptides were loaded, washed once with 1 ml water, and eluted with 70% acetonitrile containing 0.1% formic acid. Peptides were evaporated to dryness *in vacuo,* re-suspended in 10 mM triethylammonium bicarbonate (pH 8.0) and fractionated by bRPLC on an Agilent 1260 Infinity LC system equipped with an XBridge C18 5 µm 4.6 x 250 mm column. Solvent A was aqueous 10 mM triethylammonium bicarbonate at pH 7.4 and solvent B was 10 mM triethylammonium bicarbonate in acetonitrile at a flow rate of 0.5 mL/minute.

Peptides were further fractionated by a gradient in which solvent B was increased from 0% to 5% from 0 to 10 min, 5% to 35% from 10 to 70 min, 35% to 70% from 70 to 85 min, held at 70% from 85 to 95 min, and reduced to 0% from 95 to 105 min. The eluted peptides were collected in 64 fractions, which were concatenated to fifteen fractions as described (Wang et al., 2011c). Concatenated fractions were evaporated to dryness *in vacuo* and dried samples were re-suspended in 100 uL of 3% acetonitrile with 0.1% formic acid for LC-MS/MS analysis.

LC-MS/MS analyses were performed on a Q Exactive Plus mass spectrometer (Thermo Fisher Scientific, Bremen, Germany) equipped with a Proxeon nLC1000 LC (ThermoFisher Scientific) and a Nanoflex source (ThermoFisher Scientific). Peptides were resolved on an 11 cm long column with a 75 um internal diameter (New Objective, Woburn, MA, PF360–75-10-N-5) packed with 3 µm particle size

and 120 Å pore size ReproSil-Pur C18-AQ resin (Dr. Maisch GmbH, Ammerbuch-Entringen, Germany) over a 70 minute gradient at a 300nL/min flow rate. The gradient was formed utilizing 0.1% formic acid in water (solvent A) and 0.1% formic acid in acetonitrile (solvent B) whereby the percentage of B was varied as follows: 2% to 5% in 5 min, 5% to 35% over 55 min, 35% to 90% in 3 min, followed by 90% for 7 min.

A single MS1 scan from m/z 300–1800 at 70,000 resolution with an automatic gain control (AGC) value of 3e6 and max injection time of 64 msec was recorded as profile data. A top-12 method was used, whereby the 12 most intense precursors were automatically chosen for MS2 analysis and a dynamic exclusion window of 20 s was employed. For each MS2 scan, a resolution of 17,500, an AGC value of 2e5, a max injection time of 100 msec, a 2.0 m/z isolation window, and a normalized collision energy of 27 was used and centroid data were recorded.

Thermo .raw datafiles from LC-MS/MS runs were converted to mzml format using Proteowizard version 3.0.5211 (Kessner et al., 2008). The mzml files were searched using MyriMatch version 2.1.132 (Tabb et al., 2007) and MS-GF+ version 9517 (Kim and Pevzner, 2014) against the mouse Refseq database (October 16, 2014). A semi- tryptic search was employed with a maximum of four missed cleavages allowed. A fixed carbimidomethyl modification on Cys, a variable oxidation on Met, and a pyro-glu on Gln were allowed with a maximum of 2 dynamic modifications per peptide. Precursor ions were required to be within 15 ppm of expected values and fragment ions within 20 ppm. A target-decoy search was employed using a reverse sequence database to allow calculation of FDR for peptide-spectral matches. The final protein list was assembled following the rule of parsimony in IDPicker 3 version 3.1.643.0 (Ma et al., 2009) at a protein FDR of <1%. This protein list was then analyzed for spectra which were found to be 2 fold or greater different between WT and KO CHIP mice.

2.4 Results

Low-level Bioenergetic Stress Induces CHIP Expression

In neuron enriched cultures, bioenergetic stress induced by 15 minutes of OGD initiates a robust defensive program with sufficient magnitude to significantly decrease the cell death associated with a subsequent exposure to a normally lethal 90-minute period of OGD (Figure 5A). Consistent with prior reports, both bright-field photomicrographs of live cells (Figure 5B) and LDH release assays (Figure 5C) reveal that low-level bioenergetic stress protects approximately 45% of neurons from subsequent injury (McLaughlin et al., 2003; Brown et al., 2010; Zeiger et al., 2010). Importantly, this stressor does not result in neuronal cell death, as evident by phase-bright somas and intricate processes that are indistinguishable from control cells (Figure 5B). To examine the temporal and spatial time-course of CHIP expression in cells primed with by low-level bioenergetic event, we harvested neurons at various time points following 15 minutes of OGD. CHIP expression begins to increase within 1 hour (1.8-fold ±0.4 above control, Table 1), peaks 6 hours after stress (2.8-fold ±0.8 above control), and remains elevated at 24 hours (1.7-fold ±0.3 above control; Figure 5D). Notably, increases in HSP70 expression lag behind CHIP, peaking between 6 and 18 hours (2.5-fold ±0.2 above control, $p=0.01$) and returning to baseline levels at 24 hours (0.9-fold of control ±0.4; Figure 5D).

To determine the percentage of neurons that express CHIP in response to bioenergetic stress, we stained neurons 24 hours following 15-minute OGD. While we observed an increase in total CHIP expression via Western blot, by ICC we observed that CHIP is expressed in 49% of mildly stressed neurons, which was not significantly different from control cultures (Figure 5E). Given that CHIP expression undergoes temporal and spatial changes in response to stress (Figure 5C; (Stankowski et al., 2011; Palubinsky et al., 2015), we suspect that using this method failed to capture the dynamic turnover and subcellular localization of CHIP at a static timepoint of 24 hours post-OGD.

In previous work, mitochondria isolated from CHIP KO animals exhibit dysfunction in response to calcium challenge, suggesting CHIP is important for mitochondrial homeostasis during stress (Palubinsky et al., 2015). To test this hypothesis, we used the mitochondrial import receptor, TOM20 to label mitochondria and co-stained for CHIP in cells exposed to bioenergetic stress. We observed increased overlap of CHIP with TOM20-positive mitochondria as early as 3 hours after acute stress (data not shown) that was maximal at 6 hours (Figure 5F, overlap of CHIP and TOM20 in white). Taken together, these data demonstrate that CHIP localizes to mitochondria during the period in which neurons are upregulating endogenous protective pathways and HSP70. We next sought to determine how mitochondrial quality control signaling is impacted by low-level bioenergetic stressors.

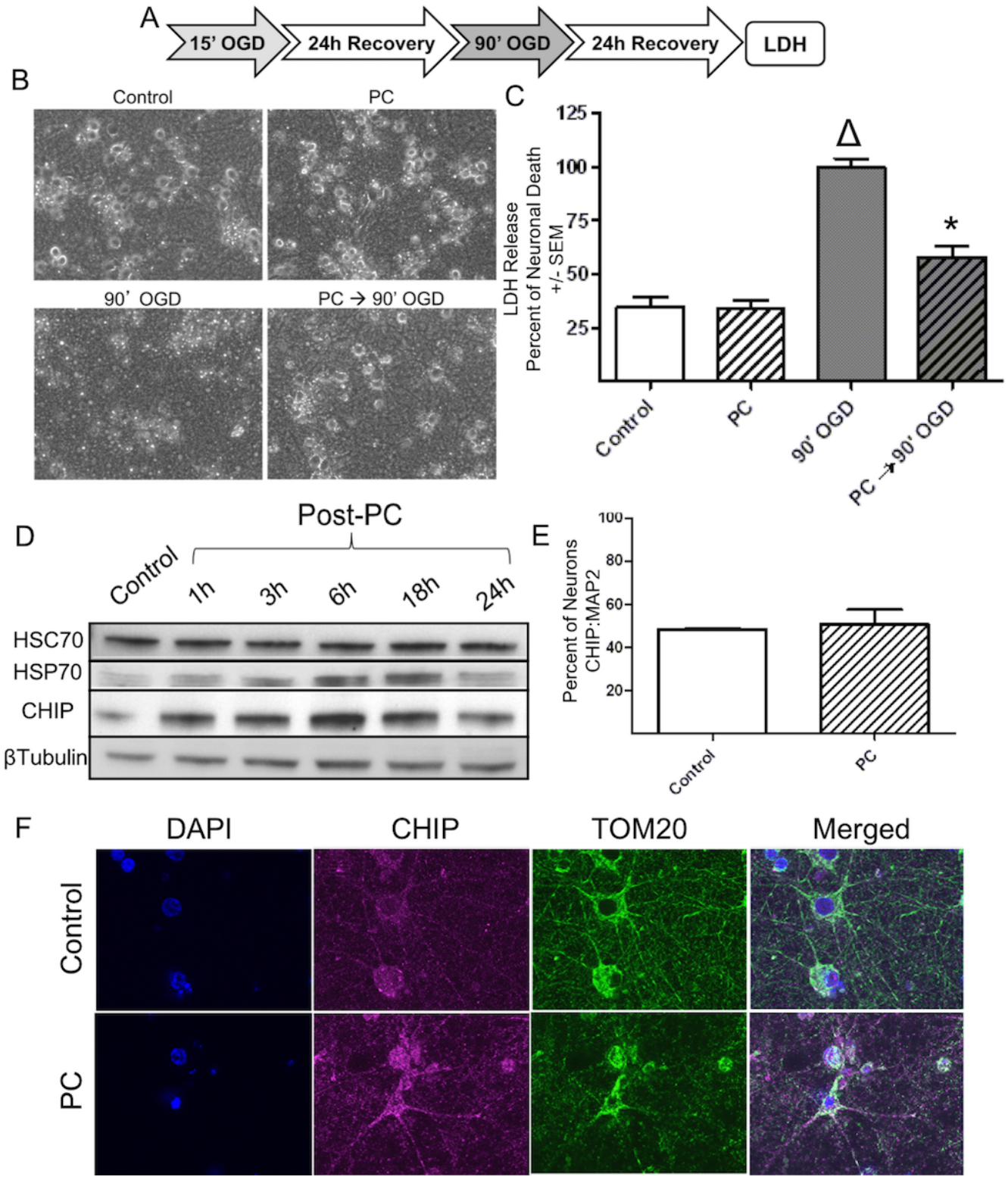

Figure 5: Low-Level Bioenergetic Stress Induces CHIP Expression. (A) Primary rat forebrain cultures were exposed to 15' OGD. Twenty-four hours later, neurons were exposed to 90' OGD, following

which cells were returned to growth media. Cell survival was assessed via LDH 24h later. (B) Representative photomicrographs taken 24h after 15' OGD (PC) reveal many phase-bright neuronal somas and intact processes that are indistinguishable from Control. Twenty-four hours after 90' OGD, there were no phase-bright neurons, indicative of total neuronal death. Cultures that were preconditioned (PC→90'OGD) contained more phase-bright neurons and intact processes compared to 90' OGD. (C) LDH release was measured, and values were normalized to 90' OGD (100% cell death) in naive cells. Data represent the mean from four independent experiments analyzed by one-way ANOVA with Bonferroni post-hoc testing. Δ Denotes statistical significance ($p<0.05$), comparing 90' OGD to control cultures. * Denotes statistical significance comparing PC→90' and all other groups ($p<0.05$). (D) Neurons exposed to 15' OGD were harvested 1, 3, 6, 18, or 24h later. Whole cell lysates were probed with antibodies against HSP70 and CHIP, as well as HSC70 and β-Tubulin as loading controls. Quantification is summarized in Table 1. (E) Twenty-four hours after PC, cultures were probed with antibodies to CHIP, MAP2, and DAPI. Cell counts were performed by blinded investigators. Basal CHIP expression is observed in 49% of MAP2-positive neurons and is not significant from control post-PC (n=3, unpaired *t*-test $p>0.05$). (F) Preconditioned neurons were PFA-fixed after 6h of recovery and probed for CHIP (magenta), TOM20 (green), and DAPI (blue).

Fold Change Normalized to Control						
	N	1h	3h	6h	18h	24h
HSC70	4	0.9 ± 0.1	0.9 ± 0.2	1.3 ± 0.5	1.0 ± 0.3	1.1 ± 0.4
HSP70	4	1.4 ± 0.4	2.1 ± 0.3	**2.5 ± 0.2**	1.0 ± 0.7	1.3 ± 0.3
CHIP	4	1.8 ± 0.4	2.2 ± 0.4	2.8 ± 0.8	2.5 ± 0.8	1.7 ± 0.3
β-Tubulin	4	1.2 ± 0.1	1.3 ± 0.1	1.2 ± 0.2	1.2 ± 0.2	1.2 ± 0.1

Table 1: Quantification of CHIP and HSP70 After Mild Bioenergetic Stress. Neurons exposed to 15' OGD were harvested 1, 3, 6, 18, or 24h later. Whole cell lysates were probed with antibodies against HSP70 and CHIP, with HSC70 and β-Tubulin as loading controls (Figure 5D). Bands were quantified

by ImageJ FIJI densitometry analysis. Values summarized in the table are the average band intensity relative to Control ± the standard error of the mean (s.e.m). Significance was determined using one-way ANOVA with Bonferonni post-hoc analysis. Increased HSP70 expression following mild bioenergetic stress was statistically significant at 6h post-OGD ($p=0.01$). CHIP increases early following OGD and remains increased above control levels, although the differences were not statistically significant.

Low-level Bioenergetic Stress Changes Mitochondrial Morphology and Increases Expression of the Mitophagy Related Protein PINK1

Mitochondria are dynamic organelles that undergo continuous fission and fusion events, as well as mitophagy. All of these processes are induced by various cell stressors, including mild hypoxic stress (Archer, 2013). To determine the morphology of mitochondria during low-level bioenergetic stress, rat primary neurons were exposed to 15 minutes of OGD then visualized with TOM20 immunostaining 24 hours later.

We found that although control and mildly stressed neurons exhibit healthy, structurally similar processes and nuclei based on MAP2 and DAPi fluorescence, mitochondrial localization is profoundly impacted by bioenergetics (Figure 6A). Mitochondria are typically well dispersed within the soma and along processes. However, low-level stress increased the number of fragmented mitochondria along neuronal processes as well as clustering of mitochondria within the soma.

During cell stress, mitochondrial membrane potential is compromised, allowing retention and accumulation of PINK1 on the outer mitochondrial membrane (Greene et al., 2012; Jin and Youle, 2013). The kinase activity of PINK1 recruits E3 ligases, such as Parkin, as well as the autophagy protein LC3, which seeds formation of an autophagosome around the mitochondrion (Kawajiri et al., 2010; Klionsky et al., 2016).

We hypothesized that stabilization of PINK1 and mitochondrial clearance may participate in neuroprotection by priming neurons for a secondary stress. To test this hypothesis, whole cell lysate was collected 3, 6, and 24 hours following bioenergetic stress and full-length, stabilized PINK1 was found to rapidly increase and remain elevated for 24 hours (3.3-fold ±2.1 above control; Figure 6B, Table 2).

To further elucidate the extent of bioenergetically-induced PINK1 stabilization in neurons, we stained for PINK1 24 hours following 15 minutes of OGD and found a significant increase in the total number of PINK1 positive cells compared to untreated cultures (28% increase; n=3, p=0.01) (Figure 6C & D). The number of MAP2-positive neurons does not change after PC, consistent with previous data (Figure 5); however, we observe that the underlying neuropil undergoes remodeling that is made apparent using immunofluorescence techniques (Figure 6C). Given that PINK1 is a rapid sensor of mitochondrial dysfunction, this data is consistent with our prior observation that 15 minutes of OGD, while a mild bioenergetic stress resulting in no neuronal cell death (Figure 5B, 1C), does cause substantive energetic and oxidative stress (Stankowski et al., 2011).

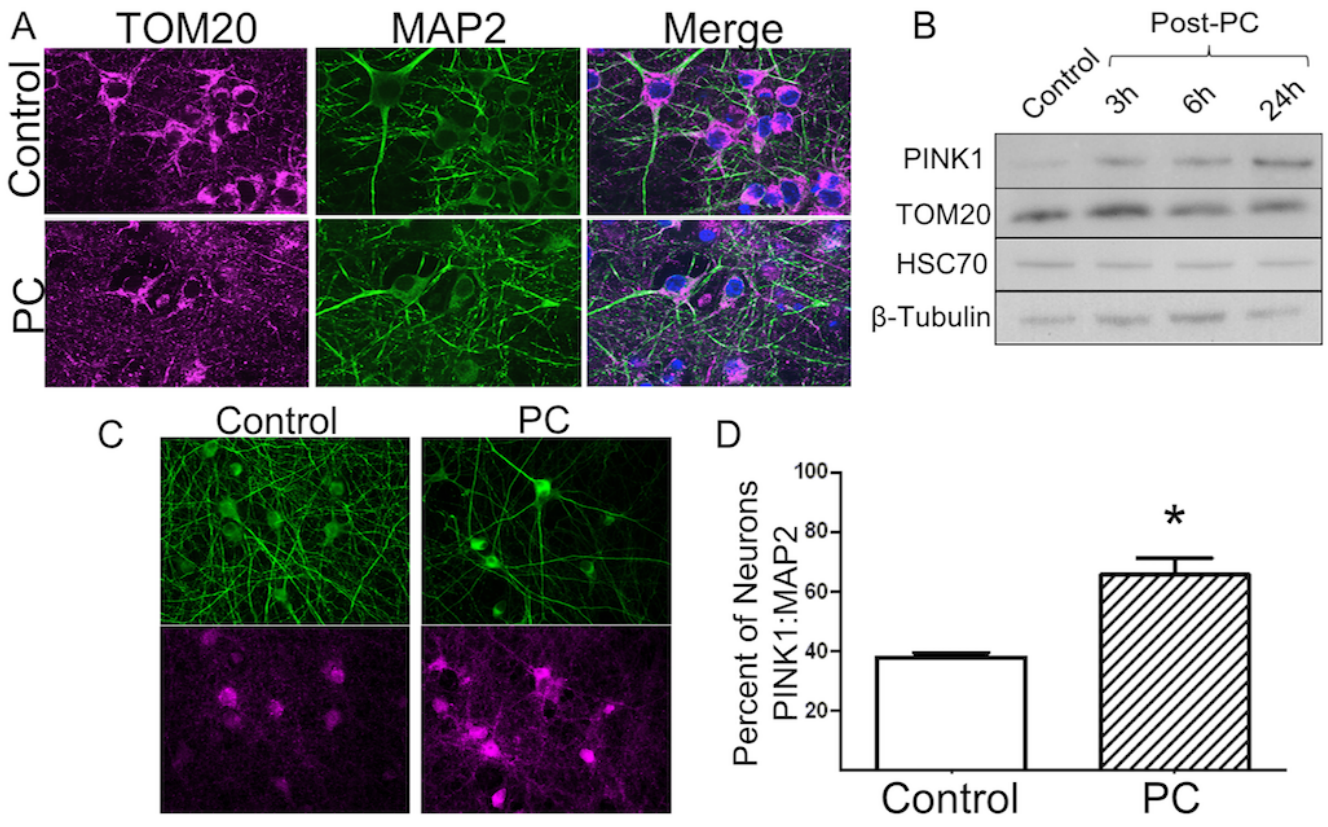

Figure 6 Low-Level Bioenergetic Stress Results in Changes in Mitochondrial Morphology and Increased Expression of the Mitophagy Related Protein PINK1. (A) Rat primary forebrain neurons were exposed to 15' OGD (PC), probed with antibodies recognizing TOM20 (magenta) and MAP2 (green), and were counterstained with nuclei marker DAPI (blue). PC was associated with fragmented mitochondria (magenta) while neuronal processes (green) remained intact, consistent with the preservation of cell viability. (B) Mitochondrial stress was assessed by evaluating stabilized PINK1 3, 6, or 24 hours after PC. Whole cell lysates were probed with antibodies against PINK1 and the mitochondrial outer membrane protein TOM20, as well as HSC70 and β-Tubulin as loading controls. Quantification is summarized in Table 2. (C) Using immunofluorescence, PINK1 (magenta) and MAP2 (green) staining revealed high levels of somatic PINK1 staining around nuclei (blue) of preconditioned cells, consistent

with the overall elevation in PINK1 signal in panel (B). (D) Cell counts of PINK1 positive neurons were performed by blinded investigators. PINK1 can be observed in 38% of MAP2-positive neurons at baseline. After PC, the number of neurons expressing stabilized PINK1 significantly increases to 68% of neurons (n=3, p=0.01; unpaired t-test).

Fold Change Normalized to Control				
	N	3h	6h	24h
PINK1	3	2.5 ± 1.0	2.6 ± 0.9	3.3 ± 2.1
TOM20	4	1.3 ± 0.1	1.3 ± 0.2	1.2 ± 0.2
HSC70	4	0.9 ± 0.2	1.3 ± 0.5	1.1 ± 0.4
β-Tubulin	4	1.3 ± 0.1	1.2 ± 0.2	1.2 ± 0.1

Table 2 Quantification of PINK1 and TOM20 after Mild Bioenergetic Stress. Neurons exposed to 15' OGD were harvested 3, 6, or 24h later. Whole cell lysates were probed with antibodies against PINK1, TOM20, with HSC70 and β-Tubulin as loading controls (Figure 6B). Bands were quantified by ImageJ FIJI densitometry analysis. Values summarized in the table are the average band intensity relative to Control ± the standard error of the mean (s.e.m). Significance was determined using one-way ANOVA with Bonferonni post-hoc analysis. PINK1 expression increases by 3h following OGD and remains increased above control levels, although the differences were not statistically significant.

Autophagic Signaling Is Required for Achieving a Protective Response

Some E3 ligases, such as Parkin, play critical roles in promoting mitophagy in response to stress, but likely not in the normal clearance of these organelles (Kubli et al., 2013). We therefore sought to determine the role of CHIP in both pathophysiological and physiological mitophagy in neurons.

To determine the contribution of mitophagy, we used the autophagy inhibitor, bafilomycin A1 (BafA) to prevent lysosome acidification during our mild bioenergetic stress (Klionsky et al., 2016). The

next day, we treated rat primary neurons with 90 minutes of OGD, which is typically lethal, and assessed cell death 24 hours later. Neurons treated with 1 nM BafA during the priming event exhibited increased cell death following secondary stress compared to those that only received the initial, mild bioenergetic priming stress ($n=4$, $p<0.05$; Figure 7A).

By measuring CHIP and HSP70 expression in this paradigm, we determined both proteins were highly expressed in primed neurons in the presence of BafA, with CHIP expression significantly increased by 24h (1.4-fold ±0.1 above control, $p=0.01$; Figure 7B, Table 3). PINK1, while increased after OGD in the presence or absence of BafA, was not statistically different. To determine autophagic flux, we quantified Western blot band intensities of LC3-I and LC3-II (Klionsky et al., 2016) and observed that LC3-II accumulated in cultures preconditioned with BafA co-treatment, revealing impeded autophagic flux (LC3-II:LC3-I is 2.1-fold ±0.3 above control, $p=0.03$; Figure 7B, Table 3). We also observed dramatically increased accumulation of LC3- and CHIP-positive autophagosomes in neurons following low-level OGD (Figure 7C: Middle). This effect was further augmented with BafA treatment (Figure 7C: Right). Taken together these data suggest that CHIP localization to mitochondria coincides with mitophagy and that mitophagy is a critical component of the neuroprotection afforded by preconditioning.

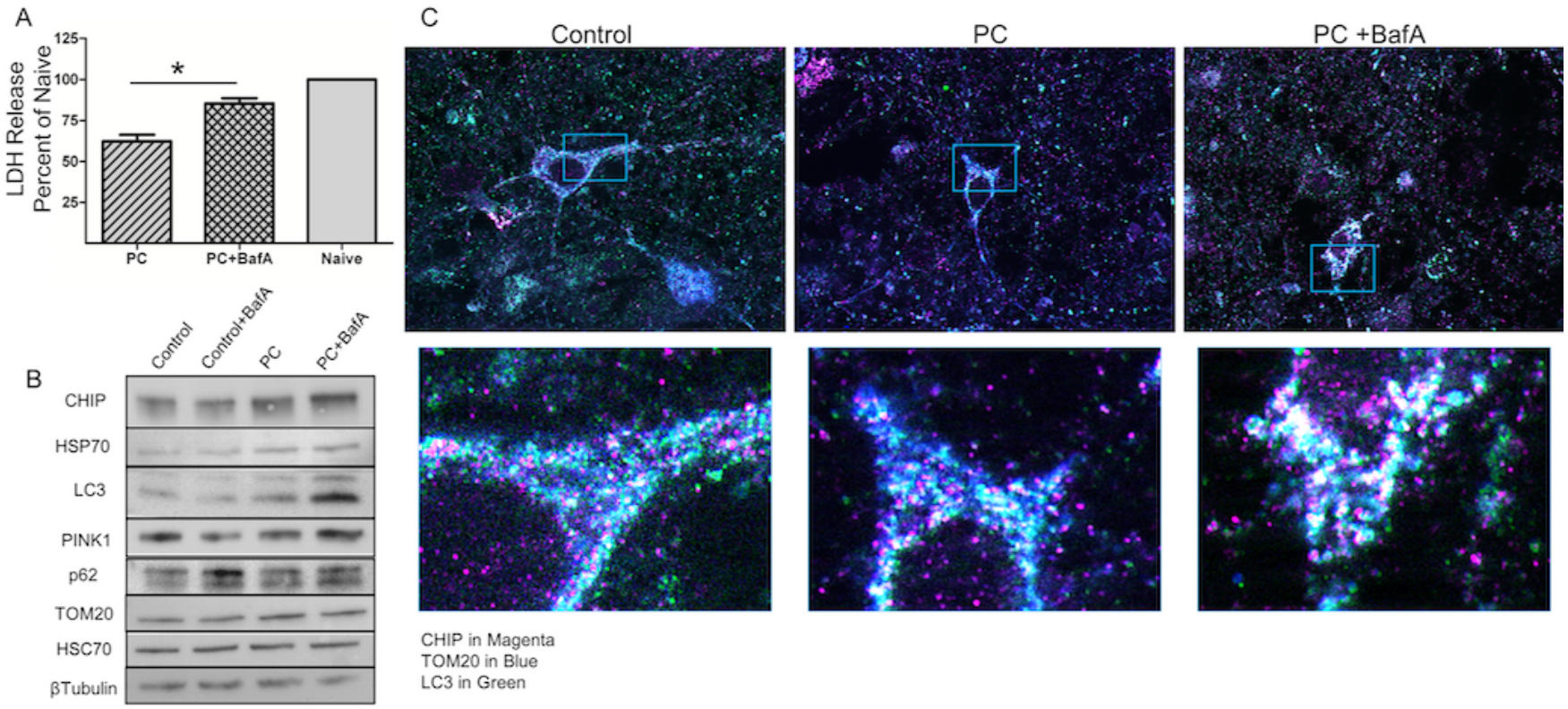
A
LDH Release
Percent of Naive
125
100
75
50
25
*
PC
PC+BafA
Naive
B
Control
Control+BafA
PC
PC+BafA
CHIP
HSP70
LC3
PINK1
p62
TOM20
HSC70
βTubulin
C
Control
PC
PC +BafA
CHIP in Magenta
TOM20 in Blue
LC3 in Green

Figure 7 Autophagic Signaling Is Required for Achieving a Protective Response. Neurons were exposed to 15' OGD in the presence or absence of the Bafilomycin A1 (BafA, 1 nM), a drug that blocks vacuolar ATPases, inhibiting fusion between autophagosomes and lysosomes. (A) Survival was assessed by LDH release 24h after subsequent 90' OGD as described in Figure 5A. Blocking autophagy resulted in 85% cell death, a significant increase compared to PC neurons without BafA. Values were normalized to 90' OGD. Data represent the mean from 4 independent experiments. *denotes significance compared to preconditioned cells ($p<0.05$). (B) Control neurons, neurons treated with BafA, preconditioned neurons (PC) and neurons preconditioned plus BafA (PC+BafA) were harvested for Western blotting 24 hours after treatment. Whole cell lysate was probed for CHIP, HSP70, LC3, PINK1, p62, TOM70, HSC70, and β-Tubulin. Accumulation of LC3-II and CHIP was evident in PC+BafA. Quantification is summarized in Table 1. (C) Preconditioned neurons were fixed 6h after PC in the presence or absence of BafA, and CHIP localization was evaluated by immunofluorescence (magenta). Autophagosomes were labeled with LC3 (green), and mitochondria labeled with TOM20 (blue). Images were taken at 63x; teal boxes were magnified to show regions of LC3 staining around CHIP-positive mitochondria. Overlap of the three labels results in white.

Fold Change Normalized to Control				
	N	Con +BafA	OGD	OGD +BafA
HSC70	4	1.0 ± 0.1	1.1 ± 0.1	1.2 ± 0.1
HSP70	4	1.1 ± 0.3	1.7 ± 0.3	1.4 ± 0.1
CHIP	3	1.0 ± 0.1	1.2 ± 0.0	**1.4 ± 0.1**
PINK1	4	0.8 ± 0.2	1.8 ± 0.6	1.9 ± 0.6
TOM20	3	2.1 ± 0.8	1.8 ± 0.4	2.8 ± 1.7
p62	3	1.5 ± 0.1	1.2 ± 0.4	2.0 ± 0.9
LC3-I	4	0.8 ± 0.2	1.0 ± 0.3	1.3 ± 0.6
LC3-II	4	0.9 ± 0.2	1.4 ± 0.4	2.3 ± 0.9
LC3-II:LC3-I	4	1.0 ± 0.1	1.5 ± 0.4	**2.1 ± 0.3**
β-Tubulin	4	1.1 ± 0.1	1.4 ± 0.1	1.3 ± 0.3

Table 3 Quantification of Proteins Following Autophagy Inhibition During Mild Bioenergetic Stress. Control neurons and neurons exposed to bafilomycin A (BafA, 1 nM), 15' OGD, or 15' OGD +BafA were harvested 24h post-treatment. Whole cell lysates were probed with antibodies against HSP70, CHIP, PINK1, TOM20, p62, and LC3, with HSC70 and β-Tubulin as loading controls (Figure 7B). Bands were quantified using ImageJ FIJI using densitometry analysis. Values summarized in the table are the average band intensity relative to Control ± the standard error of the mean (s.e.m). Significance was determined using one-way ANOVA with Bonferonni post-hoc analysis. While HSP70, PINK1, TOM20, and p62 expression increase following OGD and BafA treatment, they are not found to be statistically significant. The ratio of LC3-II to LC3-I increases following mild bioenergetic stress and was statistically different when co-treated with BafA ($p=0.01$). CHIP expression also increases after OGD with BafA co-treatment ($p=0.01$).

CHIP Deficiency Increases Mitochondrial Number and Changes Mitochondrial Morphology

Given the increased CHIP localization to mitochondria during mild bioenergetic stress, we sought to determine if CHIP also played a role in mitochondrial homeostasis during physiological

conditions. Mouse embryonic fibroblasts (MEFs) provide higher resolution imaging of mitochondrial morphology than neurons, as MEFs are large, flat, and non-polarized. We hypothesize that changes in mitochondrial morphology caused by CHIP loss is pervasive and will manifest even in mitotic, peripheral cell types.

WT and CHIP KO MEFs were prepared for transmission electron microscopy (tEM) after 15-20 passages under normal growth conditions where both cell lines underwent mitosis after ~30 hours. tEM imaging of WT MEFs reveal large, round mitochondria with intact membranes and many thin cristae (Figure 8A-C). These cells contain large lysosomes and the endoplasmic reticuli appear tubular throughout the slice. CHIP KO MEFs were appreciably different from WT cells in that the majority of mitochondria had thick, swollen cristae and smaller matrices (Figure 8D-F) consistent with mitochondrial stress and swelling even though the cells proliferated normally. KO MEFs also contained fewer lysosomes and irregularly-shaped endoplasmic reticuli.

To quantify the extent of mitochondrial morphological changes, we performed MitoTracker Orange staining in WT and CHIP KO MEFs and prepared them for ICC with β-tubulin co-stain. Using ImageJ FIJI, we quantified mitochondrial number, area, and perimeter. Area and perimeter values were then used to calculate mitochondrial circularity, where values closer to 0 are less circular (i.e. more tubular) and values close to 1 are perfectly circular.

CHIP KO MEFs contained significantly greater numbers of mitochondria than WT (Figure 8G, $p<0.0001$). Given the large amount of variability in CHIP KO mitochondrial number, we hypothesize that during the division phases of mitosis, CHIP KO fibroblasts undergo bioenergetic, mitophaghic and proteostatic pressures which result in highly variable mitochondria not observed in normal fibroblasts. These data are consistent with previous reports that mitochondrial mass is largely affected by proliferation and increased oxidative stress (Lee et al., 2002).

We observed that relative frequency distributions for mitochondrial circularity are skewed in CHIP KO MEFs, with higher frequencies for more elongated mitochondria (circularity <0.3) than in WT (Figure 8H). This finding of increased non-circular mitochondria in KO cells seems to contrast our tEM results, in which mitochondria appear smaller and lack complex structure. However, EM analysis is dependent on 2D transverse sectioning of cells, which does not capture the complex structure of mitochondrial branching or length.

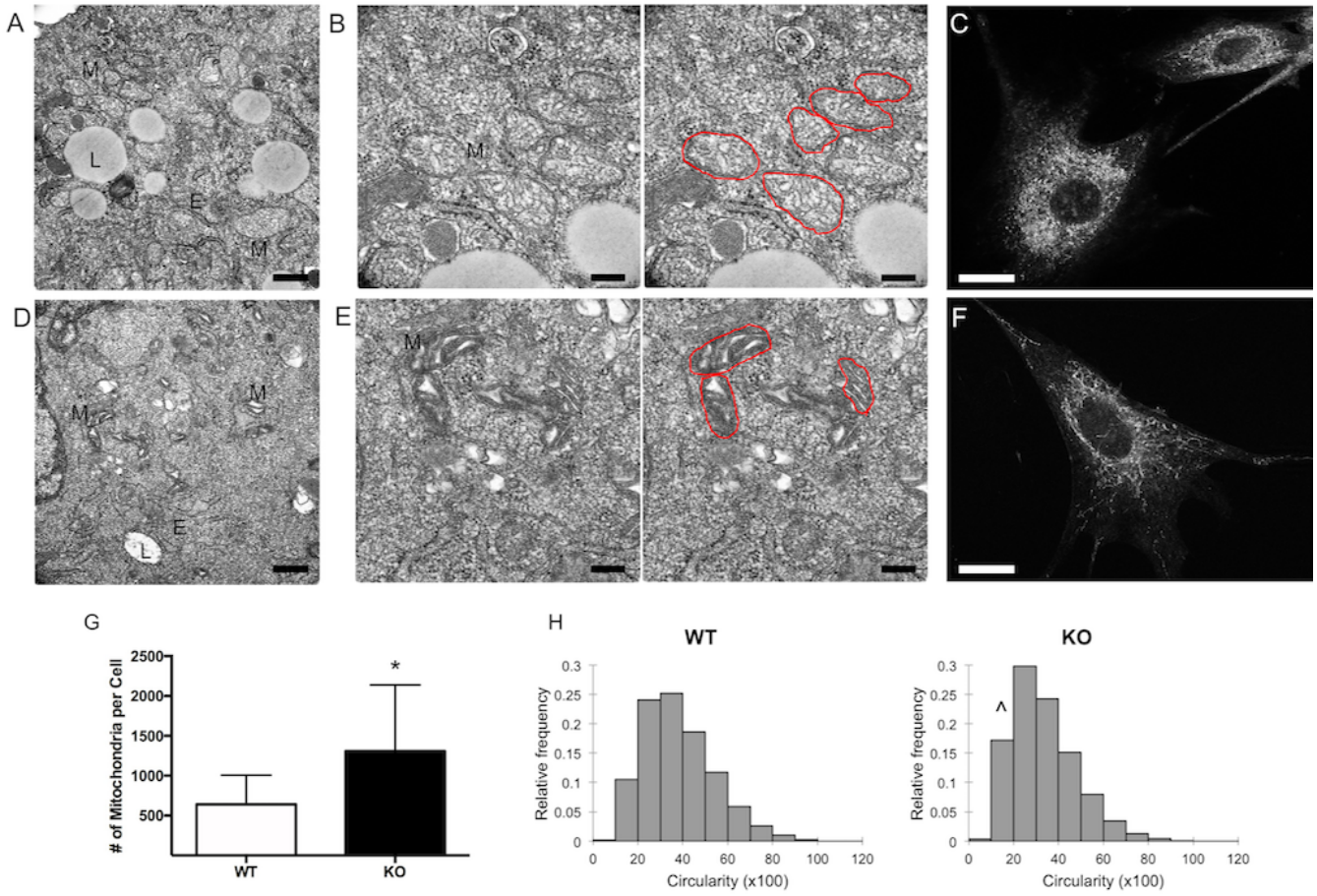

Figure 8: CHIP Deficiency Results in Significantly Increased Mitochondrial Number with Abnormal Morphological Features. Immortalized MEFs were cultured from WT and CHIP KO mice. (A,B,D,E) MEFs were grown to 60-70% confluency and fixed for tEM. Sections (70-80 nm) were imaged at 26000x (A, D; Scale bar, 500 nm) and 67000x (B, E; Scale bar, 200 nm). (A, B) WT MEFs have well-

defined mitochondrial membranes and thin inner membranes forming cristae. (D, E) KO MEFs have smaller mitochondria containing unstructured cristae and thick inner membranes. (Endoplasmic Reticulum, E; Lysosome, L; Mitochondria, M). (C, F) MEFs were stained with MitoTracker Orange and PFA-fixed. Images used for measuring mitochondrial Count, Area, and Perimeter were taken using a Zeiss Apotome (63x) and analyzed via ImageJ. Scale bar, 20 μm. (G) KO MEFs exhibit significant increases in MitoTracker Orange-positive mitochondria per cell compared to WT ($p<0.0001$, *denotes significance). (H) Circularity was calculated using Area and Perimeter measurements where values closer to 0 indicate elongated or tubular mitochondria, and a value of 1 indicates a perfect circle. Values were multiplied by 100 in order to generate histograms. KO MEFs exhibit significantly increased numbers of elongated mitochondria ($p<0.0001$, ^ denotes a shift in relative frequency compared to WT). Graphs represent data from duplicate coverslips per genotype from two independent cultures, with significance determined via Mann-Whitney analysis.

CHIP Plays a Critical Role in Acute Neuroprotection

Given that CHIP plays a critical role in maintaining normal mitochondrial morphology and its expression increases in response to acute stress (Palubinsky et al., 2015), we hypothesized that CHIP is necessary for neuroprotection. Since chronic loss of CHIP causes profound changes in the proteome and intracellular milieu (Min et al., 2008; Palubinsky et al., 2015), we chose to acutely deplete rat primary neurons of endogenous CHIP using siRNA to test this hypothesis. We achieved approximately 67.5% knockdown of CHIP 24 hours post-transfection compared to control ($p=0.0258$, $n=4$; Figure 9A). By 48 hours post transfection, CHIP expression was not significantly different from control ($p=0.661$, $n=4$; Figure 9A). Importantly, CHIP siRNA caused no changes in cellular morphology or cell viability (Figure 9B) compared to neurons that were treated with vehicle.

To test the effect of CHIP deficiency during neuroprotective priming, we transfected neurons with CHIP siRNA followed 24 hours later (during optimal CHIP knockdown) by a mild bioenergetic stress. CHIP depletion did not affect viability after low-level (15 minute) OGD compared to non-transfected neurons (Figure 9B). We next sought to determine the effect of CHIP depletion on neuroprotection against a lethal stressor. We subjected CHIP-depleted cultures to low-level OGD followed by 90-minute OGD 24 hours later. Although CHIP expression was uninhibited during 90 minutes of OGD, cells that were depleted of CHIP during the priming event were not afforded neuroprotection and exhibited levels of cell death comparable to lethal, 90 minute OGD, alone (Figure 9B).

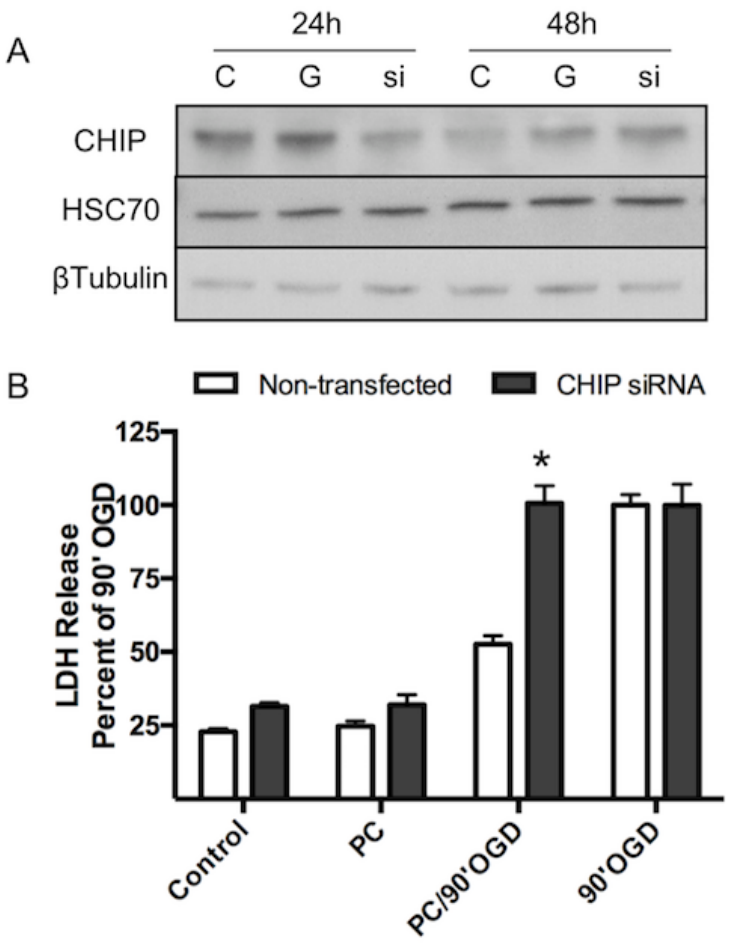

Figure 9: CHIP Expression Is Required for Achieving a Protective Response. Neurons were treated with vehicle (C), transfected with GFP (G), or transfected with GFP and 20 nM of CHIP siRNA (si). Neurons were harvested either 24 or 48 hours later, and Western blotting was performed for CHIP using HSC70 and β-Tubulin as loading controls. (A) Maximal silencing of CHIP expression (67.5%, p=0.026, n=4) was achieved 24 hours post-transfection, and this time point was chosen to determine whether blocking CHIP attenuated PC-induced neuroprotection. CHIP expression by 48h was not significantly different from control (p=0.66, n=4). No significant differences in HSC70 (p=0.97, n=4) or β-Tubulin expression were observed (p=0.55, n=4). (B) LDH released from dead or dying cells was assessed 24 hours after 90' OGD as described in Figure 9. Raw absorbance values were normalized to values obtained from 90' OGD, which leads to 100% cell death. LDH release data revealed that CHIP-deficient neurons were far

less likely to survive 90' OGD, even though they had been preconditioned. Data represent the mean from 3 independent experiments, with significance determined by two-way ANOVA and Bonferroni post-hoc analysis. *denotes significance as compared to non-transfected cells with $p<0.05$.

Mitochondrial Localization of CHIP Is Independent of its E3 Ligase Activity and HSP70 Binding

To eliminate changes attributed to cell passage and mitosis as observed in MEFs, we next used a superior physiological model of acute neuronal stress, subjecting post-mitotic CHIP KO primary neuronal cultures to a mild bioenergetic stress. We predicted that CHIP KO neurons would exhibit severe deficits in mitochondrial quality and that, even when CHIP was reintroduced into KO cells, it would colocalize to mitochondria in control cells, given that they had lacked CHIP prior to transfection.

To test these hypotheses, we exposed WT and CHIP KO neurons to 15 minutes of OGD and assessed mitophagic processes using immunofluorescence staining for TOM20 as a mitochondrial marker and LC3 as a signal for autophagosome formation 6 hours after the bioenergetic stress. WT neurons exposed to acute stress exhibited LC3-positive autophagosomes throughout the cells that contain both mitochondria and CHIP (Figure 10A). In contrast, KO neurons exhibit much more pervasive somatic redistribution of mitochondria following the stressor compared to WT controls (Figure 10A). In CHIP-deficient cells, we also observed elongated mitochondria that colocalize with LC3 after OGD, with fewer rounded autophagosome structures. Taken together with Figure 8, these data suggest that CHIP is necessary for maintaining mitochondrial morphology and suggest a role for CHIP in the mitophagic removal of dysfunctional organelles.

Quantification of colocalization was performed using FIJI Coloc2 on immunofluorescence images of WT neurons expressing TOM20 and endogenous CHIP. We found that some CHIP:TOM20 colocalization is maintained at basal levels (Figure 10B). After mild bioenergetic stress, we find that

CHIP:TOM20 colocalization does not change relative to control levels. We suspect that mitophagy occurs rapidly after the initiation of OGD.

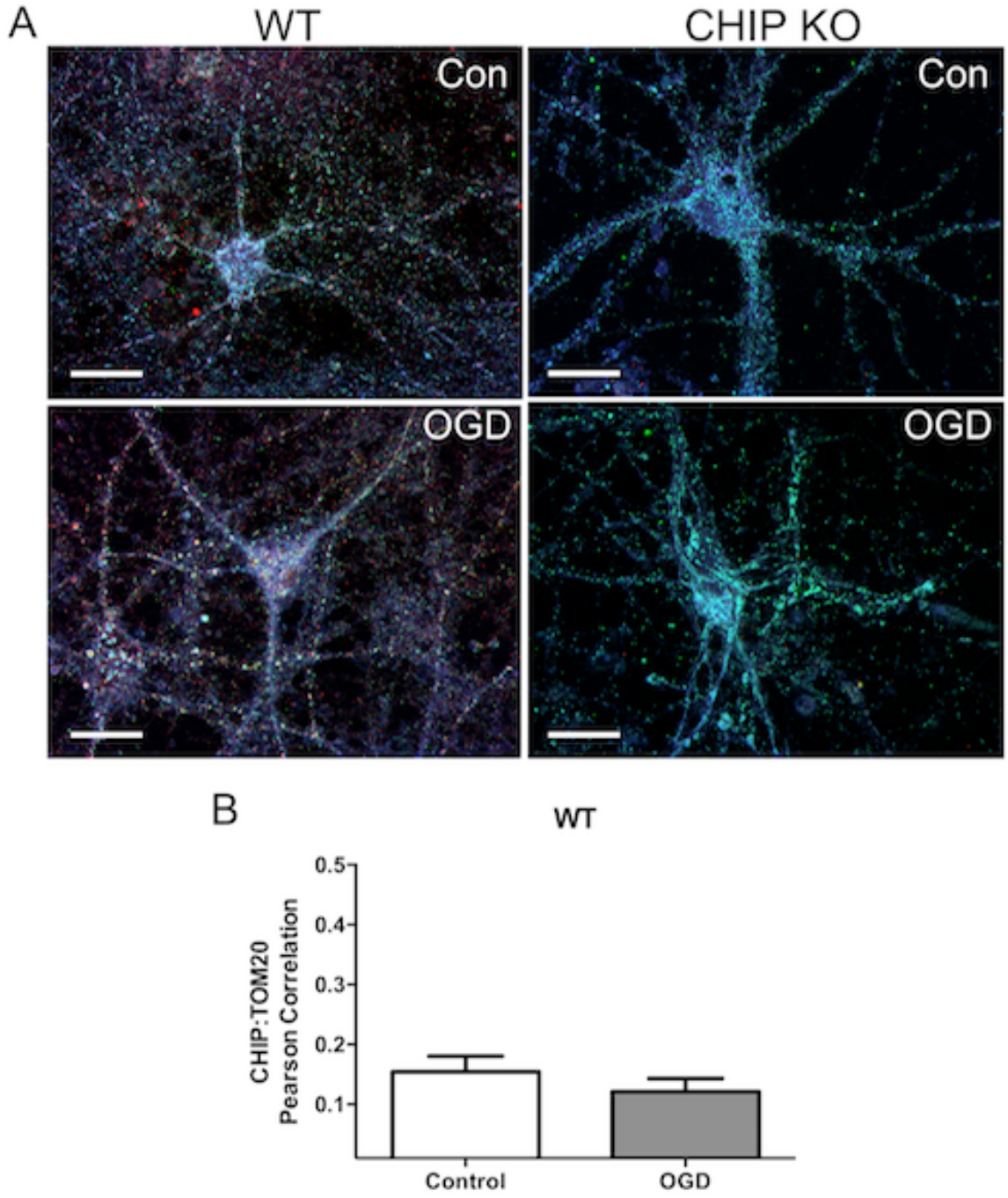

Figure 10: CHIP Localizes to Mitochondria At Baseline and After Bioenergetic Stress. (A) WT and CHIP KO primary neurons were treated with 15' OGD and fixed 6h later. Cultures were probed with

antibodies targeting TOM20 (blue), CHIP (red), and LC3 (green). Scale bar, 20 μm. CHIP and TOM20 colocalization was analyzed using Coloc2 (FIJI). KO neurons exhibit elongated mitochondria that colocalize with LC3 after OGD, with fewer rounded autophagosome structures compared to WT. (B) WT neurons exhibit a baseline colocalization of CHIP and mitochondria with an average Pearson Correlation Coefficient (PCC) of 0.15, which was not significantly different post-OGD (PCC=0.12).

As CHIP does not contain a canonical mitochondrial targeting sequence, we next sought to determine the structural domains necessary for CHIP localization to mitochondria. CHIP contains two primary functional domains: the N-terminal Tetracopeptide Repeat (TPR) domain that binds to HSPs and other TPR domain-containing enzymes and the C-terminal Ubox domain required for E3 ligase activity (Ballinger et al., 1999; Jiang et al., 2001). Mutations identified in patients with spinocerebellar ataxia are located in multiple domains of CHIP, leading to loss of either chaperone function or ubiquitin ligase activity (Heimdal et al., 2014; Shi et al., 2014; Synofzik et al., 2014; Bettencourt et al., 2015). If CHIP acts in ways similar to Parkin, the C-terminal E3 ligase domain would be necessary for mitophagy and H260Q mutants would accumulate LC3-positive organelles but fail to remove them. We also introduced a TPR K30A mutation and hypothesized that if HSC/HSP70 binding is required for mitophagy, K30A transfected cells would have no colocalization of constructs with mitochondria under baseline conditions or during bioenergetic stress.

We cultured primary forebrain neurons from CHIP KO mice and transfected plasmids expressing non-mutated CHIP driven by a human promoter (hCHIP), Ubox mutant hCHIP (H260Q), or TPR mutant hCHIP (K30A) - each fused to a mCherry expression sequence. Transfected neurons were then exposed to mild bioenergetic stress (15 minute OGD) and mCherry localization was assessed after 6 hours of recovery via ICC for TOM20 and LC3. We observed transfection of ~20% of neurons. Under baseline conditions TOM20-positive mitochondria were well-dispersed, elongated, and within a network along

processes. Six hours after a mild bioenergetic stress, staining for all inducible constructs of CHIP under the human promoter was evident (Figure 11A-C). Both human promoter-driven, non-mutated CHIP and the same construct with a H260Q Ubox inactivation mutation colocalized with mitochondria following stress (Figure 11A, 7C). Interestingly, transfected CHIP with a K30A HSP70-interaction site mutation also colocalized with mitochondria that were in close proximity to LC3 labeling (Figure 11B). These data suggest that neither E3 ligase activity nor HSP family binding is necessary for CHIP to localize to mitochondria.

Quantification of colocalization was performed using FIJI Coloc2 on immunofluorescence images of KO neurons expressing TOM20 and transfected hCHIP in KO neurons. When neurons from CHIP KO animals were transfected with either K30A mutant (Figure 11B) or H260Q mutant CHIP (Figure 11C), we observed a significant increase in CHIP:TOM20 colocalization after OGD. Similar to WT neurons (Figure 10), we did not observe a difference in colocalization between control and after bioenergetic stress in KO neurons transfected with the non-mutated human CHIP plasmid (Figure 11A). We did observe that hCHIP localizes to mitochondria at baseline in CHIP KO cultures likely due to the severe disruption of mitochondrial morphology, as seen in CHIP KO MEFs (Figure 8), as well as the limited calcium buffering ability noted in isolated CHIP KO mitochondria (Palubinsky et al., 2015).

Because we see no significant difference in mitochondrial localization of endogenous (Figure 10B) or non-mutated CHIP (Figure 11A) after OGD, we suspect that active CHIP-mediated mitophagy may be occurring rapidly following stress. Given that functional autophagic processes are necessary for mitochondrial clearance, we hypothesize that the increases observed in mutant CHIP colocalization to mitochondria after mild bioenergetic stress are likely due to deficient clearance and subsequent accumulation of CHIP-tagged mitochondria. To test this, KO neurons transfected with non-mutated hCHIP were treated with BafA to block autophagosome fusion with lysosomes following bioenergetic

stress (Figure 11A). Indeed, hCHIP increases colocalization with mitochondria after low-level stress when autophagy is blocked compared to control and low-level OGD alone, suggesting that CHIP-tagged mitochondria are directed for autophagy (Figure 11A). Taken together, these data suggest that functional Ubox and TPR domains are essential for clearance of mitochondria after bioenergetic stress but not for mitochondrial localization.

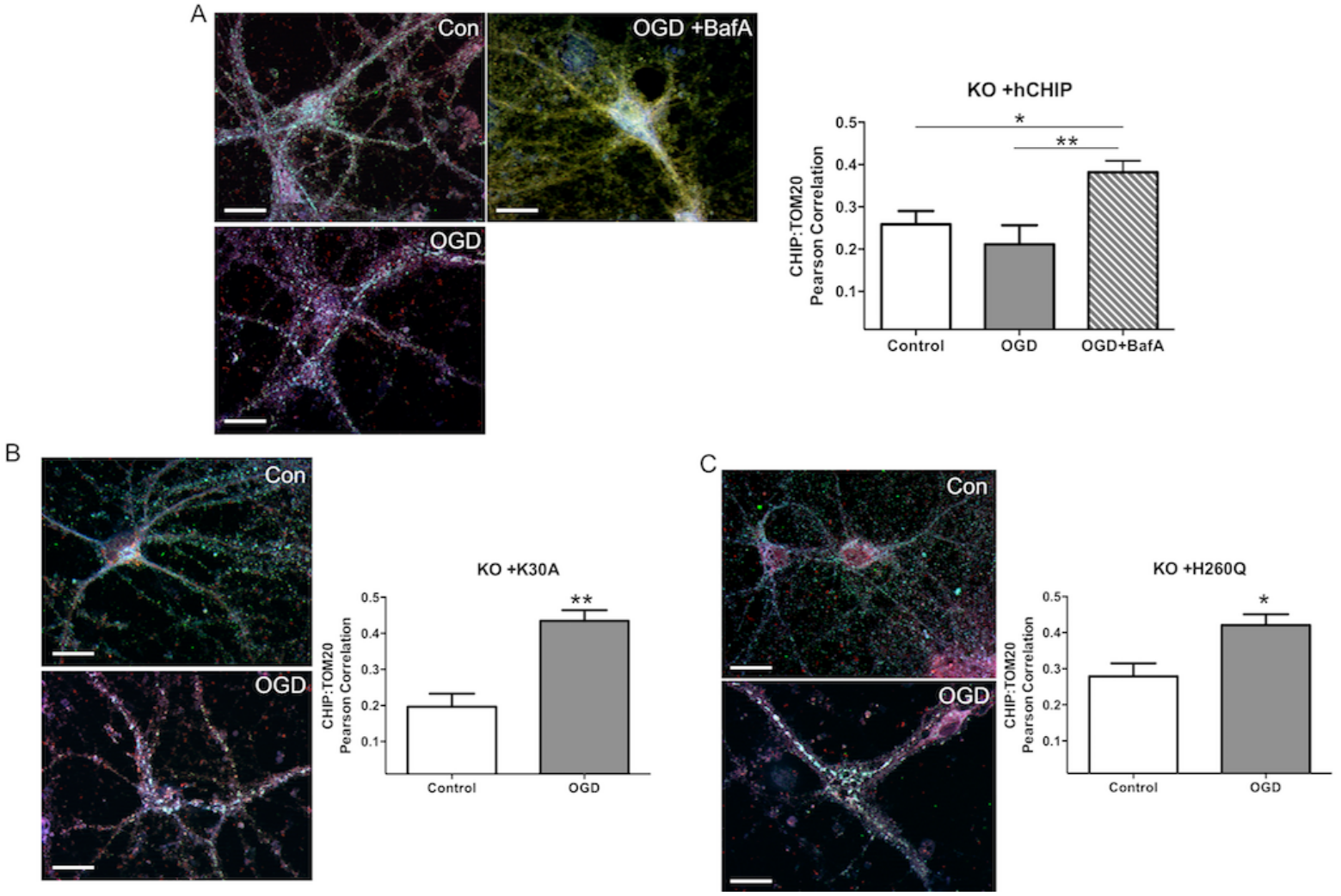
A
Con
OGD +BafA
OGD
KO +hCHIP
CHIP:TOM20
Pearson Correlation
0.5
0.4
0.3
0.2
0.1
*
**
Control
OGD
OGD+BafA
B
Con
OGD
KO +K30A
CHIP:TOM20
Pearson Correlation
0.5
0.4
0.3
0.2
0.1
**
Control
OGD
C
Con
OGD
KO +H260Q
CHIP:TOM20
Pearson Correlation
0.5
0.4
0.3
0.2
0.1
*
Control
OGD

Figure 11 CHIP is Necessary for Maintaining Mitochondrial Quality Control After Stress, Yet Mitochondrial Localization of CHIP is Independent of the TPR and Ubox Domains. (A) CHIP KO neurons were transfected with CHIP (hCHIP) (A), K30A (B), or H260Q (C). Twenty-four hours after transfection, cultures were exposed to 15' OGD or 15' OGD +BafA (1 nM) and PFA-fixed at 6h. Cultures were probed with antibodies targeting TOM20 (blue) and LC3 (green). Red fluorescence is emitted from the mCherry tag linked to transfected CHIP. Scale bar, 20 μm. (A) KO neurons transfected with non-mutated hCHIP (KO+hCHIP) exhibit baseline CHIP:TOM20 colocalization (PCC=0.26) that does not significantly differ post-OGD (PCC=0.21). Cotreatment with BafA significantly increases CHIP:TOM20 colocalization post-OGD (PCC=0.38) compared to control and OGD alone. (B) KO neurons transfected with K30A (KO+K30A) demonstrate increased colocalization post-OGD (PCC=0.43) compared to control (PCC=0.20). (C) KO neurons transfected with H260Q (KO+H260Q) show increased colocalization post-OGD (PCC=0.42) compared to control (PCC=0.28). *Denotes significance of $p<0.01$, and ** $p<0.0001$.

Loss of CHIP Changes the Expression of Critical Bioenergetic Enzymes and Mitochondrial Quality Control Proteins

Mitochondrial transport failure, altered organelle dynamics and changes in structure and function have been implicated in the primary pathology of an increasing number of neurodegenerative diseases (Morotz et al., 2012; Yan et al., 2013; Serrat et al., 2014; Zhang et al., 2015). Proteomic analyses of whole-brains harvested from PND35 WT and CHIP KO mice revealed a number of proteins essential for mitochondrial trafficking and energetic homeostasis that are significantly altered in CHIP KO animals compared to WT (Table 4).

The greatest change observed was a 10-fold increase in the expression of ganglioside-induced differentiation associated protein (Gdap-1). Like CHIP, Gdap-1 lacks a canonical mitochondrial targeting sequence, but functions as an essential mitochondrial outer membrane protein regulating mitochondrial structure and function (Niemann et al., 2005; Otera and Mihara, 2011). Artificially increasing Gdap-1 expression in cell lines results in mitochondrial hyper-fission without overt toxicity, while driving the expression of fusion proteins such as mitofusin 1 can reverse this phenotype (Niemann et al., 2005). The 10-fold increase in Gdap-1 observed in CHIP KO mice should drive mitochondrial fission and therefore manifest as small circular mitochondria. Yet our imaging analysis and quantification of mitochondria from CHIP KO MEFs demonstrate elongated and misshapen organelles. This suggests that Gdap-1 upregulation, while significant, is unsuccessful at driving fission in a CHIP-deficient model.

While less well understood in the context of mitochondrial dynamics, the dynamin protein family is essential for endocytosis, organelle fission and fusion and vesicle formation (Antonny et al., 2016). Dynamin 1 and 3 are CNS-specific and are highly expressed in neurons (Romeu and Arola, 2014). We observed a 7.5-fold increase in expression levels of Dynamin 3 (Dnm3) in CHIP KO brains. These data are consistent with our previous report of increased levels of Dynamin-related protein 1 (Drp1) in CHIP KO mice (Lizama et al., 2017) as well as a gene dose-dependent change in Drp1 oxidation (Palubinsky et al., 2015). Like Gdap-1, increased Dnm3 and Drp1 should manifest as significant mitochondrial fission, but given our analyses these proteins are also unable to drive this process in the absence of CHIP.

CHIP deficiency also resulted in a 2.3-fold increase in the expression of the mitochondrial trafficking protein Miro (Rhot1). This Rho GTPase is an outer mitochondrial membrane protein involved in regulating mitochondrial morphology and intra- and intercellular trafficking. Miro is

essential for ensuring ATP availability for energetically demanding neuronal signaling and communication (Tang, 2015). Overexpression of Miro1 or Miro2 increases mitochondrial length (Saotome et al., 2008), a finding that is consistent with the elongated phenotype of these organelles in CHIP deficient cells. In addition to changing mitochondrial shape, increased Miro expression may be causally linked to changes in CHIP expression. Phosphorylation of Miro by PINK1 (Wang et al., 2011b) targets the protein for degradation by the E3 ubiquitin ligase Parkin (Liu et al., 2012; Birsa et al., 2014). Given the number of overlapping substrates between CHIP and Parkin (Lizama et al., 2017), it is possible that CHIP promotes Miro degradation as well. Taken together with increased Gdap-1, Dnm3, and Drp1, we suspect that CHIP is a critical link between mitochondrial fission and subsequent mitophagy, although more studies are needed to confirm direct protein-protein interactions between CHIP and these mitochondrial targets.

In addition to molecules related to fission-fusion dynamics, we also identified several mitochondrial enzymes increased in brains from CHIP KO animals. Alcohol dehydrogenase (ADH), also termed s-nitroso glutathione terminase, is elevated 3-fold in CHIP deficient animals. ADH eliminates neurotoxic aldehydes generated by lipid peroxidation (O'Brien et al., 2005), consistent with our prior report that CHIP deficiency significantly increases CNS F2t-Isoprostanes and Neuroprostanes (Palubinsky et al., 2015). These species are derived from the non-enzymatic reduction of the membrane lipids arachidonic acid and docosahexaenoic acid. In addition to detoxifying aldehydes, ADH can bind A-beta peptide, forming a mitotoxic species that decreases Complex IV activity, oxygen and neural glucose utilization and ATP formation, as well as production of ROS (Yao et al., 2011).

The Krebs cycle enzyme malate dehydrogenase (MDH) is increased 2.2-fold in brains from CHIP KO animals. MDH is the final acceptor in the Krebs cycle and is increased in neural cell culture models exposed to oxidative stress (Bubber et al., 2005; Shi and Gibson, 2011). The mitochondrial-

specific isoform, MDH2, interacts with the malate-aspartate shuttle, which facilitates the transfer of reducing equivalents from the cytosol to the mitochondria for oxidation (Musrati et al., 1998). Pharmacological activators of MDH and the malate-aspartate shuttle are protective in cardiac ischemia-reperfusion injury models (Stottrup et al., 2010), suggesting that this pathway is rate-limiting and increased expression and activity may be part of an effort to adapt to the bioenergetic dysfunction caused by chronic loss of CHIP.

The observed decreases in Glutathione S-Transferase (GST) speak to the intense oxidative stress observed in CHIP deficient brain. Glutathione (GSH) is the most abundant cellular antioxidant, and maintaining a high ratio of reduced to oxidized glutathione (GSH:GSSG) is essential for cellular health (Halliwell and Gutteridge, 1989). GST catalyzes the conjugation of GSH to endogenous and exogenous oxidized lipids and proteins for detoxification (Strange et al., 2001). CHIP KO animals have a 4.1-fold decrease in GSTA4 expression. This antioxidant is particularly interesting in that it is dually located in the cytosol and mitochondria (Raza, 2011; Al Nimer et al., 2013). Within the mitochondria, GSTA4 detoxifies cells from the lipid peroxidation product 4-hydroxynoneal generated in response to oxidative stress (Singhal et al., 2015). The decrease in GSTA4 expression we identified via proteomics corroborates our previous findings of increased protein oxidation and lipid peroxidation in CHIP deficient animals (Palubinsky et al., 2015).

Other aspects of cellular protein and lipid oxidation profiles are also clearly impacted by CHIP deficiency, including a 2.8-fold decrease in DJ-1 expression. DJ-1 is a redox sensor that functions in repairing proteins damaged by glycation during oxidative stress. DJ-1 translocates to mitochondria in neural cells after bioenergetic stress and is secreted by injured neurons (Kaneko et al., 2014). Loss of DJ-1 increases susceptibility to cell death following acute ischemia-reperfusion in mice (Dongworth et al., 2014). As such, novel DJ-1-binding compounds are currently being studied in the context of

Parkinson's disease therapy (Inden et al., 2017) and have the potential to be cross-purposed as neuroprotective strategies against acute oxidative stress. These data support a model in which CHIP is a critical regulator of redox homeostasis as DJ-1 decreases significantly in its absence, refortifying an environment of protein and lipid oxidation.

Taken together, these data reveal that CHIP expression is critical to mitochondrial quality control proteins, bioenergetic enzymes, and redox sensors. These results may explain in part the severe abnormalities in mitochondrial shape, cristae structure, and calcium buffering capacity, as well as increased neuronal vulnerability to mild bioenergetic stress when CHIP is absent.

Significantly Altered Proteins (Fold Change)	
Increased in CHIP KO Mice	
Protein	**Fold Change**
Gdap-1	10.2
Dynamin 3	7.5
Miro	2.3
Alcohol dehydrogenase	3.0
Malate dehydrogenase	2.2
Decreased in CHIP KO Mice	
Protein	**Fold Change**
Glutathione S Transferase α4	4.1
DJ-1	2.8

Table 4 CHIP Loss Changes Expression of Proteins Involved In Mitochondrial Dynamics and Energetics. Whole brain lysates from WT and CHIP KO mice (4 male, 4 female for each genotype) were analyzed by LC-MS/MS. Proteins listed are >2-fold increased or decreased in KO compared to WT based on spectral count data.

2.5 Discussion

The interactions between proteins involved in mitochondrial bioenergetics, redox tone, structure, signaling, and autophagy are becoming increasingly well understood, particularly in regards to mediating responses to neurological injury and disease. Redox stress sensors like PINK1, DJ-1 and apoptosis signaling kinases (ASK) play critical roles in sensing oxidative stress, triggering mitophagy and initiating fission and fusion of organelles. The expression and distribution of these proteins are regulated by chaperones, protein-protein interactions, redox sensitivity, ubiquitination, and degradation. In this work, we show that the chaperone-binding protein, CHIP, is unique among disease-associated proteins in that it is both an E3 ligase as well as an essential regulator of mitochondrial number and morphology in both physiological and acute pathophysiological stress signaling.

CHIP was identified as a potential regulator of acute neuronal stress in studies from our lab in which we observed increases in CHIP and HSP70 expression that correlate with the time windows of neuroprotection observed in ischemic preconditioning (Stankowski et al., 2011). Cells given a low (non-lethal) level of stress are able to upregulate endogenous protective pathways and withstand any number of subsequent injuries including OGD, hypoxia, and oxidative stress (Stetler et al., 2014). We sought to evaluate the importance of CHIP using a preconditioning model, as understanding the proteins and pathways that control this endogenous form of protection could be leveraged therapeutically.

Primary neuronal cultures exposed to a short period of oxygen and glucose deprivation proved to be a highly effective means to study CHIP redistribution. Here we show that CHIP expression increases rapidly in neurons in response to bioenergetic stress, functioning as a critical regulator of neuroprotection and mitochondrial autophagic clearance. Within six hours of acute stress, CHIP relocalized to mitochondrial membranes. Silencing CHIP expression with siRNA significantly increased

neuronal death in response to subsequent stress. These data suggest that CHIP induction, and possibly redistribution, are critical events in neurons in order to fend off potentially toxic events.

We initially hypothesized that when redistributed to the mitochondria, CHIP would promote mitophagy in a manner akin to Parkin. Parkin is a well-characterized E3-ubiquitin ligase with similar functional domains to CHIP and, based on cell free assays, some redundant client proteins that are targeted for degradation (Imai et al., 2002; Kumar et al., 2012). *In vitro* studies of Parkin revealed its roles in mitochondrial quality control and mitophagy (Grunewald et al., 2010; Matsuda et al., 2010; Narendra et al., 2010; Rana et al., 2013; Seirafi et al., 2015). CHIP's ability to compensate for Parkin is not unprecedented (Imai et al., 2002), and new studies in Drosophila show that CHIP functions downstream of PINK1 signaling, with CHIP overexpression rescuing mitophagy when Parkin is deficient (Chen et al., 2017).

Taken together with biophysical data, it is perhaps not surprising that CHIP is unique among E3 ligases as it forms asymmetric homodimers with protruding TPR domains. These TPR domains transiently bind to the C-terminal domain of HSC/P70. The interfacing Ubox domains then add poly-ubiquitin chains to exposed K48 residues on client proteins (Scheufler et al., 2000; Schulman and Chen, 2005; Stankiewicz et al., 2010). Not only does CHIP lack a canonical mitochondrial localization signal, but protein relocalization continued to occur even when we introduced mutations that arrest E3 ligase function (H260Q) or block HSP70-binding (K30A).

Surprisingly, mutating these sites enhanced CHIP association with mitochondria after low-level bioenergetic stress. One interpretation of this data is that the HSP-bound/ubiquitin ligase functions of CHIP are predominantly cytosolic and that the mutations in H260Q or K30A increased a free pool of CHIP capable of moving to mitochondria. Another possible interpretation is that HSP70 binding and ubiquitin ligase sites are dispensable for relocalization to mitochondria but are needed to drive

secondary processes such as mitophagy that would then degrade CHIP/mitochondrial complexes, appearing as a decrease in CHIP/mitochondrial association. Indeed, HSC/HSP70 C-terminal CHIP-binding mutants increase cell vulnerability to stress-induced apoptosis (Mosser et al., 2000), and CHIP rescues mitochondrial dysfunction in a Ubox-dependent manner in PINK1 KO drosophila models (Chen et al., 2017).

In the absence of a canonical mitochondrial targeting sequence, our data suggest that the charged helix domains of CHIP may mediate mitochondrial localization, or that the TPR and Ubox domains may contain unidentified regions that bind with proteins or lipids that facilitate mitochondrial localization. Indeed, CHIP was recently shown to bind to lipid membranes enriched in phosphotidylinositol and phosphotidic acid, and these lipid substrates compete with chaperones for binding at the TPR domain (Kopp et al., 2017). Interestingly, however, Kopp et al. found that purified CHIP protein did not bind strongly to cardiolipin using cell-free lipid-binding assays. Cardiolipin, an inner mitochondrial membrane lipid, externalizes to the outer mitochondrial membrane in response to mitochondrial injury, interacts with LC3, and facilitates mitophagy (Chu et al., 2013). Based on our findings, interrogation of CHIP binding with mitochondrial lipids, such as cardiolipin, is warranted using physiological conditions and more sensitive detection of lipid-protein interactions, such as subcellular fractionation and mass spectrometry.

We selected the H260Q and K30A mutations based on known functions of CHIP primary domains; however, next-generation sequencing of patients with spinocerebellar ataxias has identified numerous mutations in the STUB1 gene encoding CHIP protein. In patients with SCAR16, homozygous or compound heterozygous point mutations are spread throughout the major structural domains of CHIP, resulting in a loss of function (Heimdal et al., 2014; Shi et al., 2014; Synofzik et al., 2014; Bettencourt et al., 2015; Kawarai et al., 2016). STUB1 mutations are rare and the clinical phenotype and

neuropathological features of these mutations remain poorly described. CHIP likely controls critical functions beyond the cerebellum, as patients present not only with progressive limb ataxia, gait instability, and cerebellar atrophy but also with dysarthria and mild cognitive impairment (Heimdal et al., 2014; Kawarai et al., 2016).

Genetic mutations in E3 ligases such as X-linked inhibition of apoptosis protein (XIAP), Hrd1, and Parkin are associated with Parkinson's disease and other neurological disorders (Harlin et al., 2001; Goldberg et al., 2003; Kaneko et al., 2010). However, recapitulating neuronal death, particularly in Parkin knockout mouse models, has largely proven unsuccessful (Perez and Palmiter, 2005). Our data suggest that CHIP performs a more vital role in neuronal homeostasis than Parkin. Indeed, CHIP KO animals, neurons and MEFs have high baseline levels of oxidative stress, bioenergetic dysfunction and a hair-trigger response to injuries that should be non-toxic. Mitochondria are severely deformed with swollen cristae and are present in greater numbers when CHIP has been genetically deleted. This phenotype is unique compared to observations from other E3 ligase mutants (Stevens et al., 2015; Mukherjee and Chakrabarti, 2016; Roy et al., 2016). CHIP deficiency is debilitating, as even heterozygous mice have significant motor dysfunction (McLaughlin et al., 2012). Homozygous-null mice are too frail to participate in behavioral testing and have significant oxidative dysfunction in the CNS and periphery before dying prematurely (Min et al., 2008; McLaughlin et al., 2012; Palubinsky et al., 2015). These data stand in stark contrast to Parkin deficient models, which are neurochemically, behaviorally and structurally indistinguishable from littermates (Goldberg et al., 2003; Palacino et al., 2004; Perez and Palmiter, 2005; Lizama et al., 2017).

The morphological and biochemical changes observed in CHIP deficient mitochondria do, however, strikingly parallel mutations in autophagy protein 5 (Atg5) that disrupt formation of the Atg12-Atg5 complex. The Atg12-Atg5 conjugate exhibits E3 ligase–like activity, facilitating lipidation

of LC3 family members (Otomo et al., 2013). While mice with complete deletion of Atg5 die shortly after birth (Yoshii et al., 2016), Atg5 mutations have been identified in patients with ataxia and are associated with loss of autophagic signaling in conditional KO models (Kim et al., 2016b). Our data support an 'Atg-5-like' role for CHIP in normal as well as pathological neuronal mitophagy. As CHIP-null animals are not embryonic lethal, CHIP deficient mice may also provide a rigorous animal model for studying premature aging and susceptibility to neurological injury.

CHAPTER 3

SUMMARY AND FUTURE DIRECTIONS

Summary

Since its discovery in 2003, CHIP is now known to be vital for proteostasis, signaling, metabolism, and organelle function. This work is the first to reveal the role of CHIP in neuronal preconditioning and further supports that contextually- and temporally-regulated mitophagy is neuroprotective. However, the complete profile of CHIP activity, particularly with regard to HSP70-independent or E3 ligase-independent interactions, requires a great deal more study. In this work we show that CHIP can be recruited to mitochondria under physiologically-relevant stress, and that this localization does not depend on HSP70 binding nor on E3-ligase activity. Within the last year, CHIP has been shown to bind PINK1 in a TPR-independent and Ubox-independent manner (Yoo and Chung, 2018). Additionally, CHIP was shown to bind to plasma membrane lipids in a way that competes with HSP70 binding and is dependent upon charged amino acids in the coiled-coil domain (Kopp et al., 2017). These data support the hypothesis that the unique coiled-coil domain of CHIP may be a yet unexplored mechanism for novel protein-protein and protein-lipid interactions.

3.1 CHIP Deficiency As a Model For Pathological Aging and Frailty

Given the multiple roles of CHIP in cell signaling and survival pathways, it is tempting to speculate that non-pathogenic variants of the STUB1 gene render humans that carry these variants susceptible to environmental stimuli and toxins. Similar models of gene-environment interactions exist for understanding familial and sporadic neurodegenerative diseases, such as Huntington's disease and PD (Cannon and Greenamyre, 2013; Mo et al., 2015).

Our group has shown that CHIP haploinsufficient animals (CHIP Het) exhibit motor dysfunction beginning at adolescence, despite being able to live as long as their wild-type littermates (McLaughlin et al., 2012). Preliminary data comparing WT and CHIP Het adult mice reveal that, despite similar basal metabolic rate and activity, CHIP Het animals fail to perform as well on an exercise stress test, reaching exhaustion much sooner than their WT littermates.

These phenotypes strikingly resemble symptoms of frailty, a clinical syndrome affecting more than 30% of geriatric adults in the United States (Mohler et al., 2014). Individuals with frailty exhibit a progressive physical decline that is defined by five symptoms: weight loss, diminished muscle tone, slow walking pace, low physical activity, and exhaustion (Fried et al., 2001). Frailty is associated with increased disability, elevated risk of medical co-morbidity, and increased mortality even when accounting for common age-associated diseases (Fried et al., 2001; Newman et al., 2001; Woods et al., 2005; Bandeen-Roche et al., 2006). This syndrome, apart from normal aging, renders individuals highly vulnerable to external stressors and leads to poor recovery from injury.

The causes of frailty remain to be completely elucidated. Thus far, evidence suggests that oxidative stress, mitochondrial dysfunction, and chronic inflammation are associated with increased risk of frailty. In studies looking at serum from patients, high levels of isoprostanes, oxidized glutathione, protein adduction, and DNA damage are associated with frail patients compared to age-matched control cohorts (Serviddio et al., 2009; Cesari et al., 2012; Liu et al., 2016). Frail individuals also exhibit lower mitochondrial DNA content, which suggests abnormal bioenergetic tone (Ashar et al., 2015).

Given the increasing geriatric population, mouse models of frailty are a sorely unmet need in which to test potential clinical interventions. To date, only two animal models of frailty exist: the Interleukin-10 (IL-10) knockout mouse and the Cu/Zn superoxide disumates (Sod1) knockout mouse

(Deepa et al., 2017). Like CHIP haploinsufficient animals, IL-10 and Sod1 knockout animals exhibit decreased muscle tone, elevated F_{2t}-isoprostanes, and diminished ATP pools (Deepa et al., 2017).

To assess CHIP deficiency as a mouse model of frailty, future projects characterizing the metabolic phenotype of young and aged CHIP haploinsufficent animals are needed. This can be done through metabolic and behavioral analyses on adult and geriatric WT and CHIP Het mice in collaboration with the Vanderbilt Mouse Metabolic Phenotyping Core. Using the Oxymax system, basal activity, oxygen consumption, and fat/lean mass can be monitored over a five-day period. To stress animals, exercise endurance tests can be performed while simultaneously recording metabolic rate. We suspect that while adult CHIP Het animals will exhibit no differences in basal metabolic rate and activity, stressed adult and aged CHIP Het animals will exhibit decreased activity and shifts in metabolic tone (i.e. elevated fatty acid metabolism versus oxidative phosphorylation) not observed in WT mice.

To further elucidate the age-related pathology of CHIP loss, the lipidomic and proteomic profile of aged CHIP haploinsufficient animals could be assessed using biochemical and LC/MS techniques, identifying biomarkers of frailty and aging in WT and CHIP Het tissues. We suspect that, by comparing profiles of young versus aged WT and CHIP Het animals, we will confirm previously recognized biomarkers of frailty and identify novel markers of pathological aging. For example, circulating HSP70 concentrations are correlated with inflammation and frailty in geriatric patients than in an age-matched healthy geriatric cohort (Njemini et al., 2011; Ogawa et al., 2012).

While pathogenic CHIP mutations have been identified in patients with SCA, there remain gaps in our understanding of the frequency and phenotype of CHIP heterozygosity or non-SCA-causing mutations in CHIP. To understand the frequency of CHIP variants in human populations and correlations with frailty and disease risk, we could screen deidentified electronic patient records and genomic data provided by the BioVU Synthetic Derivative to determine correlations between SNPs in

STUB1, patient frailty, and age-related co-morbidities. We hypothesize that frail patients, as identified by standardized frailty assessments, will exhibit biomarkers of frailty that corroborate our CHIP KO and Het animal models, as well as exhibit genetic variations in the *STUB1* gene.

3.2 CHIP Deficiency As a Model of Aberrant Autophagy

Autophagic protein and organelle degradation is an essential, highly conserved process that regulates normal and pathophysiological processes. The autophagy related proteins (Atgs) were first identified and characterized in yeast, but these proteins are conserved across eukaryotes and higher vertebrates. The Atgs function in sequential steps in order to orchestrate initiation of membrane formation, protein and organelle identification, and engulfment (Reviewed in (Mizushima et al., 2011) and (Galluzzi et al., 2017)). Mammalian homologues and functionally redundant proteins in the autophagic pathway continue to be identified (Galluzzi et al., 2017).

Part of the core Atg proteins, Atg5 and Atg12 work cooperatively in the formation of pre-autophagosomes and function in part as an E3 ligase to facilitate activation of LC3 (Hanada et al., 2007). Unsurprisingly, mutants and deletions of Atg5 have been shown to result in profound deficits in autophagic signaling, and mice with global deletion of Atg5 die shortly after birth (Hara et al., 2006; Yoshii et al., 2016). While autophagy dysfunction is associated with a myriad of diseases (Jiang and Mizushima, 2014), mutations in the core non-redundant autophagy proteins have not been reported in patients, with the exception of Atg5. Mutations in this gene were recently identified in two patients with ataxia with developmental delay (Kim et al., 2016b). This phenotype is consistent with that of patients with an early onset, recessive form of spinocerebellar ataxia and mutations in CHIP.

As discussed in Chapter 1, animals with CHIP deficiency exhibit profound deficits in motor and cardiovascular function and premature death, with abnormal mitochondria and autophagic flux

(Palubinsky et al., 2015). As described in Chapter 2, we found that in response to acute bioenergetic failure, CHIP relocates to mitochondria and colocalizes with the autophagy protein LC3. We are interested in continuing comparative analyses of the molecular pathology of CHIP deficiency with that of Atg5 deficiency. We seek to determine the ability of Atg5 to compensate for defects in mitophagy caused by CHIP deletion and test the hypothesis that Atg5 and CHIP are functional homologues (Figure 12).

To determine the susceptibility of CHIP KO and Atg5 KO MEF cells to proteotoxic, energetic, and oxidative stress, we could determine how loss of CHIP or loss of Atg5 affects cell viability under different stressors. Specifically, we could use acute heat shock to induce proteotoxicity, nutrient deprivation to induce energetic stress, and 4-HNE to induce oxidative stress. Using this strategy will delineate the protective roles of CHIP and Atg5 in protein triage, mitochondrial quality control, and redox homeostasis.

We have previously shown that CHIP loss leads to abnormal autophagic flux (elevated LC3 and p62) in brain tissue (Palubinsky et al., 2015). We suspect that Atg5 is also aberrantly expressed in tissues from CHIP deficient animals, particularly in tissues with high metabolic demand, such as the brain, heart, and skeletal muscle. To test this, Atg5 expression and localization will be characterized during CHIP deficiency using western blotting and immunofluorescence staining.

To assess the functional redundancy of CHIP and Atg5 in autophagic flux, we will transfect CHIP KO MEFs and primary neurons with an Atg5 overexpression plasmid. Given the rapid localization of CHIP to mitochondria during stress and the role of CHIP in maintaining basal energetic homeostasis, we hypothesize that, while Atg5 may compensate for defects in autophagy in CHIP KO, CHIP is indispensable for mitophagy in the neuronal autophagic pathway. Similarly, we will transfect

Atg5 KO MEFs with hCHIP to determine whether CHIP can ameliorate defects in protein and organelle turnover.

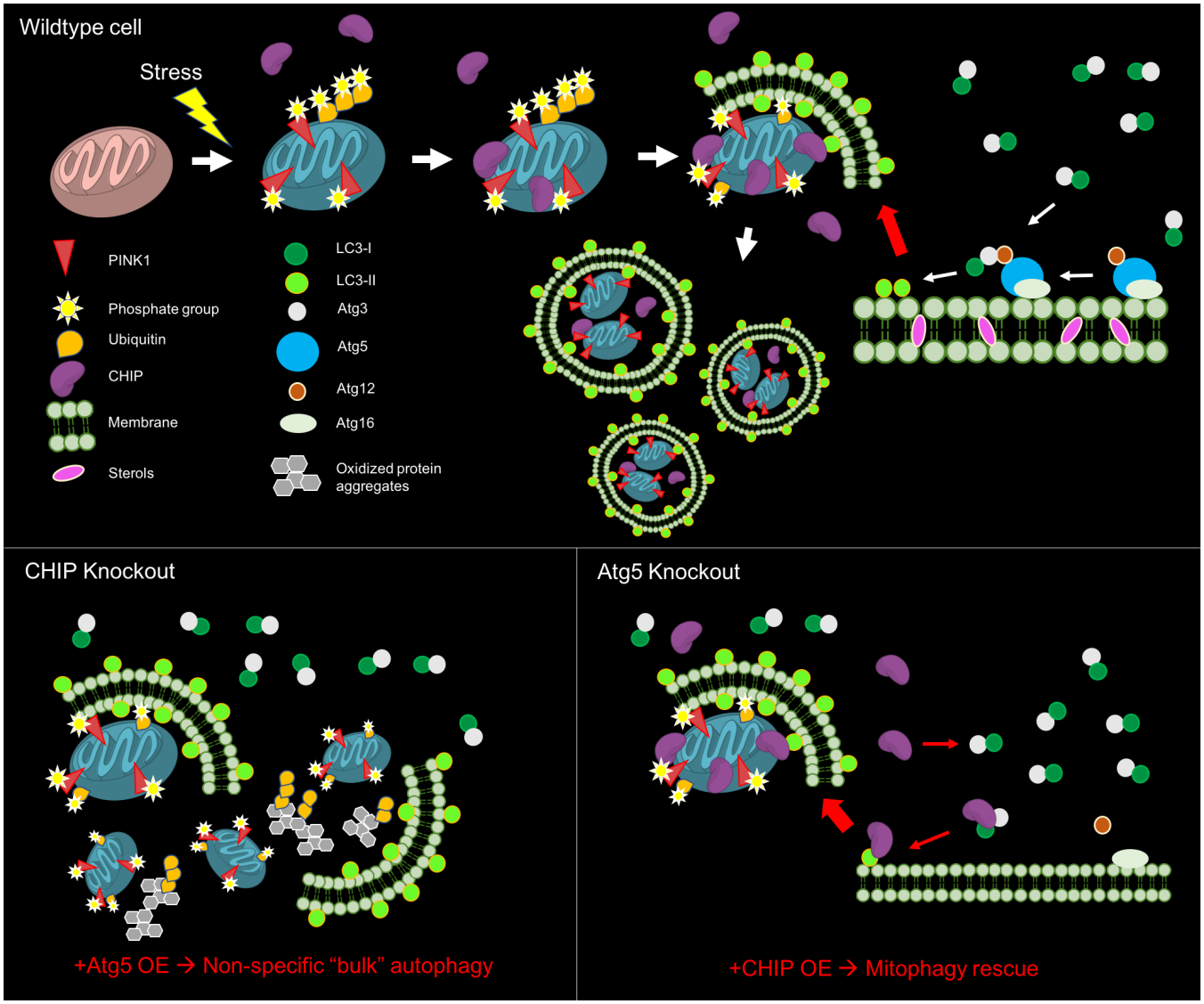

Figure 12 Hypothesized Role of CHIP and Atg5 in Mitophagy. In normal cells, damaged mitochondria are degraded via mitophagy through sequential steps. The kinase PINK1 is stabilized on the OMM of damaged mitochondria and phosphorylates OMM proteins and ubiquitin. E3 ligase CHIP is recruited to damaged mitochondria and facilitates addition of ubiquitin. Membrane-bound LC3 (LC3-II) is formed via the E3 ligase-like activity of the Atg16-Atg5-Atg12 complex and is subsequently recruited to damaged organelles for autophagosome formation. There remain significant gaps in knowledge about

the lipid and sterol composition of these phagophores, and how these membranes are affected in disease states. We hypothesize that CHIP and Atg5 may be functionally redundant. CHIP KO cells accumulate sick mitochondria and aggregates of poly-ubiquitinated and oxidized proteins. We suspect that overexpession of Atg5 in a CHIP KO system will compensate for loss of CHIP through activation of bulk autophagy, consequently improving cell viability. Given that CHIP has lipid membrane binding properties in addition to its E3 ligase activity, we suspect that overexpression of CHIP in an Atg5 KO system will compensate for the loss of activated LC3 and phagophore fomation. Moreover, we hypothesize that CHIP may specifically rescue mitophagy, given that CHIP is recruited to mitochondria during stress, to improve cell survival. Red arrows and text indicate hypothesized effects.

3.3 Therapeutic Targets and the Challenges of Reducing CHIP and Parkin-Mediated Pathology

Opportunities for Targeting E3 Ligases with Off-Label Drugs

Targeting the UPS has proven successful for the treatment of multiple myeloma and other types of cancer (Ghobrial et al., 2016; Guang and Bianchi, 2017). The first FDA approved proteasome inhibitor, bortezomib, binds to the 20S proteasome to block the degradation of pro-apoptotic proteins, inducing cell cycle arrest (Piperdi et al., 2011; Accardi et al., 2015). Since the approval for use of this landmark drug in 2003, several other proteasome inhibitors have been approved or are in late-stage clinical trials (Teicher and Tomaszewski, 2015; Manasanch and Orlowski, 2017). Although these drugs maintain high specificity and efficacy, proteasome inhibitors are not pathway-specific, targeting the latter steps of the UPS during which all protein degradation is affected.

Upon dissociation from HSP70, Parkin also promotes degradation of the Pael-R receptor during times of ER-stress (Imai et al., 2002). This positive regulation of Parkin via the HSP70 chaperone complex, as well as an increasing number of disease states in which chaperone machinery and the UPS are disrupted (Charan and LaVoie, 2015), again suggests that E3 ligases may be potential therapeutic

targets. Further support for E3s as drug targets comes from studies of proteasome inhibition with bortezomib (Ruschak et al., 2011) or carfilzomib (Kuhn et al., 2007), which, while effective, were shown to result in broad toxicity, off-target effects and increased drug resistance, suggesting that enzymes that lie upstream of the proteasome, such as E3 ligases, are a more feasible target (Goldenberg et al., 2010; Bulatov and Ciulli, 2015; Huang and Dixit, 2016). Additionally, E3 ligases represent an attractive drug target due to the limited number of substrates they target, limiting the regulatory pathways affected (Bhowmick et al., 2013; Skaar et al., 2014; Bulatov and Ciulli, 2015; Huang and Dixit, 2016). Yet, to date only two inhibitors, Nutlins (Roche) and Lenalidomide (Celgene) for the E3 ligases MDM2 and CRBN, respectively, have reached clinical trials (Patel and Player, 2008; Skaar et al., 2014).

One biochemical feature of RBR E3s that makes them slightly more complex to inhibit compared to other E3s is that they require disruption of strong protein-protein interactions, which is more difficult than simply targeting a catalytic site (Gonzalez-Ruiz and Gohlke, 2006; Arkin et al., 2014). A notable biochemical difference of RBR E3 ligases is that they act as scaffolds or adaptors to bring the components of the ubiquitination machinery in closer contact with the substrate. In doing so, the ubiquitin-conjugated E2 binds to the RING1 domain and then ubiquitin is transferred from the E2 to the E3 RING2 domain from which it is then transferred to the substrate (Bielskiene et al., 2015). Therefore, inhibiting the activity of RBR E3s requires molecules that interrupt the interaction between the ubiquitinated substrate at the substrate interaction domain in order to selectively block degradation of a small number of client proteins (Patel and Player, 2008).

The structure of CHIP makes this protein a more pliable target for small molecule binding. Given that the TPR domain is a highly conserved structure, and thousands of TPR proteins have been identified, one would suspect that the TPR domain is not a suitably druggable target. Yet, despite a

consensus sequence, TPR domain-containing proteins exhibit intra-domain heterogeneity that ultimately determines specificity through variation in hydrophobic pockets, residue type and charge, electrostatic interaction, and secondary structure flexibility (Zeytuni and Zarivach, 2012). The CHIP TPR domain binds weakly to the EEVD motif of HSC/HSP70, which suggests a transient, dynamic function of the pro-degradation chaperone complex (Wang et al., 2011a; Smith et al., 2013). Pharmacological modulators of the CHIP TPR domain may strengthen or weaken the interaction with the HSC/HSP70 complex, which may improve proteostasis in a variety of disease contexts. For example, CHIP binding to HSP70 is required for recognition of abnormal phospho-tau and will preferentially degrade these substrates when HSP90 is pharmacologically inhibited (Dickey et al., 2007b). Given the low-specificity and toxicity of most HSP90 inhibitors, combination therapy with modulators of CHIP may be a useful strategy (Butler et al., 2015).

In generating therapeutic strategies for modifying E3 ligase function, it is also important to verify which models use naturally-occurring versus synthetic mutants to divulge E3 ligase functions. For example, Parkin mutant C431S is not found in patients with PD, but its use in cell culture models identified a covalent intermediate in Parkin activation and evidence for its HECT-like activity (Lazarou et al., 2013). Additionally, synthetic mutations in CHIP, such as the K30A and H260Q mutations, have not been identified in patients but are established tools for delineating the function of CHIP domains (Xu et al., 2002).

Controlling Chaperone Activity to Dictate Protein Fate

Beyond direct control over E3 ligases and their PTM sites, an alternate strategy to change E3 expression and activity is to change the catalogue of clients presented for ubiquitination and the activity of the chaperone complex. Given the role of HSPs in combating a wide variety of cellular stressors, it is

not surprising that much research has focused on developing modulators to inhibit or activate these key proteins (Holzbeierlein et al., 2010; Neckers and Workman, 2012). The most specific and efficient compounds currently available are designed to target the structural components of HSP90, a chaperone that responds to a plethora of environmental and physiological stressors (Schopf et al., 2017). Investigators initially established HSP90′s ability to be manipulated by drugs such as geldanamycin and radicicol. These natural small molecules mimic the ATP-bound structure adopted in the chaperone's N-terminal nucleotide binding domain (NBD) and cause potent and selective blockade of ATP binding/hydrolysis, inhibition of chaperone function, depletion of oncogenic clients, and antitumor activity (Neckers and Workman, 2012).

Chaperone proteins exhibit high levels of structural conservation. For example, eleven members of the HSP70 family contain an N-terminal NBD (~40 kDa) and a C-terminal substrate-binding domain (SBD) of roughly 25 kDa connected by a short linker (Bertelsen et al., 2009). Similar to HSP90, HSP70 has unique structural components making it a suitable drug target. Many of the functions of HSP70 appear to revolve around crosstalk between ATPase activity in the NBD and substrate binding in the SBD. HSP70 binds tightly to ATP, and through an allosteric, interdomain interaction, increases the on- and off-rate of peptide binding in the adjacent SBD. In turn, nucleotide hydrolysis to ADP closes the "lid" and enhances the affinity for substrate. Likewise, interactions between the SBD and its substrates increase the rate of ATP hydrolysis in the NBD, suggesting that communication between the two domains is two-way (Mayer et al., 2000). From a drug discovery viewpoint, this unique allostery provides multiple opportunities for chemical intervention, including inhibition of ATP turnover, substrate binding, or even blocking interdomain allostery altogether (Evans et al., 2010).

The first set of specific allosteric modulators of the HSC70 complex that target the HSP40-HSC70 interacting or the ATP/ADP substrate binding domains have been developed. Importantly, these

regions are conserved across all members of the HSC70 family, including HSP70. The ATP binding domain is a critical determinant of chaperone complex activity. When HSC70 family members bind HSP40, repetitive cycles of substrate binding and release occur. The affinity of ATP binding, length of substrate interaction and strength of substrate affinity therefore determines the fate of the client protein by modulating protein refolding or degradation. When bound to the nucleotide site, pro-degradation compounds block ATP turnover and drive the complex to release denatured proteins for subsequent ubiquitination and degradation. One of these compounds, MKT-077, is being actively explored in preclinical and clinical trials as it blocks proliferation of cancer cell lines (Li et al., 2013). On the other hand, protein-refolding modulators activate the ATPase domain of HSP40 resulting in the constant clamping and release of HSP70-bound substrates required for proper protein refolding (Jinwal et al., 2009). It is interesting to speculate as to what role CHIP may play when these compounds are administered.

HSPs also indirectly regulate mitochondrial dynamics in mutant models of Parkin. For example, expression of DnaJ/Hsp40 chaperone HSJ1a and DNAJB6 was found to rescue mitophagy of depolarized mitochondria in cultures expressing a Parkin RING domain mutant (Rose et al., 2011). This C289G mutation, found in patients with early-onset autosomal-recessive parkinsonism, causes Parkin to aggregate and lose the ability to translocate to mitochondria (Lucking et al., 2000). HSP70 co-chaperones HSJ1a and DNAJB6 selectively prevented mutated Parkin from forming aggregates (Rose et al., 2011). A later study found conflicting data in which expression of these co-chaperones reduced aggregated mutant Parkin, but did not rescue mitophagy (Kakkar et al., 2016). The authors attributed these conflicting results to the use of different cell lines with differential endogenous Parkin expression. Nevertheless, DNAJ proteins were effective in preventing mutant Parkin aggregation in an HSP70-dependent manner (Kakkar et al., 2016). Therefore, targeting the expression or HSP70-binding capacity

of DNAJ co-chaperones may be an additional opportunity for treating PD and other neurodegenerative diseases caused by aggregate-prone E3 ligases. Given the role of CHIP at the mitochondria, similar studies investigating the role of CHIP in these models is of intense interest.

Beyond targeting chaperones themselves, transcription factors that influence the expression of chaperones may also be able to regulate E3 function and activity both directly and indirectly. For example, under basal physiological conditions, HSF1 is an inactive monomer held in a multiprotein complex that includes HSC/HSP70 and HSP90 (Morimoto, 1998). During heat stress, HSF1 undergoes a conformational change, trimerizes, and interacts directly with CHIP (Kim et al., 2005). This interaction allows HSF1 to localize to the nucleus and induce HSC/HSP70 expression (Dai et al., 2003; Kim et al., 2005). Thus, perhaps targeting HSF1 by promoting trimerization and subsequent binding with CHIP is a promising therapy to upregulate neuroprotective HSP70.

Activation of HSF1 occurs uniformly in response to treatment with the HSP90 inhibitors currently under clinical evaluation. While simultaneously inhibiting the oncogenic Ras/Raf signaling pathways, these agents also promote production of soluble and insoluble HSP70 pools (Bagatell et al., 2000). In neural cells, aggregation of mutant α-synuclein was shown to inhibit HSF1 expression by increasing its ubiquitination via the E3 ligase NEDD4 (Kim et al., 2016a). Conversely, introduction of a constitutively active form of HSF1 rescues neural cells from α-synuclein-induced toxicity (Liangliang et al., 2010). As such, efforts are currently underway to identify and validate modulators of HSF1, HSP70, and HSP27 and to explore their functions and validity in combination therapy with HSP90 and other chaperone inhibitors.

CNS drug discovery remains a challenge owing to issues of blood–brain barrier penetrance, first-pass metabolism, target affinity and selectivity, and therapeutic index (Chico et al., 2009; Abbott, 2013; Butlen-Ducuing et al., 2016). The more we uncover about the structure, function and activity of Parkin

and CHIP, where known mutations result in devastating disease, the more avenues we open regarding how to effectively target and treat neurodegeneration.

APPENDIX

Appendix A: Design of CHIP Plasmids

Plasmid 1: hCHIP Full Length:mCherry

Promoter: CHIP Promoter

ORF1: hCHIP

Linker: 3xGGGGS

ORF2: mCherry

Resistance: Ampicillin

Promoter Sequence:

GGGGGCGGGGCCTCTGCTGATGGGGCCGGCGGCTGGGGGCGGGGCCTCTGGATTGGGCGG

CTGCTGGGGGCGGGGCCTCTGCGGATGGGGCCGGCTGCTGGGGGCGGGGCCTCTGGATGG

GGCCGGCTGCCGGGGGAGGGGTCTCTGCGCGTTGGGACAGGGGCGGAACCCCAGGTGGTC

GGGACAGGCTGTTGCGGGAGCGCGCCCTCAGCGAAGCAAGTGAGGCATCTCACTGGGAAA

GTCGAATGTGTGTGGCGGCCGCCGCCGAGGCGGGTTCCGAAGAGACCTCAGCAGGGCAGG

CCAGGGCCTACGCGAACGCCCACCCTTAAGAGCGCGGGGACAGGGAACTGGAGCGTTCCT

CCCAGCCCCCGACGTCGCGGGCCCAGTGTCCCCGTCCAGGCTGGTTGGGCGCACGCGCGGC

CCCACTCGCCCCCACGCGTGCGTCCCCGCTGGTCCCGCCCCCGGCCGGAAGTTCCGGCGGC

GGAGCTGGGCCGGGCCCGAGCGGATCGCGGGCTCGGGCTGCGGGGCTCCGGCTGCGGGCG

CTGGGCCGCGAGGCGCGGAGCTTGGGAGCGGAGCCCAGGCCGTGCCGCGCGGCGCCAT

hCHIP:

ATGAAGGGCAAGGAGGAGAAGGAGGGCGGCGCACGGCTGGGCGCTGGCGGCGGAAGCCC
CGAGAAGAGCCCGAGCGCGCAGGAGCTCAAGGAGCAGGGCAATCGTCTGTTCGTGGGCCG
AAAGTACCCGGAGGCGGCGGCCTGCTACGGCCGCGCGATCACCCGGAACCCGCTGGTGGC
CGTGTATTACACCAACCGGGCCTTGTGCTACCTGAAGATGCAGCAGCACGAGCAGGCCCTG
GCCGACTGCCGGCGCGCCCTGGAGCTGGACGGGCAGTCTGTGAAGGCGCACTTCTTCCTGG
GGCAGTGCCAGCTGGAGATGGAGAGCTATGATGAGGCCATCGCCAATCTGCAGCGAGCTT
ACAGCCTGGCCAAGGAGCAGCGGCTGAACTTCGGGGACGACATCCCCAGCGCTCTTCGAAT
CGCGAAGAAGAAGCGCTGGAACAGCATTGAGGAGCGGCGCATCCACCAGGAGAGCGAGCT
GCACTCCTACCTCTCCAGGCTCATTGCCGCGGAGCGTGAGAGGGAGCTGGAAGAGTGCCAG
CGAAACCACGAGGGTGATGAGGACGACAGCCACGTCCGGGCCCAGCAGGCCTGCATTGAG
GCCAAGCACGACAAGTACATGGCGGACATGGACGAGCTTTTTTCTCAGGTGGATGAGAAG
AGGAAGAAGCGAGACATCCCCGACTACCTGTGTGGCAAGATCAGCTTTGAGCTGATGCGG
GAGCCGTGCATCACGCCCAGTGGCATCACCTACGACCGCAAGGACATCGAGGAGCACCTG
CAGCGTGTGGGTCATTTTGACCCCGTGACCCGGAGCCCCCTGACCCAGGAACAGCTCATCC
CCAACTTGGCTATGAAGGAGGTTATTGACGCATTCATCTCTGAGAATGGCTGGGTGGAGGA
CTACTAA

Linker:

TCTGGTGGCGGAGGCTCGGGCGGAGGTGGGTCGGGTGGCGGCGGATCA

mCherry:

ATGGTGAGCAAGGGCGAGGAGGATAACATGGCCATCATCAAGGAGTTCATGCGCTTCAAG

GTGCACATGGAGGGCTCCGTGAACGGCCACGAGTTCGAGATCGAGGGCGAGGGCGAGGGC

CGCCCCTACGAGGGCACCCAGACCGCCAAGCTGAAGGTGACCAAGGGTGGCCCCCTGCCC

TTCGCCTGGGACATCCTGTCCCCTCAGTTCATGTACGGCTCCAAGGCCTACGTGAAGCACCC

CGCCGACATCCCCGACTACTTGAAGCTGTCCTTCCCCGAGGGCTTCAAGTGGGAGCGCGTG

ATGAACTTCGAGGACGGCGGCGTGGTGACCGTGACCCAGGACTCCTCCCTGCAGGACGGC

GAGTTCATCTACAAGGTGAAGCTGCGCGGCACCAACTTCCCCTCCGACGGCCCCGTAATGC

AGAAGAAGACCATGGGCTGGGAGGCCTCCTCCGAGCGGATGTACCCCGAGGACGGCGCCC

TGAAGGGCGAGATCAAGCAGAGGCTGAAGCTGAAGGACGGCGGCCACTACGACGCTGAGG

TCAAGACCACCTACAAGGCCAAGAAGCCCGTGCAGCTGCCCGGCGCCTACAACGTCAACA

TCAAGTTGGACATCACCTCCCACAACGAGGACTACACCATCGTGGAACAGTACGAACGCGC

CGAGGGCCGCCACTCCACCGGCGGCATGGACGAGCTGTACAAGTAA

Plasmid 2: hCHIP UBox Mutant:mCherry

Promoter: CHIP Promoter

ORF1: hCHIP UBox Mutant

Linker: 3xGGGGS

ORF2: mCherry

Resistance: Ampicillin

Promoter Sequence:

GGGGGCGGGGCCTCTGCTGATGGGGCCGGCGGCTGGGGGCGGGGCCTCTGGATTGGGCGG

CTGCTGGGGGCGGGGCCTCTGCGGATGGGGCCGGCTGCTGGGGGCGGGGCCTCTGGATGG

GGCCGGCTGCCGGGGGAGGGGTCTCTGCGCGTTGGGACAGGGGCGGAACCCCAGGTGGTC

GGGACAGGCTGTTGCGGGAGCGCGCCCTCAGCGAAGCAAGTGAGGCATCTCACTGGGAAA

GTCGAATGTGTGTGGCGGCCGCCGCCGAGGCGGGTTCCGAAGAGACCTCAGCAGGGCAGG

CCAGGGCCTACGCGAACGCCCACCCTTAAGAGCGCGGGGACAGGGAACTGGAGCGTTCCT

CCCAGCCCCCGACGTCGCGGGCCCAGTGTCCCCGTCCAGGCTGGTTGGGCGCACGCGCGGC

CCCACTCGCCCCCACGCGTGCGTCCCCGCTGGTCCCGCCCCCGGCCGGAAGTTCCGGCGGC

GGAGCTGGGCCGGGCCCGAGCGGATCGCGGGCTCGGGCTGCGGGGCTCCGGCTGCGGGCG

CTGGGCCGCGAGGCGCGGAGCTTGGGAGCGGAGCCCAGGCCGTGCCGCGCGGCGCCAT

hCHIP UBox Mutant (H260Q)

ATGAAGGGCAAGGAGGAGAAGGAGGGCGGCGCACGGCTGGGCGCTGGCGGCGGAAGCCC

CGAGAAGAGCCCGAGCGCGCAGGAGCTCAAGGAGCAGGGCAATCGTCTGTTCGTGGGCCG

AAAGTACCCGGAGGCGGCGGCCTGCTACGGCCGCGCGATCACCCGGAACCCGCTGGTGGC

CGTGTATTACACCAACCGGGCCTTGTGCTACCTGAAGATGCAGCAGCACGAGCAGGCCCTG

GCCGACTGCCGGCGCGCCCTGGAGCTGGACGGGCAGTCTGTGAAGGCGCACTTCTTCCTGG

GGCAGTGCCAGCTGGAGATGGAGAGCTATGATGAGGCCATCGCCAATCTGCAGCGAGCTT

ACAGCCTGGCCAAGGAGCAGCGGCTGAACTTCGGGGACGACATCCCCAGCGCTCTTCGAAT

CGCGAAGAAGAAGCGCTGGAACAGCATTGAGGAGCGGCGCATCCACCAGGAGAGCGAGCT

GCACTCCTACCTCTCCAGGCTCATTGCCGCGGAGCGTGAGAGGGAGCTGGAAGAGTGCCAG

CGAAACCACGAGGGTGATGAGGACGACAGCCACGTCCGGGCCCAGCAGGCCTGCATTGAG

GCCAAGCACGACAAGTACATGGCGGACATGGACGAGCTTTTTTCTCAGGTGGATGAGAAG

AGGAAGAAGCGAGACATCCCCGACTACCTGTGTGGCAAGATCAGCTTTGAGCTGATGCGG

GAGCCGTGCATCACGCCCAGTGGCATCACCTACGACCGCAAGGACATCGAGGAGCAACTG

CAGCGTGTGGGTCATTTTGACCCCGTGACCCGGAGCCCCCTGACCCAGGAACAGCTCATCC
CCAACTTGGCTATGAAGGAGGTTATTGACGCATTCATCTCTGAGAATGGCTGGGTGGAGGA
CTACTGATAA

Linker:

TCTGGTGGCGGAGGCTCGGGCGGAGGTGGGTCGGGTGGCGGCGGATCA

mCherry:

ATGGTGAGCAAGGGCGAGGAGGATAACATGGCCATCATCAAGGAGTTCATGCGCTTCAAG
GTGCACATGGAGGGCTCCGTGAACGGCCACGAGTTCGAGATCGAGGGCGAGGGCGAGGGC
CGCCCCTACGAGGGCACCCAGACCGCCAAGCTGAAGGTGACCAAGGGTGGCCCCCTGCCC
TTCGCCTGGGACATCCTGTCCCCTCAGTTCATGTACGGCTCCAAGGCCTACGTGAAGCACCC
CGCCGACATCCCCGACTACTTGAAGCTGTCCTTCCCCGAGGGCTTCAAGTGGGAGCGCGTG
ATGAACTTCGAGGACGGCGGCGTGGTGACCGTGACCCAGGACTCCTCCCTGCAGGACGGC
GAGTTCATCTACAAGGTGAAGCTGCGCGGCACCAACTTCCCCTCCGACGGCCCCGTAATGC
AGAAGAAGACCATGGGCTGGGAGGCCTCCTCCGAGCGGATGTACCCCGAGGACGGCGCCC
TGAAGGGCGAGATCAAGCAGAGGCTGAAGCTGAAGGACGGCGGCCACTACGACGCTGAGG
TCAAGACCACCTACAAGGCCAAGAAGCCCGTGCAGCTGCCCGGCGCCTACAACGTCAACA
TCAAGTTGGACATCACCTCCCACAACGAGGACTACACCATCGTGGAACAGTACGAACGCGC
CGAGGGCCGCCACTCCACCGGCGGCATGGACGAGCTGTACAAGTAA

Plasmid 3: hCHIP TPR Mutant:mCherry

Promoter: CHIP Promoter

ORF1: hCHIP TPR Mutant

Linker: 3xGGGGS

ORF2: mCherry

Resistance: Ampicillin

Promoter Sequence:

GGGGGCGGGGCCTCTGCTGATGGGGCCGGCGGCTGGGGGCGGGGCCTCTGGATTGGGCGG

CTGCTGGGGGCGGGGCCTCTGCGGATGGGGCCGGCTGCTGGGGGCGGGGCCTCTGGATGG

GGCCGGCTGCCGGGGGAGGGGTCTCTGCGCGTTGGGACAGGGGCGGAACCCCAGGTGGTC

GGGACAGGCTGTTGCGGGAGCGCGCCCTCAGCGAAGCAAGTGAGGCATCTCACTGGGAAA

GTCGAATGTGTGTGGCGGCCGCCGCCGAGGCGGGTTCCGAAGAGACCTCAGCAGGGCAGG

CCAGGGCCTACGCGAACGCCCACCCTTAAGAGCGCGGGGACAGGGAACTGGAGCGTTCCT

CCCAGCCCCCGACGTCGCGGGCCCAGTGTCCCCGTCCAGGCTGGTTGGGCGCACGCGCGGC

CCCACTCGCCCCCACGCGTGCGTCCCCGCTGGTCCCGCCCCCGGCCGGAAGTTCCGGCGGC

GGAGCTGGGCCGGGCCCGAGCGGATCGCGGGCTCGGGCTGCGGGGCTCCGGCTGCGGGCG

CTGGGCCGCGAGGCGCGGAGCTTGGGAGCGGAGCCCAGGCCGTGCCGCGCGGCGCCAT

hCHIP TPR Mutant (K30A):

ATGAAGGGCAAGGAGGAGAAGGAGGGCGGCGCACGGCTGGGCGCTGGCGGCGGAAGCCC

CGAGAAGAGCCCGAGCGCGCAGGAGCTCGCGGAGCAGGGCAATCGTCTGTTCGTGGGCCG

AAAGTACCCGGAGGCGGCGGCCTGCTACGGCCGCGCGATCACCCGGAACCCGCTGGTGGC

CGTGTATTACACCAACCGGGCCTTGTGCTACCTGAAGATGCAGCAGCACGAGCAGGCCCTG

GCCGACTGCCGGCGCGCCCTGGAGCTGGACGGGCAGTCTGTGAAGGCGCACTTCTTCCTGG

GGCAGTGCCAGCTGGAGATGGAGAGCTATGATGAGGCCATCGCCAATCTGCAGCGAGCTT
ACAGCCTGGCCAAGGAGCAGCGGCTGAACTTCGGGGACGACATCCCCAGCGCTCTTCGAAT
CGCGAAGAAGAAGCGCTGGAACAGCATTGAGGAGCGGCGCATCCACCAGGAGAGCGAGCT
GCACTCCTACCTCTCCAGGCTCATTGCCGCGGAGCGTGAGAGGGAGCTGGAAGAGTGCCAG
CGAAACCACGAGGGTGATGAGGACGACAGCCACGTCCGGGCCCAGCAGGCCTGCATTGAG
GCCAAGCACGACAAGTACATGGCGGACATGGACGAGCTTTTTTCTCAGGTGGATGAGAAG
AGGAAGAAGCGAGACATCCCCGACTACCTGTGTGGCAAGATCAGCTTTGAGCTGATGCGG
GAGCCGTGCATCACGCCCAGTGGCATCACCTACGACCGCAAGGACATCGAGGAGCACCTG
CAGCGTGTGGGTCATTTTGACCCCGTGACCCGGAGCCCCCTGACCCAGGAACAGCTCATCC
CCAACTTGGCTATGAAGGAGGTTATTGACGCATTCATCTCTGAGAATGGCTGGGTGGAGGA
CTACTGATAA

Linker:

TCTGGTGGCGGAGGCTCGGGCGGAGGTGGGTCGGGTGGCGGCGGATCA

mCherry:

ATGGTGAGCAAGGGCGAGGAGGATAACATGGCCATCATCAAGGAGTTCATGCGCTTCAAG
GTGCACATGGAGGGCTCCGTGAACGGCCACGAGTTCGAGATCGAGGGCGAGGGCGAGGGC
CGCCCCTACGAGGGCACCCAGACCGCCAAGCTGAAGGTGACCAAGGGTGGCCCCCTGCCC
TTCGCCTGGGACATCCTGTCCCCTCAGTTCATGTACGGCTCCAAGGCCTACGTGAAGCACCC
CGCCGACATCCCCGACTACTTGAAGCTGTCCTTCCCCGAGGGCTTCAAGTGGGAGCGCGTG
ATGAACTTCGAGGACGGCGGCGTGGTGACCGTGACCCAGGACTCCTCCCTGCAGGACGGC
GAGTTCATCTACAAGGTGAAGCTGCGCGGCACCAACTTCCCCTCCGACGGCCCCGTAATGC

AGAAGAAGACCATGGGCTGGGAGGCCTCCTCCGAGCGGATGTACCCCGAGGACGGCGCCC

TGAAGGGCGAGATCAAGCAGAGGCTGAAGCTGAAGGACGGCGGCCACTACGACGCTGAGG

TCAAGACCACCTACAAGGCCAAGAAGCCCGTGCAGCTGCCCGGCGCCTACAACGTCAACA

TCAAGTTGGACATCACCTCCCACAACGAGGACTACACCATCGTGGAACAGTACGAACGCGC

CGAGGGCCGCCACTCCACCGGCGGCATGGACGAGCTGTACAAGTA

Abbott NJ (2013) Blood-brain barrier structure and function and the challenges for CNS drug delivery. J Inherit Metab Dis 36:437-449.

Accardi F, Toscani D, Bolzoni M, Dalla Palma B, Aversa F, Giuliani N (2015) Mechanism of Action of Bortezomib and the New Proteasome Inhibitors on Myeloma Cells and the Bone Microenvironment: Impact on Myeloma-Induced Alterations of Bone Remodeling. Biomed Res Int 2015:172458.

Adelborg K, Szepligeti S, Sundboll J, Horvath-Puho E, Henderson VW, Ording A, Pedersen L, Sorensen HT (2017) Risk of Stroke in Patients With Heart Failure: A Population-Based 30-Year Cohort Study. Stroke; a journal of cerebral circulation 48:1161-1168.

Aguirre JD, Dunkerley KM, Mercier P, Shaw GS (2017) Structure of phosphorylated UBL domain and insights into PINK1-orchestrated parkin activation. Proceedings of the National Academy of Sciences of the United States of America 114:298-303.

Ahlqvist G, Landin S, Wroblewski R (1975) Ultrastructure of skeletal muscle in patients with Parkinson's disease and upper motor lesions. Lab Invest 32:673-679.

Al Nimer F, Strom M, Lindblom R, Aeinehband S, Bellander BM, Nyengaard JR, Lidman O, Piehl F (2013) Naturally occurring variation in the Glutathione-S-Transferase 4 gene determines neurodegeneration after traumatic brain injury. Antioxidants & redox signaling 18:784-794.

Antonny B, Burd C, De Camilli P, Chen E, Daumke O, Faelber K, Ford M, Frolov VA, Frost A, Hinshaw JE, Kirchhausen T, Kozlov MM, Lenz M, Low HH, McMahon H, Merrifield C, Pollard TD, Robinson PJ, Roux A, Schmid S (2016) Membrane fission by dynamin: what we know and what we need to know. The EMBO journal 35:2270-2284.

Aravind L, Koonin EV (2000) The U box is a modified RING finger - a common domain in ubiquitination. Curr Biol 10:R132-134.

Archer SL (2013) Mitochondrial dynamics--mitochondrial fission and fusion in human diseases. The New England journal of medicine 369:2236-2251.

Arkin MR, Tang Y, Wells JA (2014) Small-molecule inhibitors of protein-protein interactions: progressing toward the reality. Chem Biol 21:1102-1114.

Arndt V, Rogon C, Hohfeld J (2007) To be, or not to be--molecular chaperones in protein degradation. Cellular and molecular life sciences : CMLS 64:2525-2541.

Ashar FN, Moes A, Moore AZ, Grove ML, Chaves PHM, Coresh J, Newman AB, Matteini AM, Bandeen-Roche K, Boerwinkle E, Walston JD, Arking DE (2015) Association of mitochondrial DNA levels with frailty and all-cause mortality. J Mol Med (Berl) 93:177-186.

Bagatell R, Paine-Murrieta GD, Taylor CW, Pulcini EJ, Akinaga S, Benjamin IJ, Whitesell L (2000) Induction of a heat shock factor 1-dependent stress response alters the cytotoxic activity of hsp90-binding agents. Clin Cancer Res 6:3312-3318.

Ballinger CA, Connell P, Wu Y, Hu Z, Thompson LJ, Yin LY, Patterson C (1999) Identification of CHIP, a novel tetratricopeptide repeat-containing protein that interacts with heat shock proteins and negatively regulates chaperone functions. Molecular and cellular biology 19:4535-4545.

Bandeen-Roche K, Xue QL, Ferrucci L, Walston J, Guralnik JM, Chaves P, Zeger SL, Fried LP (2006) Phenotype of frailty: characterization in the women's health and aging studies. J Gerontol A Biol Sci Med Sci 61:262-266.

Beal F, Lang A (2006) The proteasomal inhibition model of Parkinson's disease: "Boon or bust"? Ann Neurol 60:158-161.

Bellmann K, Jaattela M, Wissing D, Burkart V, Kolb H (1996) Heat shock protein hsp70 overexpression confers resistance against nitric oxide. FEBS letters 391:185-188.
Bernardo BC, Sapra G, Patterson NL, Cemerlang N, Kiriazis H, Ueyama T, Febbraio MA, McMullen JR (2015) Long-Term Overexpression of Hsp70 Does Not Protect against Cardiac Dysfunction and Adverse Remodeling in a MURC Transgenic Mouse Model with Chronic Heart Failure and Atrial Fibrillation. PloS one 10:e0145173.
Bertelsen EB, Chang L, Gestwicki JE, Zuiderweg ER (2009) Solution conformation of wild-type E. coli Hsp70 (DnaK) chaperone complexed with ADP and substrate. Proceedings of the National Academy of Sciences of the United States of America 106:8471-8476.
Betarbet R, Sherer TB, Di Monte DA, Greenamyre JT (2002) Mechanistic approaches to Parkinson's disease pathogenesis. Brain Pathol 12:499-510.
Bettencourt C, de Yebenes JG, Lopez-Sendon JL, Shomroni O, Zhang X, Qian SB, Bakker IM, Heetveld S, Ros R, Quintans B, Sobrido MJ, Bevova MR, Jain S, Bugiani M, Heutink P, Rizzu P (2015) Clinical and Neuropathological Features of Spastic Ataxia in a Spanish Family with Novel Compound Heterozygous Mutations in STUB1. Cerebellum 14:378-381.
Bhowmick P, Pancsa R, Guharoy M, Tompa P (2013) Functional diversity and structural disorder in the human ubiquitination pathway. PloS one 8:e65443.
Bielskiene K, Bagdoniene L, Mozuraitiene J, Kazbariene B, Janulionis E (2015) E3 ubiquitin ligases as drug targets and prognostic biomarkers in melanoma. Medicina (Kaunas) 51:1-9.
Birsa N, Norkett R, Wauer T, Mevissen TE, Wu HC, Foltynie T, Bhatia K, Hirst WD, Komander D, Plun-Favreau H, Kittler JT (2014) Lysine 27 ubiquitination of the mitochondrial transport protein Miro is dependent on serine 65 of the Parkin ubiquitin ligase. The Journal of biological chemistry 289:14569-14582.
Brichta L, Greengard P (2014) Molecular determinants of selective dopaminergic vulnerability in Parkinson's disease: an update. Front Neuroanat 8:152.
Brown JE, Zeiger SL, Hettinger JC, Brooks JD, Holt B, Morrow JD, Musiek ES, Milne G, McLaughlin B (2010) Essential role of the redox-sensitive kinase p66shc in determining energetic and oxidative status and cell fate in neuronal preconditioning. The Journal of neuroscience : the official journal of the Society for Neuroscience 30:5242-5252.
Bubber P, Haroutunian V, Fisch G, Blass JP, Gibson GE (2005) Mitochondrial abnormalities in Alzheimer brain: mechanistic implications. Ann Neurol 57:695-703.
Bulatov E, Ciulli A (2015) Targeting Cullin-RING E3 ubiquitin ligases for drug discovery: structure, assembly and small-molecule modulation. The Biochemical journal 467:365-386.
Burman JL, Pickles S, Wang C, Sekine S, Vargas JNS, Zhang Z, Youle AM, Nezich CL, Wu X, Hammer JA, Youle RJ (2017) Mitochondrial fission facilitates the selective mitophagy of protein aggregates. The Journal of cell biology 216:3231-3247.
Butlen-Ducuing F, Petavy F, Guizzaro L, Zienowicz M, Haas M, Alteri E, Salmonson T, Corruble E (2016) Regulatory watch: Challenges in drug development for central nervous system disorders: a European Medicines Agency perspective. Nat Rev Drug Discov 15:813-814.
Butler LM, Ferraldeschi R, Armstrong HK, Centenera MM, Workman P (2015) Maximizing the Therapeutic Potential of HSP90 Inhibitors. Mol Cancer Res 13:1445-1451.
Cagalinec M, Safiulina D, Liiv M, Liiv J, Choubey V, Wareski P, Veksler V, Kaasik A (2013) Principles of the mitochondrial fusion and fission cycle in neurons. Journal of cell science 126:2187-2197.
Cannon JR, Greenamyre JT (2013) Gene-environment interactions in Parkinson's disease: specific evidence in humans and mammalian models. Neurobiol Dis 57:38-46.

Casarejos MJ, Perucho J, Lopez-Sendon JL, Garcia de Yebenes J, Bettencourt C, Gomez A, Ruiz C, Heutink P, Rizzu P, Mena MA (2014) Trehalose improves human fibroblast deficits in a new CHIP-mutation related ataxia. PloS one 9:e106931.

Cesari M, Kritchevsky SB, Nicklas B, Kanaya AM, Patrignani P, Tacconelli S, Tranah GJ, Tognoni G, Harris TB, Incalzi RA, Newman AB, Pahor M, Health ABCs (2012) Oxidative damage, platelet activation, and inflammation to predict mobility disability and mortality in older persons: results from the health aging and body composition study. J Gerontol A Biol Sci Med Sci 67:671-676.

Chan DC (2012) Fusion and fission: interlinked processes critical for mitochondrial health. Annual review of genetics 46:265-287.

Chang DT, Reynolds IJ (2006) Differences in mitochondrial movement and morphology in young and mature primary cortical neurons in culture. Neuroscience 141:727-736.

Charan RA, LaVoie MJ (2015) Pathologic and therapeutic implications for the cell biology of parkin. Mol Cell Neurosci 66:62-71.

Chen CM, Wu YR, Cheng ML, Liu JL, Lee YM, Lee PW, Soong BW, Chiu DT (2007) Increased oxidative damage and mitochondrial abnormalities in the peripheral blood of Huntington's disease patients. Biochemical and biophysical research communications 359:335-340.

Chen D, Gao F, Li B, Wang H, Xu Y, Zhu C, Wang G (2010) Parkin mono-ubiquitinates Bcl-2 and regulates autophagy. The Journal of biological chemistry 285:38214-38223.

Chen H, Chan DC (2006) Critical dependence of neurons on mitochondrial dynamics. Current opinion in cell biology 18:453-459.

Chen H, Chan DC (2009) Mitochondrial dynamics--fusion, fission, movement, and mitophagy--in neurodegenerative diseases. Human molecular genetics 18:R169-176.

Chen J, Xue J, Ruan J, Zhao J, Tang B, Duan R (2017) Drosophila CHIP protects against mitochondrial dysfunction by acting downstream of Pink1 in parallel with Parkin. FASEB journal : official publication of the Federation of American Societies for Experimental Biology 31:5234-5245.

Chen Y, Stevens B, Chang J, Milbrandt J, Barres BA, Hell JW (2008) NS21: re-defined and modified supplement B27 for neuronal cultures. Journal of neuroscience methods 171:239-247.

Cherra SJ, 3rd, Chu CT (2008) Autophagy in neuroprotection and neurodegeneration: A question of balance. Future neurology 3:309-323.

Chico LK, Van Eldik LJ, Watterson DM (2009) Targeting protein kinases in central nervous system disorders. Nat Rev Drug Discov 8:892-909.

Choi HJ, Kim SW, Lee SY, Hwang O (2003) Dopamine-dependent cytotoxicity of tetrahydrobiopterin: a possible mechanism for selective neurodegeneration in Parkinson's disease. Journal of neurochemistry 86:143-152.

Chu CT et al. (2013) Cardiolipin externalization to the outer mitochondrial membrane acts as an elimination signal for mitophagy in neuronal cells. Nat Cell Biol 15:1197-1205.

Cummings CJ, Sun YL, Opal P, Antalffy B, Mestril R, Orr HT, Dillmann WH, Zoghbi HY (2001) Over-expression of inducible HSP70 chaperone suppresses neuropathology and improves motor function in SCA1 mice. Human molecular genetics 10:1511-1518.

Dai Q, Zhang CL, Wu YX, McDonough H, Whaley RA, Godfrey V, Li HH, Madamanchi N, Xu W, Neckers L, Cyr D, Patterson C (2003) CHIP activates HSF1 and confers protection against apoptosis and cellular stress. Embo Journal 22:5446-5458.

Deepa SS, Bhaskaran S, Espinoza S, Brooks SV, McArdle A, Jackson MJ, Van Remmen H, Richardson A (2017) A new mouse model of frailty: the Cu/Zn superoxide dismutase knockout mouse. Geroscience 39:187-198.
Detmer SA, Chan DC (2007) Functions and dysfunctions of mitochondrial dynamics. Nature reviews Molecular cell biology 8:870-879.
Dickey CA, Patterson C, Dickson D, Petrucelli L (2007a) Brain CHIP: removing the culprits in neurodegenerative disease. Trends in Molecular Medicine 13:32-38.
Dickey CA, Kamal A, Lundgren K, Klosak N, Bailey RM, Dunmore J, Ash P, Shoraka S, Zlatkovic J, Eckman CB, Patterson C, Dickson DW, Nahman NS, Jr., Hutton M, Burrows F, Petrucelli L (2007b) The high-affinity HSP90-CHIP complex recognizes and selectively degrades phosphorylated tau client proteins. Journal of Clinical Investigation 117:648-658.
Ding WX, Yin XM (2012) Mitophagy: mechanisms, pathophysiological roles, and analysis. Biol Chem 393:547-564.
Ding WX, Ni HM, Li M, Liao Y, Chen X, Stolz DB, Dorn GW, 2nd, Yin XM (2010) Nix is critical to two distinct phases of mitophagy, reactive oxygen species-mediated autophagy induction and Parkin-ubiquitin-p62-mediated mitochondrial priming. The Journal of biological chemistry 285:27879-27890.
Dixit S, Fessel JP, Harrison FE (2017) Mitochondrial dysfunction in the APP/PSEN1 mouse model of Alzheimer's disease and a novel protective role for ascorbate. Free radical biology & medicine 112:515-523.
Dongworth RK, Mukherjee UA, Hall AR, Astin R, Ong SB, Yao Z, Dyson A, Szabadkai G, Davidson SM, Yellon DM, Hausenloy DJ (2014) DJ-1 protects against cell death following acute cardiac ischemia-reperfusion injury. Cell Death Dis 5:e1082.
Doris KS, Rumsby EL, Morgan BA (2012) Oxidative stress responses involve oxidation of a conserved ubiquitin pathway enzyme. Molecular and cellular biology 32:4472-4481.
Dorsey ER, Constantinescu R, Thompson JP, Biglan KM, Holloway RG, Kieburtz K, Marshall FJ, Ravina BM, Schifitto G, Siderowf A, Tanner CM (2007) Projected number of people with Parkinson disease in the most populous nations, 2005 through 2030. Neurology 68:384-386.
Egan DF, Shackelford DB, Mihaylova MM, Gelino S, Kohnz RA, Mair W, Vasquez DS, Joshi A, Gwinn DM, Taylor R, Asara JM, Fitzpatrick J, Dillin A, Viollet B, Kundu M, Hansen M, Shaw RJ (2011) Phosphorylation of ULK1 (hATG1) by AMP-activated protein kinase connects energy sensing to mitophagy. Science 331:456-461.
Erecinska M, Silver IA (1989) ATP and brain function. Journal of cerebral blood flow and metabolism : official journal of the International Society of Cerebral Blood Flow and Metabolism 9:2-19.
Evans CG, Chang L, Gestwicki JE (2010) Heat shock protein 70 (hsp70) as an emerging drug target. J Med Chem 53:4585-4602.
Faucheux BA, Martin ME, Beaumont C, Hauw JJ, Agid Y, Hirsch EC (2003) Neuromelanin associated redox-active iron is increased in the substantia nigra of patients with Parkinson's disease. Journal of neurochemistry 86:1142-1148.
Fiesel FC, Moussaud-Lamodiere EL, Ando M, Springer W (2014) A specific subset of E2 ubiquitin-conjugating enzymes regulate Parkin activation and mitophagy differently. Journal of cell science 127:3488-3504.

Franklin TB, Krueger-Naug AM, Clarke DB, Arrigo AP, Currie RW (2005) The role of heat shock proteins Hsp70 and Hsp27 in cellular protection of the central nervous system. Int J Hyperthermia 21:379-392.
Fried LP, Tangen CM, Walston J, Newman AB, Hirsch C, Gottdiener J, Seeman T, Tracy R, Kop WJ, Burke G, McBurnie MA, Cardiovascular Health Study Collaborative Research G (2001) Frailty in older adults: evidence for a phenotype. J Gerontol A Biol Sci Med Sci 56:M146-156.
Galluzzi L et al. (2017) Molecular definitions of autophagy and related processes. The EMBO journal 36:1811-1836.
Gardner RC, Burke JF, Nettiksimmons J, Goldman S, Tanner CM, Yaffe K (2015) Traumatic brain injury in later life increases risk for Parkinson disease. Ann Neurol 77:987-995.
Geisler S, Holmstrom KM, Skujat D, Fiesel FC, Rothfuss OC, Kahle PJ, Springer W (2010) PINK1/Parkin-mediated mitophagy is dependent on VDAC1 and p62/SQSTM1. Nature Cell Biology 12:119-U170.
Gestwicki JE, Garza D (2012) Protein quality control in neurodegenerative disease. Prog Mol Biol Transl Sci 107:327-353.
Ghobrial IM, Savona MR, Vij R, Siegel DS, Badros A, Kaufman JL, Raje N, Jakubowiak A, Obreja M, Berdeja JG (2016) Final Results from a Multicenter, Open-Label, Dose-Escalation Phase 1b/2 Study of Single-Agent Oprozomib in Patients with Hematologic Malignancies. Blood 128.
Gidday JM (2006) Cerebral preconditioning and ischaemic tolerance. Nature reviews Neuroscience 7:437-448.
Gispert S et al. (2009) Parkinson phenotype in aged PINK1-deficient mice is accompanied by progressive mitochondrial dysfunction in absence of neurodegeneration. PloS one 4:e5777.
Go AS et al. (2013) Heart disease and stroke statistics--2013 update: a report from the American Heart Association. Circulation 127:e6-e245.
Goldberg MS, Fleming SM, Palacino JJ, Cepeda C, Lam HA, Bhatnagar A, Meloni EG, Wu NP, Ackerson LC, Klapstein GJ, Gajendiran M, Roth BL, Chesselet MF, Maidment NT, Levine MS, Shen J (2003) Parkin-deficient mice exhibit nigrostriatal deficits but not loss of dopaminergic neurons. Journal of Biological Chemistry 278:43628-43635.
Goldenberg SJ, Marblestone JG, Mattern MR, Nicholson B (2010) Strategies for the identification of ubiquitin ligase inhibitors. Biochem Soc Trans 38:132-136.
Golpich M, Amini E, Mohamed Z, Azman Ali R, Mohamed Ibrahim N, Ahmadiani A (2017) Mitochondrial Dysfunction and Biogenesis in Neurodegenerative diseases: Pathogenesis and Treatment. CNS Neurosci Ther 23:5-22.
Gonzalez-Ruiz D, Gohlke H (2006) Targeting protein-protein interactions with small molecules: challenges and perspectives for computational binding epitope detection and ligand finding. Current medicinal chemistry 13:2607-2625.
Gorell JM, Johnson CC, Rybicki BA, Peterson EL, Richardson RJ (1998) The risk of Parkinson's disease with exposure to pesticides, farming, well water, and rural living. Neurology 50:1346-1350.
Gorell JM, Johnson CC, Rybicki BA, Peterson EL, Kortsha GX, Brown GG, Richardson RJ (1997) Occupational exposures to metals as risk factors for Parkinson's disease. Neurology 48:650-658.
Grabbe C, Husnjak K, Dikic I (2011) The spatial and temporal organization of ubiquitin networks. Nature reviews Molecular cell biology 12:295-307.

Greene AW, Grenier K, Aguileta MA, Muise S, Farazifard R, Haque ME, McBride HM, Park DS, Fon EA (2012) Mitochondrial processing peptidase regulates PINK1 processing, import and Parkin recruitment. EMBO reports 13:378-385.
Groitl B, Jakob U (2014) Thiol-based redox switches. Biochim Biophys Acta 1844:1335-1343.
Grunewald A, Voges L, Rakovic A, Kasten M, Vandebona H, Hemmelmann C, Lohmann K, Orolicki S, Ramirez A, Schapira AH, Pramstaller PP, Sue CM, Klein C (2010) Mutant Parkin impairs mitochondrial function and morphology in human fibroblasts. PloS one 5:e12962.
Guang MHZ, Bianchi G (2017) Targeting Protein Synthesis and Degradation In Multiple Myeloma: A Look At What's On the Horizon. American Journal of Hematology/Oncology 13:4-14.
Halliwell B, Gutteridge JMC (1989) Free radicals in biology and medicine, 2nd Edition. Oxford
New York: Clarendon Press ;
Oxford University Press.
Ham AJ (2005) Proteolytic Digestion Protocols. In: The Encyclopedia of Mass Spectrometry (Caprioli RM, Gross ML, eds), pp 10-17. Kidlington, Oxford, UK: Elsevier Ltd.
Hammond-Martel I, Yu H, Affar el B (2012) Roles of ubiquitin signaling in transcription regulation. Cell Signal 24:410-421.
Hampe C, Ardila-Osorio H, Fournier M, Brice A, Corti O (2006) Biochemical analysis of Parkinson's disease-causing variants of Parkin, an E3 ubiquitin-protein ligase with monoubiquitylation capacity. Human molecular genetics 15:2059-2075.
Hanada T, Noda NN, Satomi Y, Ichimura Y, Fujioka Y, Takao T, Inagaki F, Ohsumi Y (2007) The Atg12-Atg5 conjugate has a novel E3-like activity for protein lipidation in autophagy. The Journal of biological chemistry 282:37298-37302.
Hara T, Nakamura K, Matsui M, Yamamoto A, Nakahara Y, Suzuki-Migishima R, Yokoyama M, Mishima K, Saito I, Okano H, Mizushima N (2006) Suppression of basal autophagy in neural cells causes neurodegenerative disease in mice. Nature 441:885-889.
Harlin H, Reffey SB, Duckett CS, Lindsten T, Thompson CB (2001) Characterization of XIAP-deficient mice. Molecular and cellular biology 21:3604-3608.
Hartwig A (2001) Zinc finger proteins as potential targets for toxic metal ions: differential effects on structure and function. Antioxidants & redox signaling 3:625-634.
Hatakeyama S, Yada M, Matsumoto M, Ishida N, Nakayama KI (2001) U box proteins as a new family of ubiquitin-protein ligases. The Journal of biological chemistry 276:33111-33120.
Hauser DN, Hastings TG (2013) Mitochondrial dysfunction and oxidative stress in Parkinson's disease and monogenic parkinsonism. Neurobiol Dis 51:35-42.
Hayer SN, Deconinck T, Bender B, Smets K, Zuchner S, Reich S, Schols L, Schule R, De Jonghe P, Baets J, Synofzik M (2017) STUB1/CHIP mutations cause Gordon Holmes syndrome as part of a widespread multisystemic neurodegeneration: evidence from four novel mutations. Orphanet J Rare Dis 12:31.
Heimdal K, Sanchez-Guixe M, Aukrust I, Bollerslev J, Bruland O, Jablonski GE, Erichsen AK, Gude E, Koht JA, Erdal S, Fiskerstrand T, Haukanes BI, Boman H, Bjorkhaug L, Tallaksen CM, Knappskog PM, Johansson S (2014) STUB1 mutations in autosomal recessive ataxias - evidence for mutation-specific clinical heterogeneity. Orphanet J Rare Dis 9:146.
Hohfeld J, Cyr DM, Patterson C (2001) From the cradle to the grave: molecular chaperones that may choose between folding and degradation. EMBO reports 2:885-890.
Holzbeierlein JM, Windsperger A, Vielhauer G (2010) Hsp90: a drug target? Curr Oncol Rep 12:95-101.

Hristova VA, Beasley SA, Rylett RJ, Shaw GS (2009) Identification of a Novel Zn2+-binding Domain in the Autosomal Recessive Juvenile Parkinson-related E3 Ligase Parkin. Journal of Biological Chemistry 284:14978-14986.
Huang X, Dixit VM (2016) Drugging the undruggables: exploring the ubiquitin system for drug development. Cell Res 26:484-498.
Husnjak K, Dikic I (2012) Ubiquitin-binding proteins: decoders of ubiquitin-mediated cellular functions. Annual review of biochemistry 81:291-322.
Imai Y, Soda M, Hatakeyama S, Akagi T, Hashikawa T, Nakayama KI, Takahashi R (2002) CHIP is associated with Parkin, a gene responsible for familial Parkinson's disease, and enhances its ubiquitin ligase activity. Molecular cell 10:55-67.
Inden M, Yanagisawa D, Hijioka M, Ariga H, Kitamura Y (2017) Therapeutic Activities of DJ-1 and Its Binding Compounds Against Neurodegenerative Diseases. Advances in experimental medicine and biology 1037:187-202.
Itakura E, Kishi-Itakura C, Koyama-Honda I, Mizushima N (2012) Structures containing Atg9A and the ULK1 complex independently target depolarized mitochondria at initial stages of Parkin-mediated mitophagy. Journal of cell science 125:1488-1499.
Jiang J, Ballinger CA, Wu Y, Dai Q, Cyr DM, Hohfeld J, Patterson C (2001) CHIP is a U-box-dependent E3 ubiquitin ligase: identification of Hsc70 as a target for ubiquitylation. The Journal of biological chemistry 276:42938-42944.
Jiang P, Mizushima N (2014) Autophagy and human diseases. Cell Res 24:69-79.
Jin SM, Youle RJ (2013) The accumulation of misfolded proteins in the mitochondrial matrix is sensed by PINK1 to induce PARK2/Parkin-mediated mitophagy of polarized mitochondria. Autophagy 9:1750-1757.
Jinwal UK, Miyata Y, Koren J, 3rd, Jones JR, Trotter JH, Chang L, O'Leary J, Morgan D, Lee DC, Shults CL, Rousaki A, Weeber EJ, Zuiderweg ER, Gestwicki JE, Dickey CA (2009) Chemical manipulation of hsp70 ATPase activity regulates tau stability. The Journal of neuroscience : the official journal of the Society for Neuroscience 29:12079-12088.
Joo JH, Dorsey FC, Joshi A, Hennessy-Walters KM, Rose KL, McCastlain K, Zhang J, Iyengar R, Jung CH, Suen DF, Steeves MA, Yang CY, Prater SM, Kim DH, Thompson CB, Youle RJ, Ney PA, Cleveland JL, Kundu M (2011) Hsp90-Cdc37 chaperone complex regulates Ulk1- and Atg13-mediated mitophagy. Molecular cell 43:572-585.
Joshi V, Amanullah A, Upadhyay A, Mishra R, Kumar A, Mishra A (2016) A Decade of Boon or Burden: What Has the CHIP Ever Done for Cellular Protein Quality Control Mechanism Implicated in Neurodegeneration and Aging? Front Mol Neurosci 9:93.
Kageyama Y, Hoshijima M, Seo K, Bedja D, Sysa-Shah P, Andrabi SA, Chen W, Hoke A, Dawson VL, Dawson TM, Gabrielson K, Kass DA, Iijima M, Sesaki H (2014) Parkin-independent mitophagy requires Drp1 and maintains the integrity of mammalian heart and brain. The EMBO journal 33:2798-2813.
Kakkar V, Kuiper EF, Pandey A, Braakman I, Kampinga HH (2016) Versatile members of the DNAJ family show Hsp70 dependent anti-aggregation activity on RING1 mutant parkin C289G. Sci Rep 6:34830.
Kanack AJ, Newsom OJ, Scaglione KM (2018) Most mutations that cause spinocerebellar ataxia autosomal recessive type 16 (SCAR16) destabilize the protein quality-control E3 ligase CHIP. The Journal of biological chemistry 293:2735-2743.

Kane LA, Lazarou M, Fogel AI, Li Y, Yamano K, Sarraf SA, Banerjee S, Youle RJ (2014) PINK1 phosphorylates ubiquitin to activate Parkin E3 ubiquitin ligase activity. The Journal of cell biology 205:143-153.
Kaneko M, Koike H, Saito R, Kitamura Y, Okuma Y, Nomura Y (2010) Loss of HRD1-mediated protein degradation causes amyloid precursor protein accumulation and amyloid-beta generation. The Journal of neuroscience : the official journal of the Society for Neuroscience 30:3924-3932.
Kaneko Y, Tajiri N, Shojo H, Borlongan CV (2014) Oxygen-glucose-deprived rat primary neural cells exhibit DJ-1 translocation into healthy mitochondria: a potent stroke therapeutic target. CNS Neurosci Ther 20:275-281.
Kang JF, Tang BS, Guo JF (2016) The Progress of Induced Pluripotent Stem Cells as Models of Parkinson's Disease. Stem Cells Int 2016:4126214.
Kawajiri S, Saiki S, Sato S, Sato F, Hatano T, Eguchi H, Hattori N (2010) PINK1 is recruited to mitochondria with parkin and associates with LC3 in mitophagy. FEBS letters 584:1073-1079.
Kawarai T, Miyamoto R, Shimatani Y, Orlacchio A, Kaji R (2016) Choreoathetosis, Dystonia, and Myoclonus in 3 Siblings With Autosomal Recessive Spinocerebellar Ataxia Type 16. JAMA Neurol 73:888-890.
Kazlauskaite A, Kelly V, Johnson C, Baillie C, Hastie CJ, Peggie M, Macartney T, Woodroof HI, Alessi DR, Pedrioli PG, Muqit MM (2014) Phosphorylation of Parkin at Serine65 is essential for activation: elaboration of a Miro1 substrate-based assay of Parkin E3 ligase activity. Open Biol 4:130213.
Kee Y, Huibregtse JM (2007) Regulation of catalytic activities of HECT ubiquitin ligases. Biochemical and biophysical research communications 354:329-333.
Kessner D, Chambers M, Burke R, Agus D, Mallick P (2008) ProteoWizard: open source software for rapid proteomics tools development. Bioinformatics 24:2534-2536.
Kim E, Wang B, Sastry N, Masliah E, Nelson PT, Cai H, Liao FF (2016a) NEDD4-mediated HSF1 degradation underlies α-synucleinopathy. Human molecular genetics 25:211-222.
Kim M et al. (2016b) Mutation in ATG5 reduces autophagy and leads to ataxia with developmental delay. Elife 5.
Kim S, Pevzner PA (2014) MS-GF+ makes progress towards a universal database search tool for proteomics. Nat Commun 5:5277.
Kim SA, Yoon JH, Kim DK, Kim SG, Ahn SG (2005) CHIP interacts with heat shock factor 1 during heat stress. FEBS letters 579:6559-6563.
Kim Y, Park J, Kim S, Song S, Kwon SK, Lee SH, Kitada T, Kim JM, Chung J (2008) PINK1 controls mitochondrial localization of Parkin through direct phosphorylation. Biochemical and biophysical research communications 377:975-980.
Kitada T, Tong Y, Gautier CA, Shen J (2009) Absence of nigral degeneration in aged parkin/DJ-1/PINK1 triple knockout mice. Journal of neurochemistry 111:696-702.
Kitagawa K, Matsumoto M, Tagaya M, Hata R, Ueda H, Niinobe M, Handa N, Fukunaga R, Kimura K, Mikoshiba K, et al. (1990) 'Ischemic tolerance' phenomenon found in the brain. Brain research 528:21-24.
Klein C, Westenberger A (2012) Genetics of Parkinson's disease. Cold Spring Harb Perspect Med 2:a008888.
Klionsky DJ et al. (2016) Guidelines for the use and interpretation of assays for monitoring autophagy (3rd edition). Autophagy 12:1-222.

Komatsu M, Waguri S, Chiba T, Murata S, Iwata J, Tanida I, Ueno T, Koike M, Uchiyama Y, Kominami E, Tanaka K (2006) Loss of autophagy in the central nervous system causes neurodegeneration in mice. Nature 441:880-884.
Kopp Y, Lang WH, Schuster TB, Martinez-Limon A, Hofbauer HF, Ernst R, Calloni G, Vabulas RM (2017) CHIP as a membrane-shuttling proteostasis sensor. Elife 6.
Kornberg A (1989) For the love of enzymes : the odyssey of a biochemist. Cambridge, Mass.: Harvard University Press.
Koyano F, Okatsu K, Kosako H, Tamura Y, Go E, Kimura M, Kimura Y, Tsuchiya H, Yoshihara H, Hirokawa T, Endo T, Fon EA, Trempe J-F, Saeki Y, Tanaka K, Matsuda N (2014) Ubiquitin is phosphorylated by PINK1 to activate parkin. Nature 510:162-+.
Krebs RA, Feder ME (1997) Deleterious consequences of Hsp70 overexpression in Drosophila melanogaster larvae. Cell Stress Chaperones 2:60-71.
Kubli DA, Zhang X, Lee Y, Hanna RA, Quinsay MN, Nguyen CK, Jimenez R, Petrosyan S, Murphy AN, Gustafsson AB (2013) Parkin protein deficiency exacerbates cardiac injury and reduces survival following myocardial infarction. The Journal of biological chemistry 288:915-926.
Kuhn DJ, Chen Q, Voorhees PM, Strader JS, Shenk KD, Sun CM, Demo SD, Bennett MK, van Leeuwen FW, Chanan-Khan AA, Orlowski RZ (2007) Potent activity of carfilzomib, a novel, irreversible inhibitor of the ubiquitin-proteasome pathway, against preclinical models of multiple myeloma. Blood 110:3281-3290.
Kumar P, Pradhan K, Karunya R, Ambasta RK, Querfurth HW (2012) Cross-functional E3 ligases Parkin and C-terminus Hsp70-interacting protein in neurodegenerative disorders. Journal of neurochemistry 120:350-370.
Kwakye GF, McMinimy RA, Aschner M (2016) Disease-Toxicant Interactions in Parkinson's Disease Neuropathology. Neurochem Res.
Lazarou M, Narendra DP, Jin SM, Tekle E, Banerjee S, Youle RJ (2013) PINK1 drives Parkin self-association and HECT-like E3 activity upstream of mitochondrial binding. The Journal of cell biology 200:163-172.
Lazarou M, Sliter DA, Kane LA, Sarraf SA, Wang C, Burman JL, Sideris DP, Fogel AI, Youle RJ (2015) The ubiquitin kinase PINK1 recruits autophagy receptors to induce mitophagy. Nature 524:309-314.
Lee HC, Yin PH, Chi CW, Wei YH (2002) Increase in mitochondrial mass in human fibroblasts under oxidative stress and during replicative cell senescence. J Biomed Sci 9:517-526.
Lee JY, Nagano Y, Taylor JP, Lim KL, Yao TP (2010) Disease-causing mutations in parkin impair mitochondrial ubiquitination, aggregation, and HDAC6-dependent mitophagy. The Journal of cell biology 189:671-679.
Lee S, Zhang C, Liu X (2015) Role of glucose metabolism and ATP in maintaining PINK1 levels during Parkin-mediated mitochondrial damage responses. The Journal of biological chemistry 290:904-917.
Lee Y, Lee HY, Hanna RA, Gustafsson AB (2011) Mitochondrial autophagy by Bnip3 involves Drp1-mediated mitochondrial fission and recruitment of Parkin in cardiac myocytes. American journal of physiology Heart and circulatory physiology 301:H1924-1931.
Li X, Srinivasan SR, Connarn J, Ahmad A, Young ZT, Kabza AM, Zuiderweg ER, Sun D, Gestwicki JE (2013) Analogs of the Allosteric Heat Shock Protein 70 (Hsp70) Inhibitor, MKT-077, as Anti-Cancer Agents. ACS Med Chem Lett 4.

Liangliang X, Yonghui H, Shunmei E, Shoufang G, Wei Z, Jiangying Z (2010) Dominant-positive HSF1 decreases alpha-synuclein level and alpha-synuclein-induced toxicity. Mol Biol Rep 37:1875-1881.
Liu CK, Lyass A, Larson MG, Massaro JM, Wang N, D'Agostino RB, Sr., Benjamin EJ, Murabito JM (2016) Biomarkers of oxidative stress are associated with frailty: the Framingham Offspring Study. Age (Dordr) 38:1.
Liu S, Sawada T, Lee S, Yu W, Silverio G, Alapatt P, Millan I, Shen A, Saxton W, Kanao T, Takahashi R, Hattori N, Imai Y, Lu B (2012) Parkinson's disease-associated kinase PINK1 regulates Miro protein level and axonal transport of mitochondria. PLoS Genet 8:e1002537.
Lizama BN, Palubinsky AM, McLaughlin B (2017) Alterations in the E3 ligases Parkin and CHIP result in unique metabolic signaling defects and mitochondrial quality control issues. Neurochem Int.
Lizama BN, Palubinsky, Amy M., Raveendran, Vineeth A., Moore, Annah G., Federspiel, Joel D., Liebler, Daniel C., McLaughlin, BethAnn (Under Review) Mitochondrial C-terminus of HSC70-Interacting Protein Localization is Critical to Neuronal
Survival After Acute Stress.
Lucking CB, Durr A, Bonifati V, Vaughan J, De Michele G, Gasser T, Harhangi BS, Meco G, Denefle P, Wood NW, Agid Y, Brice A, French Parkinson's Disease Genetics Study G, European Consortium on Genetic Susceptibility in Parkinson's D (2000) Association between early-onset Parkinson's disease and mutations in the parkin gene. The New England journal of medicine 342:1560-1567.
Ma ZQ, Dasari S, Chambers MC, Litton MD, Sobecki SM, Zimmerman LJ, Halvey PJ, Schilling B, Drake PM, Gibson BW, Tabb DL (2009) IDPicker 2.0: Improved protein assembly with high discrimination peptide identification filtering. J Proteome Res 8:3872-3881.
Manasanch EE, Orlowski RZ (2017) Proteasome inhibitors in cancer therapy. Nat Rev Clin Oncol 14:417-433.
Margaill I, Plotkine M, Lerouet D (2005) Antioxidant strategies in the treatment of stroke. Free radical biology & medicine 39:429-443.
Matsuda N, Sato S, Shiba K, Okatsu K, Saisho K, Gautier CA, Sou YS, Saiki S, Kawajiri S, Sato F, Kimura M, Komatsu M, Hattori N, Tanaka K (2010) PINK1 stabilized by mitochondrial depolarization recruits Parkin to damaged mitochondria and activates latent Parkin for mitophagy. The Journal of cell biology 189:211-221.
Mayer MP, Schroder H, Rudiger S, Paal K, Laufen T, Bukau B (2000) Multistep mechanism of substrate binding determines chaperone activity of Hsp70. Nat Struct Biol 7:586-593.
McLaughlin B, Buendia MA, Saborido TP, Palubinsky AM, Stankowski JN, Stanwood GD (2012) Haploinsufficiency of the E3 ubiquitin ligase C-terminus of heat shock cognate 70 interacting protein (CHIP) produces specific behavioral impairments. PloS one 7:e36340.
McLaughlin B, Hartnett KA, Erhardt JA, Legos JJ, White RF, Barone FC, Aizenman E (2003) Caspase 3 activation is essential for neuroprotection in preconditioning. Proceedings of the National Academy of Sciences of the United States of America 100:715-720.
McWilliams TG, Prescott AR, Montava-Garriga L, Ball G, Singh F, Barini E, Muqit MMK, Brooks SP, Ganley IG (2018) Basal Mitophagy Occurs Independently of PINK1 in Mouse Tissues of High Metabolic Demand. Cell Metab 27:439-449 e435.
Mears JA, Lackner LL, Fang S, Ingerman E, Nunnari J, Hinshaw JE (2011) Conformational changes in Dnm1 support a contractile mechanism for mitochondrial fission. Nat Struct Mol Biol 18:20-26.

Metzger MB, Hristova VA, Weissman AM (2012) HECT and RING finger families of E3 ubiquitin ligases at a glance. Journal of cell science 125:531-537.
Mez J et al. (2017) Clinicopathological Evaluation of Chronic Traumatic Encephalopathy in Players of American Football. JAMA 318:360-370.
Min J-N, Whaley RA, Sharpless NE, Lockyer P, Portbury AL, Patterson C (2008) CHIP deficiency decreases longevity, with accelerated aging phenotypes accompanied by altered protein quality control. Molecular and cellular biology 28:4018-4025.
Mishra P, Varuzhanyan G, Pham AH, Chan DC (2015) Mitochondrial Dynamics is a Distinguishing Feature of Skeletal Muscle Fiber Types and Regulates Organellar Compartmentalization. Cell Metab 22:1033-1044.
Mizushima N, Yoshimori T, Ohsumi Y (2011) The role of Atg proteins in autophagosome formation. Annu Rev Cell Dev Biol 27:107-132.
Mo C, Hannan AJ, Renoir T (2015) Environmental factors as modulators of neurodegeneration: insights from gene-environment interactions in Huntington's disease. Neurosci Biobehav Rev 52:178-192.
Mohler MJ, Fain MJ, Wertheimer AM, Najafi B, Nikolich-Zugich J (2014) The Frailty syndrome: clinical measurements and basic underpinnings in humans and animals. Exp Gerontol 54:6-13.
Moon HE, Paek SH (2015) Mitochondrial Dysfunction in Parkinson's Disease. Exp Neurobiol 24:103-116.
Moore DJ, West AB, Dikeman DA, Dawson VL, Dawson TM (2008) Parkin mediates the degradation-independent ubiquitination of Hsp70. Journal of neurochemistry 105:1806-1819.
Morimoto RI (1998) Regulation of the heat shock transcriptional response: cross talk between a family of heat shock factors, molecular chaperones, and negative regulators. Genes Dev 12:3788-3796.
Morotz GM, De Vos KJ, Vagnoni A, Ackerley S, Shaw CE, Miller CC (2012) Amyotrophic lateral sclerosis-associated mutant VAPBP56S perturbs calcium homeostasis to disrupt axonal transport of mitochondria. Human molecular genetics 21:1979-1988.
Mosser DD, Caron AW, Bourget L, Meriin AB, Sherman MY, Morimoto RI, Massie B (2000) The chaperone function of hsp70 is required for protection against stress-induced apoptosis. Molecular and cellular biology 20:7146-7159.
Mukherjee R, Chakrabarti O (2016) Regulation of Mitofusin1 by Mahogunin Ring Finger-1 and the proteasome modulates mitochondrial fusion. Biochim Biophys Acta 1863:3065-3083.
Murphy TH, Miyamoto M, Sastre A, Schnaar RL, Coyle JT (1989) Glutamate toxicity in a neuronal cell line involves inhibition of cystine transport leading to oxidative stress. Neuron 2:1547-1558.
Musrati RA, Kollarova M, Mernik N, Mikulasova D (1998) Malate dehydrogenase: Distribution, function and properties. Gen Physiol Biophys 17:193-210.
Narendra DP, Jin SM, Tanaka A, Suen DF, Gautier CA, Shen J, Cookson MR, Youle RJ (2010) PINK1 is selectively stabilized on impaired mitochondria to activate Parkin. PLoS biology 8:e1000298.
Neckers L, Workman P (2012) Hsp90 molecular chaperone inhibitors: are we there yet? Clin Cancer Res 18:64-76.

Newman AB, Gottdiener JS, McBurnie MA, Hirsch CH, Kop WJ, Tracy R, Walston JD, Fried LP, Cardiovascular Health Study Research G (2001) Associations of subclinical cardiovascular disease with frailty. J Gerontol A Biol Sci Med Sci 56:M158-166.
Nguyen TN, Padman BS, Lazarou M (2016) Deciphering the Molecular Signals of PINK1/Parkin Mitophagy. Trends Cell Biol 26:733-744.
Niemann A, Ruegg M, La Padula V, Schenone A, Suter U (2005) Ganglioside-induced differentiation associated protein 1 is a regulator of the mitochondrial network: new implications for Charcot-Marie-Tooth disease. The Journal of cell biology 170:1067-1078.
Njemini R, Bautmans I, Onyema OO, Van Puyvelde K, Demanet C, Mets T (2011) Circulating heat shock protein 70 in health, aging and disease. BMC Immunol 12:24.
Novak I, Kirkin V, McEwan DG, Zhang J, Wild P, Rozenknop A, Rogov V, Lohr F, Popovic D, Occhipinti A, Reichert AS, Terzic J, Dotsch V, Ney PA, Dikic I (2010) Nix is a selective autophagy receptor for mitochondrial clearance. EMBO reports 11:45-51.
O'Brien PJ, Siraki AG, Shangari N (2005) Aldehyde sources, metabolism, molecular toxicity mechanisms, and possible effects on human health. Crit Rev Toxicol 35:609-662.
Ogawa K, Kim HK, Shimizu T, Abe S, Shiga Y, Calderwood SK (2012) Plasma heat shock protein 72 as a biomarker of sarcopenia in elderly people. Cell Stress Chaperones 17:349-359.
Olzmann JA, Chin LS (2008) Parkin-mediated K63-linked polyubiquitination: a signal for targeting misfolded proteins to the aggresome-autophagy pathway. Autophagy 4:85-87.
Otera H, Mihara K (2011) Molecular mechanisms and physiologic functions of mitochondrial dynamics. Journal of biochemistry 149:241-251.
Otomo C, Metlagel Z, Takaesu G, Otomo T (2013) Structure of the human ATG12~ATG5 conjugate required for LC3 lipidation in autophagy. Nat Struct Mol Biol 20:59-66.
Pakdaman Y, Sanchez-Guixe M, Kleppe R, Erdal S, Bustad HJ, Bjorkhaug L, Haugarvoll K, Tzoulis C, Heimdal K, Knappskog PM, Johansson S, Aukrust I (2017) In vitro characterization of six STUB1 variants in spinocerebellar ataxia 16 reveals altered structural properties for the encoded CHIP proteins. Bioscience reports 37.
Palacino JJ, Sagi D, Goldberg MS, Krauss S, Motz C, Wacker M, Klose J, Shen J (2004) Mitochondrial dysfunction and oxidative damage in parkin-deficient mice. The Journal of biological chemistry 279:18614-18622.
Palubinsky AM, Lizama BN, Winland AJ, Heinreich M, Gestwicki JE (In Preparation) IDH3α and αKG are Targets of Chaperone Mediated Protein
Refolding Following Acute Ischemic Stress Resulting in Increased Neuronal
Survival. In.
Palubinsky AM, Stankowski JN, Kale AC, Codreanu SG, Singer RJ, Liebler DC, Stanwood GD, McLaughlin B (2015) CHIP Is an Essential Determinant of Neuronal Mitochondrial Stress Signaling. Antioxidants & redox signaling 23:535-549.
Patel S, Player MR (2008) Small-molecule inhibitors of the p53-HDM2 interaction for the treatment of cancer. Expert Opin Investig Drugs 17:1865-1882.
Pearce N, Gallo V, McElvenny D (2015) Head trauma in sport and neurodegenerative disease: an issue whose time has come? Neurobiol Aging 36:1383-1389.
Pearl LH, Prodromou C, Workman P (2008) The Hsp90 molecular chaperone: an open and shut case for treatment. The Biochemical journal 410:439-453.
Perez FA, Palmiter RD (2005) Parkin-deficient mice are not a robust model of parkinsonism. Proceedings of the National Academy of Sciences of the United States of America 102:2174-2179.

Periquet M, Corti O, Jacquier S, Brice A (2005) Proteomic analysis of parkin knockout mice: alterations in energy metabolism, protein handling and synaptic function. Journal of neurochemistry 95:1259-1276.
Piperdi B, Ling YH, Liebes L, Muggia F, Perez-Soler R (2011) Bortezomib: understanding the mechanism of action. Mol Cancer Ther 10:2029-2030.
Powers WJ, Rabinstein AA, Ackerson T, Adeoye OM, Bambakidis NC, Becker K, Biller J, Brown M, Demaerschalk BM, Hoh B, Jauch EC, Kidwell CS, Leslie-Mazwi TM, Ovbiagele B, Scott PA, Sheth KN, Southerland AM, Summers DV, Tirschwell DL, American Heart Association Stroke C (2018) 2018 Guidelines for the Early Management of Patients With Acute Ischemic Stroke: A Guideline for Healthcare Professionals From the American Heart Association/American Stroke Association. Stroke; a journal of cerebral circulation 49:e46-e110.
Pysh JJ, Khan T (1972) Variations in mitochondrial structure and content of neurons and neuroglia in rat brain: an electron microscopic study. Brain research 36:1-18.
Qian SB, McDonough H, Boellmann F, Cyr DM, Patterson C (2006) CHIP-mediated stress recovery by sequential ubiquitination of substrates and Hsp70. Nature 440:551-555.
Rana A, Rera M, Walker DW (2013) Parkin overexpression during aging reduces proteotoxicity, alters mitochondrial dynamics, and extends lifespan. Proceedings of the National Academy of Sciences of the United States of America 110:8638-8643.
Raza H (2011) Dual localization of glutathione S-transferase in the cytosol and mitochondria: implications in oxidative stress, toxicity and disease. FEBS J 278:4243-4251.
Reddy PH, Reddy TP, Manczak M, Calkins MJ, Shirendeb U, Mao PZ (2011) Dynamin-related protein 1 and mitochondrial fragmentation in neurodegenerative diseases. Brain Res Rev 67:103-118.
Rial D, Castro AA, Machado N, Garcao P, Goncalves FQ, Silva HB, Tome AR, Kofalvi A, Corti O, Raisman-Vozari R, Cunha RA, Prediger RD (2014) Behavioral phenotyping of Parkin-deficient mice: looking for early preclinical features of Parkinson's disease. PloS one 9:e114216.
Riley BE, Lougheed JC, Callaway K, Velasquez M, Brecht E, Nguyen L, Shaler T, Walker D, Yang Y, Regnstrom K, Diep L, Zhang Z, Chiou S, Bova M, Artis DR, Yao N, Baker J, Yednock T, Johnston JA (2013) Structure and function of Parkin E3 ubiquitin ligase reveals aspects of RING and HECT ligases. Nat Commun 4:1982.
Romeu A, Arola L (2014) Classical dynamin DNM1 and DNM3 genes attain maximum expression in the normal human central nervous system. BMC Res Notes 7:188.
Rose JM, Novoselov SS, Robinson PA, Cheetham ME (2011) Molecular chaperone-mediated rescue of mitophagy by a Parkin RING1 domain mutant. Human molecular genetics 20:16-27.
Rosser MFN, Washburn E, Muchowski PJ, Patterson C, Cyr DM (2007) Chaperone functions of the E3 ubiquitin ligase CHIP. Journal of Biological Chemistry 282:22267-22277.
Rotblat B et al. (2014) HACE1 reduces oxidative stress and mutant Huntingtin toxicity by promoting the NRF2 response. Proceedings of the National Academy of Sciences of the United States of America 111:3032-3037.
Roy M, Itoh K, Iijima M, Sesaki H (2016) Parkin suppresses Drp1-independent mitochondrial division. Biochemical and biophysical research communications 475:283-288.
Rubel C, Soss S, McDonough H, Chazin W, Patterson C, Schisler J (2015) The Unfolding Tail of CHIP Mutation in Gordon Holmes Syndrome. Faseb Journal 29.

Ruschak AM, Slassi M, Kay LE, Schimmer AD (2011) Novel proteasome inhibitors to overcome bortezomib resistance. J Natl Cancer Inst 103:1007-1017.
Santos D, Cardoso SM (2012) Mitochondrial dynamics and neuronal fate in Parkinson's disease. Mitochondrion 12:428-437.
Saotome M, Safiulina D, Szabadkai G, Das S, Fransson A, Aspenstrom P, Rizzuto R, Hajnoczky G (2008) Bidirectional Ca2+-dependent control of mitochondrial dynamics by the Miro GTPase. Proceedings of the National Academy of Sciences of the United States of America 105:20728-20733.
Scheufler C, Brinker A, Bourenkov G, Pegoraro S, Moroder L, Bartunik H, Hartl FU, Moarefi I (2000) Structure of TPR domain-peptide complexes: critical elements in the assembly of the Hsp70-Hsp90 multichaperone machine. Cell 101:199-210.
Schlossmacher MG, Frosch MP, Gai WP, Medina M, Sharma N, Forno L, Ochiishi T, Shimura H, Sharon R, Hattori N, Langston JW, Mizuno Y, Hyman BT, Selkoe DJ, Kosik KS (2002) Parkin localizes to the Lewy bodies of Parkinson disease and dementia with Lewy bodies. Am J Pathol 160:1655-1667.
Schopf FH, Biebl MM, Buchner J (2017) The HSP90 chaperone machinery. Nature reviews Molecular cell biology 18:345-360.
Schulman BA, Chen ZJ (2005) Protein ubiquitination: CHIPping away the symmetry. Molecular cell 20:653-655.
Seirafi M, Kozlov G, Gehring K (2015) Parkin structure and function. FEBS J 282:2076-2088.
Serrat R, Mirra S, Figueiro-Silva J, Navas-Perez E, Quevedo M, Lopez-Domenech G, Podlesniy P, Ulloa F, Garcia-Fernandez J, Trullas R, Soriano E (2014) The Armc10/SVH gene: genome context, regulation of mitochondrial dynamics and protection against Abeta-induced mitochondrial fragmentation. Cell Death Dis 5:e1163.
Serviddio G, Romano AD, Greco A, Rollo T, Bellanti F, Altomare E, Vendemiale G (2009) Frailty syndrome is associated with altered circulating redox balance and increased markers of oxidative stress. Int J Immunopathol Pharmacol 22:819-827.
Shi CH, Schisler JC, Rubel CE, Tan S, Song B, McDonough H, Xu L, Portbury AL, Mao CY, True C, Wang RH, Wang QZ, Sun SL, Seminara SB, Patterson C, Xu YM (2014) Ataxia and hypogonadism caused by the loss of ubiquitin ligase activity of the U box protein CHIP. Human molecular genetics 23:1013-1024.
Shi Q, Gibson GE (2011) Up-regulation of the mitochondrial malate dehydrogenase by oxidative stress is mediated by miR-743a. Journal of neurochemistry 118:440-448.
Shimura H, Hattori N, Kubo S, Mizuno Y, Asakawa S, Minoshima S, Shimizu N, Iwai K, Chiba T, Tanaka K, Suzuki T (2000) Familial Parkinson disease gene product, parkin, is a ubiquitin-protein ligase. Nat Genet 25:302-305.
Singhal SS, Singh SP, Singhal P, Horne D, Singhal J, Awasthi S (2015) Antioxidant role of glutathione S-transferases: 4-Hydroxynonenal, a key molecule in stress-mediated signaling. Toxicol Appl Pharmacol 289:361-370.
Skaar JR, Pagan JK, Pagano M (2014) SCF ubiquitin ligase-targeted therapies. Nat Rev Drug Discov 13:889-903.
Smith MC, Scaglione KM, Assimon VA, Patury S, Thompson AD, Dickey CA, Southworth DR, Paulson HL, Gestwicki JE, Zuiderweg ER (2013) The E3 ubiquitin ligase CHIP and the molecular chaperone Hsc70 form a dynamic, tethered complex. Biochemistry 52:5354-5364.

Song S, Jang S, Park J, Bang S, Choi S, Kwon KY, Zhuang X, Kim E, Chung J (2013) Characterization of PINK1 (PTEN-induced putative kinase 1) mutations associated with Parkinson disease in mammalian cells and Drosophila. The Journal of biological chemistry 288:5660-5672.
Sriram SR, Li X, Ko HS, Chung KK, Wong E, Lim KL, Dawson VL, Dawson TM (2005) Familial-associated mutations differentially disrupt the solubility, localization, binding and ubiquitination properties of parkin. Human molecular genetics 14:2571-2586.
Stankiewicz M, Nikolay R, Rybin V, Mayer MP (2010) CHIP participates in protein triage decisions by preferentially ubiquitinating Hsp70-bound substrates. Febs Journal 277:3353-3367.
Stankowski JN, Zeiger SL, Cohen EL, DeFranco DB, Cai J, McLaughlin B (2011) C-terminus of heat shock cognate 70 interacting protein increases following stroke and impairs survival against acute oxidative stress. Antioxidants & redox signaling 14:1787-1801.
Stetler RA, Zhang F, Liu C, Chen J (2009) Ischemic tolerance as an active and intrinsic neuroprotective mechanism. Handb Clin Neurol 92:171-195.
Stetler RA, Leak RK, Gan Y, Li P, Zhang F, Hu X, Jing Z, Chen J, Zigmond MJ, Gao Y (2014) Preconditioning provides neuroprotection in models of CNS disease: paradigms and clinical significance. Prog Neurobiol 114:58-83.
Stevens DA, Lee Y, Kang HC, Lee BD, Lee YI, Bower A, Jiang H, Kang SU, Andrabi SA, Dawson VL, Shin JH, Dawson TM (2015) Parkin loss leads to PARIS-dependent declines in mitochondrial mass and respiration. Proceedings of the National Academy of Sciences of the United States of America 112:11696-11701.
Stottrup NB, Lofgren B, Birkler RD, Nielsen JM, Wang L, Caldarone CA, Kristiansen SB, Contractor H, Johannsen M, Botker HE, Nielsen TT (2010) Inhibition of the malate-aspartate shuttle by pre-ischaemic aminooxyacetate loading of the heart induces cardioprotection. Cardiovasc Res 88:257-266.
Strange RC, Spiteri MA, Ramachandran S, Fryer AA (2001) Glutathione-S-transferase family of enzymes. Mutat Res 482:21-26.
Surmeier DJ, Obeso JA, Halliday GM (2017) Selective neuronal vulnerability in Parkinson disease. Nature reviews Neuroscience 18:101-113.
Surmeier DJ, Guzman JN, Sanchez-Padilla J, Goldberg JA (2010) What causes the death of dopaminergic neurons in Parkinson's disease? Prog Brain Res 183:59-77.
Surmeier DJ, Guzman JN, Sanchez-Padilla J, Schumacker PT (2011) The role of calcium and mitochondrial oxidant stress in the loss of substantia nigra pars compacta dopaminergic neurons in Parkinson's disease. Neuroscience 198:221-231.
Synofzik M, Schule R, Schulze M, Gburek-Augustat J, Schweizer R, Schirmacher A, Krageloh-Mann I, Gonzalez M, Young P, Zuchner S, Schols L, Bauer P (2014) Phenotype and frequency of STUB1 mutations: next-generation screenings in Caucasian ataxia and spastic paraplegia cohorts. Orphanet J Rare Dis 9:57.
Tabb DL, Fernando CG, Chambers MC (2007) MyriMatch: highly accurate tandem mass spectral peptide identification by multivariate hypergeometric analysis. J Proteome Res 6:654-661.
Tang BL (2015) MIRO GTPases in Mitochondrial Transport, Homeostasis and Pathology. Cells 5.
Taylor KS, Cook JA, Counsell CE (2007) Heterogeneity in male to female risk for Parkinson's disease. J Neurol Neurosurg Psychiatry 78:905-906.
Teicher BA, Tomaszewski JE (2015) Proteasome inhibitors. Biochem Pharmacol 96:1-9.
Tipton KF, Singer TP (1993) Advances in our understanding of the mechanisms of the neurotoxicity of MPTP and related compounds. Journal of neurochemistry 61:1191-1206.

Trempe JF, Sauve V, Grenier K, Seirafi M, Tang MY, Menade M, Al-Abdul-Wahid S, Krett J, Wong K, Kozlov G, Nagar B, Fon EA, Gehring K (2013) Structure of parkin reveals mechanisms for ubiquitin ligase activation. Science 340:1451-1455.
Van Den Eeden SK, Tanner CM, Bernstein AL, Fross RD, Leimpeter A, Bloch DA, Nelson LM (2003) Incidence of Parkinson's disease: variation by age, gender, and race/ethnicity. Am J Epidemiol 157:1015-1022.
van der Bliek AM (2009) Fussy mitochondria fuse in response to stress. The EMBO journal 28:1533-1534.
Wang B, Abraham N, Gao G, Yang Q (2016) Dysregulation of autophagy and mitochondrial function in Parkinson's disease. Transl Neurodegener 5:19.
Wang L, Liu Y-T, Hao R, Chen L, Chang Z, Wang H-R, Wang Z-X, Wu J-W (2011a) Molecular Mechanism of the Negative Regulation of Smad1/5 Protein by Carboxyl Terminus of Hsc70-interacting Protein (CHIP). Journal of Biological Chemistry 286.
Wang X, Winter D, Ashrafi G, Schlehe J, Wong YL, Selkoe D, Rice S, Steen J, LaVoie MJ, Schwarz TL (2011b) PINK1 and Parkin target Miro for phosphorylation and degradation to arrest mitochondrial motility. Cell 147:893-906.
Wang Y, Yang F, Gritsenko MA, Wang Y, Clauss T, Liu T, Shen Y, Monroe ME, Lopez-Ferrer D, Reno T, Moore RJ, Klemke RL, Camp DG, 2nd, Smith RD (2011c) Reversed-phase chromatography with multiple fraction concatenation strategy for proteome profiling of human MCF10A cells. Proteomics 11:2019-2026.
Weihofen A, Ostaszewski B, Minami Y, Selkoe DJ (2008) Pink1 Parkinson mutations, the Cdc37/Hsp90 chaperones and Parkin all influence the maturation or subcellular distribution of Pink1. Human molecular genetics 17:602-616.
Wolf PA, Abbott RD, Kannel WB (1991) Atrial fibrillation as an independent risk factor for stroke: the Framingham Study. Stroke; a journal of cerebral circulation 22:983-988.
Woods NF, LaCroix AZ, Gray SL, Aragaki A, Cochrane BB, Brunner RL, Masaki K, Murray A, Newman AB, Women's Health I (2005) Frailty: emergence and consequences in women aged 65 and older in the Women's Health Initiative Observational Study. J Am Geriatr Soc 53:1321-1330.
Writing Group M et al. (2016) Executive Summary: Heart Disease and Stroke Statistics--2016 Update: A Report From the American Heart Association. Circulation 133:447-454.
Xu J (2005) Preparation, culture, and immortalization of mouse embryonic fibroblasts. Curr Protoc Mol Biol Chapter 28:Unit 28 21.
Xu W, Marcu M, Yuan X, Mimnaugh E, Patterson C, Neckers L (2002) Chaperone-dependent E3 ubiquitin ligase CHIP mediates a degradative pathway for c-ErbB2/Neu. Proceedings of the National Academy of Sciences of the United States of America 99:12847-12852.
Xu Z, Kohli E, Devlin KI, Bold M, Nix JC, Misra S (2008) Interactions between the quality control ubiquitin ligase CHIP and ubiquitin conjugating enzymes. BMC Struct Biol 8:26.
Yan MH, Wang X, Zhu X (2013) Mitochondrial defects and oxidative stress in Alzheimer disease and Parkinson disease. Free radical biology & medicine 62:90-101.
Yao J, Du H, Yan S, Fang F, Wang C, Lue LF, Guo L, Chen D, Stern DM, Gunn Moore FJ, Xi Chen J, Arancio O, Yan SS (2011) Inhibition of amyloid-beta (Abeta) peptide-binding alcohol dehydrogenase-Abeta interaction reduces Abeta accumulation and improves mitochondrial function in a mouse model of Alzheimer's disease. The Journal of neuroscience : the official journal of the Society for Neuroscience 31:2313-2320.

Ye Z, Needham PG, Estabrooks SK, Whitaker SK, Garcia BL, Misra S, Brodsky JL, Camacho CJ (2017) Symmetry breaking during homodimeric assembly activates an E3 ubiquitin ligase. Sci Rep 7:1789.
Yoo L, Chung KC (2018) The ubiquitin E3 ligase CHIP promotes proteasomal degradation of the serine/threonine protein kinase PINK1 during staurosporine-induced cell death. The Journal of biological chemistry 293:1286-1297.
Yoshii SR, Kuma A, Akashi T, Hara T, Yamamoto A, Kurikawa Y, Itakura E, Tsukamoto S, Shitara H, Eishi Y, Mizushima N (2016) Systemic Analysis of Atg5-Null Mice Rescued from Neonatal Lethality by Transgenic ATG5 Expression in Neurons. Dev Cell 39:116-130.
Young C, Tenkova T, Dikranian K, Olney JW (2004) Excitotoxic versus apoptotic mechanisms of neuronal cell death in perinatal hypoxia/ischemia. Current molecular medicine 4:77-85.
Zeiger SL, McKenzie JR, Stankowski JN, Martin JA, Cliffel DE, McLaughlin B (2010) Neuron specific metabolic adaptations following multi-day exposures to oxygen glucose deprivation. Biochim Biophys Acta 1802:1095-1104.
Zeytuni N, Zarivach R (2012) Structural and functional discussion of the tetra-trico-peptide repeat, a protein interaction module. Structure 20:397-405.
Zhang F, Wang W, Siedlak SL, Liu Y, Liu J, Jiang K, Perry G, Zhu X, Wang X (2015) Miro1 deficiency in amyotrophic lateral sclerosis. Front Aging Neurosci 7:100.
Zhang M, Windheim M, Roe SM, Peggie M, Cohen P, Prodromou C, Pearl LH (2005) Chaperoned ubiquitylation--crystal structures of the CHIP U box E3 ubiquitin ligase and a CHIP-Ubc13-Uev1a complex. Molecular cell 20:525-538.
Zhang Y, Gao J, Chung KK, Huang H, Dawson VL, Dawson TM (2000) Parkin functions as an E2-dependent ubiquitin- protein ligase and promotes the degradation of the synaptic vesicle-associated protein, CDCrel-1. Proceedings of the National Academy of Sciences of the United States of America 97:13354-13359.
Zhao Y, Brickner JR, Majid MC, Mosammaparast N (2014) Crosstalk between ubiquitin and other post-translational modifications on chromatin during double-strand break repair. Trends Cell Biol 24:426-434.